VOLUME I

TESTING AND EVALUATION OF GROUT STRENGTHENED AND REPAIRED TUBULAR MEMBERS

FINAL REPORT

TEES Projects 32525-30900, 30920, 30930, 30980, 41720

by

T. L. Kohutek, J. M. Nunn, and S. L. Faseler

Texas Engineering Experiment Station
Texas A&M University
College Station, Texas

August 1993

ACKNOWLEDGMENTS

This project was funded by five companies representing oil and gas operators, contractors, and regulators. The technical representatives from each of these organizations are an essential part of the research team. The authors would like to express their appreciation to them for their financial support and input throughout all phases of this project.

The following is a list of the participants and their representatives:

ARCO Exploration and Production Tech.
Mr. Steve Guynes
2300 W. Plano Parkway
Plano, TX 75075-8499
(214) 754-3077

Mobil Research and Development Corp.
Mr. Douglas R. Angevine
13777 Midway Road
Dallas, TX 75244-4390
(214) 851-8359

Shell Oil Company
Mr. Kris A. Digre
E&P Civil Engineering
Deepwater Division
Shell Offshore, Inc.
P. O. Box 576
Houston, TX 77001-0576
(713) 544-4104

Minerals Management Services
Mr. Charles Smith
381 Elden Street, MS 647
Herndon, VA 22070-4817
(703) 787-1559

Phillips Petroleum Co.
Mr. Roger L. Thomas
Corporate Engineering
10D4 Phillips Building
Bartlesville, OK 74004
(918) 661-4903

TABLE OF CONTENTS

TABLE OF CONTENTS (Continued)

TABLE OF CONTENTS (Continued)

LIST OF FIGURES

LIST OF FIGURES (Continued)

LIST OF TABLES

LIST OF TABLES (Continued)

EXECUTIVE SUMMARY

This report documents the work performed and the results obtained from the joint industry project, "Testing and Evaluation of Grout Strengthened and Repaired Tubular Members." The project was funded by five industry participants and was conducted by the Texas Engineering Experiment Station at Texas A&M University. The Principal Investigators on the project were Terry L. Kohutek, P.E., Ph.D. and Loren D. Lutes, P.E., Ph.D.

The purpose of the project was to determine the increase in axial capacity that grout provides when placed in undamaged and dent-damaged members. This was accomplished by performing three primary tasks: 1) conduct a comprehensive study of all previous research on grouted tubular members, 2) conduct axial compression tests on full-scale members, and 3) analyze experimental data and compare capacities to those computed by existing analytical methods.

An extensive literature review was performed in Task 1 to collect data from all research that had been conducted on grouted tubular members. In this review, it was found that 71 tests had been conducted on grouted tubulars. Sixty-four of these tests were performed on damaged, grout-repaired members. However, only four of these tests were conducted on members with diameters greater than 7 in. and lengths greater than 10 ft. In addition, the damaged members tested usually contained small dents (dent depth/diameter = $d/D < 0.20$) perpendicular to the longitudinal axis that are not representative of the more severe dents found on members of in-service platforms. Thus, there was a need to obtain data on members that are more representative of full-scale members with severe longitudinal dent damage ($d/D > 0.33$). A test matrix was formulated for Task 2 to meet this need.

Task 2 was accomplished by conducting axial compression tests on 12 members that are representative of full-scale jacket braces. The configurations of members tested included: undamaged/ungrouted, undamaged/grouted, dented/ungrouted, and dented/grouted. Within these four different configuration, members with three different diameter-to-thickness ratios (D/t = 34.0, 42.7, and 51.0) were tested. Longitudinally oriented dents with the same depth-to-diameter ratio ($d/D = 0.40$) were used for all damaged members.

In Task 3, the experimental data was analyzed on the basis of the ultimate capacity of an undamaged/ungrouted member. It was assumed that the Cox-LRFD formula provides an accurate lower bound value for these members. A member (specimen 12) was tested to further verify the validity of this assumption. To account for the effects of bending that occurred during the tests, the Cox-LRFD formula was used with the AISC-LRFD interaction formula to obtain a "corrected" predicted ultimate axial capacity. In addition, the experimentally determined ultimate axial capacity of each member was compared to the ultimate capacity predicted by several existing analytical methods.

The major findings of this study are:

1) Severe dent damage will significantly reduce the capacity of a member. The two dented/ungrouted members tested, specimens 01 and 10 (d/D = 0.40), experienced 24% and 38% reductions in their original ultimate capacities.

2) Based on the experimental data from specimen 12 and previous research efforts, the Cox-LRFD (with moment correction) formula appears to provide a reasonable lower bound value for undamaged/ungrouted members.

3) Grouting is a viable method for strengthening undamaged tubular members. Based on the experimental data, grouting members without any initial damage can increase the strength 32% to 104% above the original ultimate capacity based on the Cox-LRFD equation (with moment correction). Specimen 07 contained an extremely poor quality of grout; however, the grout still increased the strength of the member 32% above the original ultimate capacity. In the case of specimen 09, which contained quality grout the full length of the member, the capacity was 104% above the original ultimate capacity.

4) Grouting is also a viable method for repairing dent-damaged tubular members. Grout can inhibit local buckling and prevent any further reduction of the cross section at the location of the dent. In all the grout-repaired/dented members tested, the ultimate

capacity exceeded the original (undamaged/ungrouted) capacity of the member based on the Cox-LRFD equation (with moment correction). This increase in strength above the original capacity varied from 15% to 46%. This results in an 83% to 85% increase above the dented/ungrouted capacity.

5) The actual yield strength, F_y, of all members exceeded the specified minimum yield strength, 35 ksi, for API 5L Gr. B steel. The original **design** capacity (using 35 ksi and excluding the resistance factor) for all members was computed based on the Cox-LRFD equation (with moment correction). The capacity of the grouted members was 35% to 228% greater than the original **design** capacity.

6) Grouting may be a viable repair method for members with dent-damage and significant initial out-of-straightness. Grout increased the strength of a member (specimen 11) with an initial out-of-straightness/member length = 0.0095 and dent depth/diameter = 0.40 to 15% above the original (undamaged/ungrouted) ultimate capacity.

7) Most of the existing analytical methods provided very conservative (lower bound) values for the predicted ultimate strength. In some members, the predicted strength was 1/3 of the experimentally measured capacity. These analytical methods are based on relatively short, shallow dents oriented perpendicular to the longitudinal axis of the member. The dents produced in this study were relatively deep (d/D = 0.40), long (L_D = 36 in.) dents oriented along the longitudinal axis of the member. These dents appear to be "stiffer" than the assumed analytical dents and could account for the significant difference in the predicted and measured capacities.

8) Two of the analytical methods (ACI and Poston) produced unconservative (overpredicted) ultimate capacities. The ACI method overpredicts the capacity of <u>all</u> undamaged/grouted specimens (from 18% to 31%). The Poston method significantly overpredicts the capacity (by as much as 21%) of two specimens (07 and 08). It is not significant that the capacity of specimen 07 was not accurately predicted due to the fact

that the member did not contain quality grout the full length of the member. The capacity of specimen 08 was overpredicted because the initial out-of-straightness of the member was 2.0 in.; however, Poston used a value of 1.25 in. for his analysis.

9) Post-test destructive examination of the grouted members revealed significant differences in the quality and completeness of the grout. Members that were pumped full of grout, without interruption, generally contained a higher volume of quality grout.

1.0 INTRODUCTION

1.1 Background.

This report addresses the issue of strengthening undamaged and repairing damaged offshore jacket bracing. Members in offshore platforms are normally designed to withstand elements of load from wind, waves, equipment, etc. However, there are also events not considered in the design that produce loads on the structure that can damage a component or member. These events include: 1) falling material or equipment, 2) inadvertent collisions from a service craft docking at the platform, or 3) damage from explosives used for fishing near the platforms. The loads from these events may cause damage in the form of denting, holes, and/or out-of-straightness. Corrosion also causes significant damage to these components. When structural members sustain any of these forms of damage, the reduction in capacity needs to be assessed. If the reduction is significant, the member may require repair or, in more severe cases, replacement.

There are several methods commonly used to repair damaged tubular members. These include: 1) welding a sleeve around the outside of the member in the location of the damage, 2) applying an externally grouted clamp, and 3) applying internal grout. Ideally, the repair method should increase the strength of the member to its original design capacity.

A common, and generally the most economical, method used to repair members in offshore platforms is internal grouting. This grouting can occur over the entire length of the member or may be confined to the damaged area. There is limited experimental data on internally grouted tubular members, particularly on full-scale members. Experimental testing and analysis of grouted, full-scale members is needed to evaluate grouting as a repair method.

1.2 Objective of the Research

The primary objective of this research is to provide data needed to evaluate internal grouting as a method of strengthening and repairing members of offshore platforms. Of particular interest are dent-damaged members.

Presented in the next section are the test parameters and results from 71 tests that have been conducted on grouted tubular members. Of these tests, 64 were conducted on damaged, grout repaired members. All of these tests indicate that grouting increases the capacity of damaged members. However, only four of these tests were conducted on members with diameters greater than 7-in. and lengths greater than 10-ft. In addition, the damaged members tested contained dents that were relatively shallow (dent depth/diameter = d/D < 0.20) and perpendicular to the longitudinal axis of the member. These dents are not representative of the more severe dents that are found on members of in-service platforms. Thus, no data exists for full-scale members with severe dent damage (d/D > 0.33) that have been repaired by grouting.

Twelve full-scale, undamaged and dent-damaged, ungrouted and internally grouted, tubular members were tested in axial compression to obtain these data. The damaged members contained dents that are representative (d/D = 0.40) of the more severe dents found on in-service platforms. The ultimate capacity of these members was compared to capacities based on various analytical models and formulae developed for undamaged, damaged/ungrouted, undamaged/grouted, and damaged/grouted members.

1.3 Literature Review

1.3.1 Standard Notation. Different researchers use different notations when reporting the results of their work. To eliminate the confusion that often occurs when comparing the work of others, a standard notation has been adopted for the remainder of this chapter. In addition, all work reported in metric units has been converted to English units.

The following notations and units are used in this chapter:

F_y = yield strength of steel (ksi),

F_u = compressive strength of grout (ksi),

P_u = ultimate experimental axial capacity of the member (kips),

D = outside diameter of specimen (in.),

t = wall thickness of specimen (in.),

L = length of specimen (ft. or in.),

r = radius of gyration of specimen (in.),

d = maximum depth of dent (in.),

δ = maximum out-of-straightness of specimen (in.),

f_b = bending or flexural stress (ksi)

f_a = axial stress (ksi)

w/c = water to cement ratio, by weight (lb/lb)

KL = effective length. in buckling of specimen (ft. or in.)

KL/r = slenderness ratio of specimen (in./in.)

1.3.2 Previous Work. Wimpey Offshore (1984) tested the six fully grouted, undamaged specimens shown in Table 1.1. The members were subjected to combined axial and bending loads. The eccentricity of the load was varied to produce bending stress/axial stress (f_b/f_a) ratios from 1.00 to 10.00. It was found that the grout primarily reinforces the tubular wall which eliminated the possibility of local buckling and reduction of the cross section. Hence, the grout is most beneficial in members with high diameter-to-thickness ratios (D/t) where local buckling is the controlling limit state. Compact members (small L/D), which generally fail in a squash mode rather than a global buckling mode, did not fail in a squash mode due to the presence of grout in the member. Thus, the grout significantly increased the capacity of the member. In addition, it was found that the strength of members which fail in a squash mode can be further increased by increasing grout strength. However, the grout strength does not affect global stability, and thus the strength of members subject to global buckling is not affected by grout strength. This research also shows that steel yield stress has little effect on the ultimate capacity of the member.

S. Parsanejad (1987) later conducted pure axial compression tests on the ten fully grouted, tubular members shown in Table 1.2. Four specimens (A 1&2 and C 1&2) contained minimal damage with out-of-straightness ratios (δ/L less than 0.00012) and dent depth-to-diameter ratios (d/D less than 0.075). The remaining six specimens (B 1&2, D 1&2, and E 1&2) contained more substantial denting and out-of-straightness damage as shown in Table 1.2. All members contained a dent that was oriented transverse to the longitudinal axis of the member. The results of these tests indicated that specimens with a larger dent exhibited a smaller post-ultimate strength at large displacements. In addition, it was found that in all the specimens, the stress in the dented region exceeded the yield stress prior to reaching the ultimate load. This indicated

that the grout supported the tube wall and prevented local buckling. The ultimate capacity of ungrouted, undamaged tubular members, with the same geometrical and material properties, was computed using AISC specifications (AISC, 1969). It was found that the grout increased the strength in five of the eight damaged specimens above this computed design capacity. The capacity of the other three specimens (B2, D2 and E1) was less than the original design capacity. These specimens contained a combination of a larger dent ($d/D > 0.135$) and a larger out-of-straightness ($\delta/L \geq 0.00214$). It was stated by the author that this level of damage is rarely encountered in practice.

S. Parsanejad, S. Tyler, and K.Y. Chin (1987) performed pure axial compression tests on four fully grouted and five partially grouted members. Table 1.3 contains a summary of the test parameters and results for these members. All members contained a dent that was oriented transverse to the longitudinal axis of the member. It was found that specimens with larger dents have a smaller post-ultimate strength at larger displacements and that the grout prevents local buckling at the dent by reinforcing the tube wall. For the partially grouted specimens, buckling occurred near the end of the grouted length. The experimental capacities for all specimens were compared to analytical values. The analytical values were based on beam-column theory using a first yield failure criterion. In the four, fully grouted specimens, the differences between experimental and analytical capacities were acceptably small ($< 15\%$), with the analytical method providing a lower bound value. It was also found that grouting the full length of the member more than compensated for the loss of strength due to the damage. For the partially grouted specimens, the capacities based on the analytical method exceeded the experimental capacities.

S. Parsanejad and P. Gusheh (1988) conducted pure axial compression tests on the ten, partially grouted, damaged tubular members shown in Table 1.4. All specimens had D/t ratios of approximately 48 and a dent oriented transverse to the longitudinal axis of the member. Four members essentially contained dent damage only (J 5&6, and K 3&4) since the out-of-straightness was practically negligible ($\delta/L < 0.0002$). The remaining six specimens had initial out-of-straightness and dent damage. As in the other research efforts, it was found that the grout provided sufficient support of the tube wall to prevent local buckling. For all ten specimens the difference between the experimental and analytical capacities was less than 20%. The analytical

method used in this study was developed by S. Parsanejad for his 1987 study. For the four specimens with denting only, the grout increased the strength of the member to the original undamaged capacity. For one specimen, the damaged, grout repaired capacity was 19% greater than the original design capacity. For the other six specimens which contained out-of-straightness and a dent, the grout repaired capacity was up to 95% of the undamaged, ungrouted capacity. Again the authors concluded that grout can compensate for the loss in strength due to the damage.

L.F. Boswell and C.A. D'Mello (1989) conducted pure axial compression tests on 37, 1/5, 1/3, and approximately full-scale, fully grouted tubular members. Table 1.5 contains a summary of the geometric properties and ultimate capacity for each test specimen. Table 1.6 contains a summary of all of the geometric ratios for each specimen. The ends of each specimen were fitted with fixtures to approximate pinned end conditions and were tested in a horizontal position. Generally these tests showed that as the dent depth increases, the ultimate capacity decreases. In addition, the effect of D/t and L/r coupled with the dent damage on the capacity was observed. It was found that there was no significant interaction between dent damage and D/t. However, the data showed that there is interaction between dent damage and L/r. The L/r ratio had little effect at low D/t ratios (23.4) but a reduction in the effectiveness of grout in restoring capacity was observed at higher D/t ratios (28.5 and 48.0). The experimental capacity of all specimens except one exceeded the ultimate capacity for undamaged, ungrouted members based on the American Petroleum Institute (API, 1982) ASD formulation. The capacity of the other specimen was 94% of the API capacity. In addition, it was found that specimens with smaller dent depths had a more significant increase in capacity due to the grout.

J. P. Renoult and J. P. Quillevere (1990) of Elf Aquitane conducted pure axial tests on three fully grouted tubular members. Table 1.7 contains a summary of the test specimens. These members contained dent and out-of-straightness damage. The dents were oriented along the longitudinal axis of the member. The results from the tests showed that the ultimate strength of the damaged members was increased by the grout by 67% for d/D of 0.51 and 48% for d/D of 0.64 when compared to identical damaged ungrouted members. A finite element model was developed for the grouted damaged members using 20 node, brick elements. The model verified

the experimental observation that the main effect of internal grouting is to prevent or delay the occurrence of a hinge due to local buckling.

J. M. Ricles, T. E. Gillum, and W. B. Lamport (1993) conducted an extensive testing program on thirteen dent-damaged/grouted, dent-damaged/ungrouted, and undamaged/grouted members. One of the members tested had been repaired by means of an externally grouted clamp while three of the members tested were repaired by internal grouting. The other nine members were not grouted. Table 1.8 contains a summary of the test parameters and results for the three internally grouted members. All of these members had a nominal diameter of 8.625 in. and were nominally 15 ft. in length. The wall thicknesses of the members were varied to provide D/t ratios of 34.9, 46.2, and 64.0. All members contained a nominal dent depth of 0.8625 in. (d/D=0.10) and were subjected to an eccentric axial compressive load at 0.2D. Again, it should be noted that the dents were produced by a knife-edged indentor head applied transverse to the longitudinal axis of the member. The capacities of the members tested were compared to the predicted capacity based on Parsanejad's formulation (1987). These values and comparisons are also presented in Table 1.8.

The major findings for the internally grouted specimens from the Ricles, et. al., study were:

1) Internal grouting can restore a 0.1D dent-damaged member's strength beyond the original undamaged member strength. The repaired strength was from 13% to 88% greater than undamaged member strength and from 110% to 165% greater than the damaged member strength.

2) The behavior of the member and extent to which grout strengthens the member is affected by the D/t ratio. Members with higher D/t ratios (>46) are susceptible to local buckling. This local buckling prevents the repaired member from developing a capacity that is equivalent to the capacity of a dented section with full composite action.

3) The capacity predicted by Parsanejad's method provides a close lower bound value for the experimental data.

Table 1.1. Data from Experimental Research Performed by Wimpey Offshore (1984)

Specimen No.	Diameter (in.)	Length (ft.)	Thickness (in.)	Dent Depth (in.)	L/D
1 & 2	8.50	7.09	0.118	0	10
3 & 4	6.63	11.02	0.177	0	20
5 & 6	6.09	14.63	0.374	0	28.8

Specimen No.	D/t	d/D	kL/r	f_b/f_a	F_y (ksi)	P_u (kips)	F_u (ksi)
1 & 2	72.00	N.A.	28.71	1.0 5.0	58.1	304 75	10.2 8.1
3 & 4	37.40	N.A.	57.94	1.0 10.0	60.2	147 32	8.5 8.2
5 & 6	16.30	N.A.	86.69	1.0 10.0	68.9	131 40	9.3 9.1

Notes: 1) All member properties:
Steel: BS4360 Grade 50d standards
Grout: API Oilwell "B" grout, w/c = 0.34

Table 1.2. Data from Experimental Research Performed by S. Parsanejad (1987)

Specimen No.	Diameter (in.)	Length (ft.)	Thickness (in.)	Dent Depth (in.)	L/D	D/t
A (2)	1.70	4.12	0.055	0.127	29.06	31.10
B (2)	1.70	4.12	0.055	0.081	29.06	31.05
C (2)	2.70	6.10	0.055	0.208	27.16	48.55
D (2)	2.70	6.10	0.055	0.405	27.16	48.85
E (2)	1.70	4.12	0.058	0.232	29.06	29.25

Specimen No.	d/D	δ/L	kL/r	F_y (ksi)	P_u (kips)	F_u (ksi)
A (2)	0.075	0.00010	84.96	84.5 85.1	16.2 15.7	4.6
B (2)	0.138	0.00214	84.96	81.7 83.6	13.9 10.8	4.6
C (2)	0.070	0.00012	78.26	73.1 77.6	28.8 27.4	4.6
D (2)	0.150	0.00232	78.26	71.5 75.1	23.8 19.8	4.6
E (2)	0.136	0.00267	85.11	53.4 50.9	8.8 11.9	4.3

Note: (*) indicates the number of specimens

Table 1.3. Data from Experimental Research Performed by S. Parsanejad, S. Tyler, and K. Y. Chin (1987)

Specimen No.	Diameter (in.)	Length (ft.)	Grout Length (ft.)	Thickness (in.)	Dent Depth (in.)	L/D
I 1	2.70	6.32	2.95	0.052	0.275	28.1
I 2	2.70	6.32	1.97	0.053	0.259	28.1
I 3	2.70	6.32	0.98	0.054	0.270	28.1
H 2	3.43	6.32	0.98	0.060	0.505	22.0
G 1	2.70	6.25	6.25	0.055	0.193	27.8
G 2	2.70	6.25	6.25	0.055	0.397	27.8
G 3	2.70	6.25	6.25	0.055	0.346	27.8
F 1	1.72	4.39	4.39	0.028	0.248	30.6
H 1	3.43	6.25	6.25	0.061	0.499	21.9

Specimen No.	D/t	d/D	δ/L	kL/r	F_y (ksi)	F_u (ksi)
I 1	51.7	0.102	0.0028	97.3	33.5	2.7
I 2	51.2	0.096	0.0031	96.9	33.4	2.7
I 3	49.7	0.100	0.0032	96.7	33.8	2.7
H 2	57.4	0.146	0.0007	77.4	31.8	2.3
G 1	49.2	0.071	0.0001	92.8	31.8	2.3
G 2	49.2	0.142	0.0006	99.4	33.7	2.3
G 3	49.2	0.128	0.0043	97.1	33.5	2.3
F 1	61.4	0.144	0.0017	111.5	26.0	2.3
H 1	56.3	0.146	0.0022	77.7	32.5	2.3

Notes:
1) kL/r values as given in report
2) All members; grout properties: W/C = 0.45
3) The ultimate capacities were not presented in this report.

Table 1.4. Data from Experimental Research Performed by S. Parsanejad and P. Gusheh (1988)

Specimen No.	Diameter (in.)	Length (ft.)	Grout Length (ft.)	Thickness (in.)	Dent Depth (in.)	L/D
J 1	2.70	5.35	2.96	0.056	0.259	23.8
J 2	2.70	5.35	2.29	0.056	0.194	23.8
J 3	2.70	5.35	1.59	0.056	0.208	23.8
J 4	2.70	5.35	1.00	0.056	0.194	23.8
J 5	2.70	5.35	2.91	0.055	0.318	23.8
J 6	2.70	5.35	1.62	0.055	0.310	23.8
K 1	2.70	7.48	2.92	0.056	0.202	33.2
K 2	2.70	7.48	1.63	0.055	0.219	33.2
K 3	2.70	7.48	4.22	0.056	0.310	33.2
K 4	2.70	7.48	1.65	0.056	0.308	33.2

Specimen No.	D/t	d/D	δ/L	kL/r	F_y (ksi)	P_u (kips)	F_u (ksi)
J 1	48.0	0.092	0.0031	62.2	36.9	11.5	5.2
J 2	48.3	0.072	0.0040	62.9	38.2	12.8	5.2
J 3	48.3	0.077	0.0037	64.0	44.3	12.4	5.2
J 4	47.8	0.072	0.0038	65.1	37.9	12.4	5.2
J 5	48.9	0.118	0.0002	63.1	37.0	13.9	5.2
J 6	48.7	0.115	0.0002	64.8	37.6	14.6	5.2
K 1	48.4	0.075	0.0040	88.4	36.9	10.1	5.2
K 2	49.1	0.081	0.0038	90.8	38.6	9.7	5.2
K 3	48.5	0.115	0.0001	88.1	38.6	14.6	5.2
K 4	48.3	0.114	0.0002	91.4	37.9	12.1	5.2

Notes: 1) kL/r values as given in report
2) All members; grout properties: W/C = 0.45

Table 1.5. Geometry Data from Experimental Research Performed by L. F. Boswell and C. A. D'Mello (1989)

Specimen No.	Diameter (in.)	Length (ft.)	Thickness (in.)	P_u (kips) avg.	Dent Depth (in.)
A(5)	1.75	2.95	0.049	16.8	0.201
B(4)	1.75	2.95	0.062	17.5	0.213
C(3)	3.00	5.12	0.104	88.1	0.131
D(2)	3.00	5.12	0.104	54.1	0.470
F(2)	3.00	5.94	0.126	78.9	0.291
G(2)	3.00	5.09	0.130	84.6	0.284
H(2)	3.00	4.23	0.128	85.9	0.290
J(2)	3.00	6.07	0.063	48.5	0.303
K(2)	3.00	5.18	0.063	52.7	0.293
L(2)	3.00	4.33	0.063	59.4	0.299
M(2)	3.00	5.97	0.107	73.7	0.291
N(2)	3.00	5.12	0.104	67.3	0.302
O(2)	3.00	4.27	0.106	77.9	0.305
P(1)	3.00	5.12	0.104	69.7	N.A.
Q(4)	8.62	6.11	0.318	473.2	0.987

Note: (*) indicates the number of specimens tested

Table 1.6. Geometric Ratio Data from Experimental Research Performed by L. F. Boswell and C. A. D'Mello (1989)

Specimen No.	L/D	D/t	d/D	kL/r
A(5)	20.23	35.55	0.116	58.84
B(4)	20.23	27.95	0.123	59.28
C(3)	20.48	28.90	0.040	59.97
D(2)	20.48	29.00	0.160	59.97
F(2)	23.74	23.80	0.100	70.08
G(2)	20.33	23.20	0.100	60.13
H(2)	16.92	23.50	0.100	49.94
J(2)	24.26	47.70	0.100	70.13
K(2)	20.72	58.00	0.100	59.85
L(2)	17.31	58.00	0.100	50.03
M(2)	23.87	28.00	0.100	69.99
N(2)	20.46	29.00	0.100	59.97
O(2)	17.05	28.20	0.100	50.24
P(1)	20.46	28.90	N.A.	59.97
Q(4)	22.43	27.15	0.110	65.81

Note: (*) indicates the number of specimens tested.

Table 1.7. Data from Experimental Research Performed by J. P. Renault and J. P. Quillevere (1990)

Specimen No.	Diameter (in.)	Length (ft.)	Thickness (in.)	Dent Depth (in.)	L/D
5 A	6.81	15.75	0.31	3.47	27.75
5 B	6.81	15.75	0.31	3.47	27.75
6 B	6.81	15.75	0.31	4.36	27.75

Specimen No.	D/t	d/D	δ/L	P_u (kips)	kL/r
5 A	21.97	0.51	0.0092	378	57.5
5 B	21.97	0.51	0.0105	387	57.5
6 B	21.97	0.64	0.0174	283	57.5

Notes:
1) All members fully grouted
2) All members have pinned-fixed end conditions (k = 0.7)
3) All members tested meet API 5L Grade B steel standards
4) All members; grout properties: w/c = 0.44, F_u = 6.2 ksi

Table 1.8. Data from Experimental Research Performed
by J. M. Ricles, T. E. Gillum, and W. B. Lamport (1993)

Specimen No.	Diameter (in.)	Length (ft.)	Thickness (in.)	Dent Depth (in.)	L/D	D/t	δ/L	L/r
A3	8.625	14.90	0.247	0.857	20.73	34.9	0.0006	60.6
B3	8.634	14.91	0.187	0.863	20.72	46.2	0.0011	60.1
C3	8.643	15.00	0.135	0.860	20.83	64.0	0.0009	59.7

Specimen No.	F_y (ksi)	F_u (ksi)	P_u (kips)	P_{th}(Parsanejad)[2] (kips)	$\frac{P_u}{P_{th}}$
A3	34.8	4.38	191	134	1.43
B3	33.4	3.89	117	100	1.17
C3	39.4	6.89	122	109	1.12

Note: 1) All members eccentrically loaded at 0.2D.
2) (Parsanejad 1987)
3) Dent width = 5.0 in., Dent length = 24.0 in.

2.0 EXPERIMENTAL TEST PROGRAM

The experimental program was conducted to determine the pre- and post-buckling behavior and the ultimate capacity of twelve full-scale tubular members. The program consisted of: 1) denting members, 2) grouting members, 3) instrumenting members, 4) compression testing of grout cylinders, 5) full-scale compression testing of members, 6) reducing full-scale test data, 7) tensile coupon testing, and 8) evaluating full-scale test results. Denting and grouting operations were conducted at the Texas A&M University Riverside Campus while the remaining tasks were conducted at the Texas A&M University Testing and Materials Research Laboratory. The details of these events are described in this chapter.

2.1 Test Matrix Description

Meetings were held with the technical representatives of the sponsors to determine the test matrix for the program. This was done to assure that the data obtained from the test would be relevant to member types, damage, repair methods, etc., typically found in existing offshore platforms. The results from specimens 01-04 tests were used to determine the parameters for specimens 05-08. Specimens 05-08 were tested before determining the parameters for specimens 09-12.

A summary of the test parameters is presented in Table 2.1. All specimens had either 12.75 or 16.00-in. outside diameter, wall thickness of 0.375 or 0.250-in., and were approximately 40-ft. in length. **The wall thickness and diameter of each specimen was not measured during the experimental program. The specified nominal values were used in all calculations.** This resulted in three different D/t ratios (34.0, 42.7, and 51.0) and slenderness ratios (kL/r) between 40 and 90. These values are typical of those found in jacket braces.

A typical dent cross-section and profile at maximum dent depth are shown in Figures 2.1 and 2.2. Relatively long (L_d = 36-in.), deep (d/D = 0.39 - 0.40) dents were selected for two reasons: 1) these dents currently exist in many in-service members; 2) d/D = 0.40 represents "severe" dent damage. A dent of this size probably represents an upper limit on the size that would be repaired by internal grouting. Thus, it was presumed that if the original ultimate capacity of these members could be restored by internal grouting, the strength would also be

restored in members with less severe dent damage. **It should be noted that the dents used in this study differ significantly from the dents used in most of the previous research efforts.** As shown in Figures 2.3 and 2.4, an indentor was used that made a longitudinal dent rather than a transverse dent that has been used in other studies. A grout with a nominal 28 day compressive strength of 4000 psi was used because it is typical for grouts currently used for various grouting operations on offshore platforms.

The first four tests were conducted before the test parameters were defined for the final four tests (specimens 05 - 08). The increase in capacity due to grouting as indicated by the data from the first four tests proved to be greater than expected. To validate these findings, it was decided that replicate tests should be conducted. Three of the first four tests were duplicated in the second half of the test program (specimens 02 and 05, 03 and 06, 04 and 08). The ungrouted, damaged tubular member (specimen 01) was replaced by a thin walled (t = 0.250-in.), grouted, undamaged tubular member (specimen 07). A third set of four specimens (09-12) were conducted on 16.00-in. O.D., t = 0.375-in., to obtain data on larger members. The four specimens represent all possible combinations of the undamaged, dent-damaged, ungrouted, and grouted conditions.

2.2 Specimen Preparation

2.2.1 Denting Procedure. Seven of the twelve specimens tested were dented. These members were dented using a 100 ton jack and the load frame shown in Figure 2.3. A plywood cradle was used to support the tubular member during the indentation process to minimize any out-of-roundness (ovality) and reduce out-of-straightness. A loading head was designed and fabricated to dent the members to the profiles and cross sections shown in Figures 2.1 and 2.2. The head was fabricated by welding a 1/2-in. x 4-in. x 24-in. steel plate to the web of a WT5x15 section. A photograph of the head and a typical dent are shown in Figure 2.4.

The member was placed in the load frame so that the midspan of the tubular member was in line with the center of the head. After the tubular member was properly positioned, the loading head was pressed into the tubular member. When the stroke of the jack was believed to be close to

the specified dent depth, the jack was offloaded and a more accurate measurement was taken. Several of these cycles were necessary in order to achieve the proper dent depth.

During the denting procedure, some out-of-straightness was also introduced in the member. In order to correct this out-of-straightness, a fork lift was utilized to lift up the member at midspan while the two ends were chained to the ground using existing tie downs. This method worked well on the 12.75-in. members but proved ineffective on the 16.00-in. members. As shown in Table 2.1, some out-of-straightness was still present in some specimens after this procedure. However, only a fraction of the out-of-straightness was a result of the indentation process. The majority of the out-of-straightness was caused by the weight of the grout because the members were grouted in a near-horizontal position.

2.2.2 Grouting. All grouted members required some additional preparation prior to the grouting procedure. First, end caps (t = 3/4-in.) were welded to the ends of the tubular members to contain the grout. For specimens 02, 03, and 04, the end cap plates were cut so that they could be welded to the inside of the member's wall. However, these caps were not welded flush with the specimen ends which later caused problems during full-scale testing. For this situation all the load must be transmitted from the caps to the specimen wall through the weld. Segments of the welds failed during the tests which allowed the cap plate to deflect and the ends of the specimen to rotate. This problem was eliminated for specimens 05, 06, 07, 08, 09, and 11 by cutting the end plates so that they could be welded to the outside wall of the member. For this situation, the weld simply serves to hold the cap to the end and all the load is transmitted by bearing between the cap and the end.

Holes were cut in the side of the specimen near each end to serve as inflow and outflow ports for the grout. Two-in. diameter couplings, valves, and nipples were used for specimens 02-08. As will be discussed later, there were some problems during the grouting procedure directly related to using 2-in. fittings. Therefore, 3-in. diameter couplings, valves, and nipples were used for specimens 09 and 11. A typical inflow apparatus is shown in Figure 2.5. The components for the inflow apparatus are: 1) standard coupling (welded to the hole in the side of the specimen), 2) 6-in. long nipple, 3) standard gate or ball valves, and 4) 24-in. long nipple.

A standard gate valve was used for specimens 02-08. However, there were some problems encountered in closing the valves when the pumping of the grout ended. Therefore, ball valves were used for specimens 09 and 11. These valves performed much better than the gate valves. A 24-in. long nipple was used at the outflow end to increase the hydraulic head acting on the grout.

All members were placed at a 10 degree (approximate) angle before grouting as shown in Figure 2.6. The 10 degree angle was used because it is the most horizontal orientation and, thus, the most difficult grouting position that would be found in an in-service member. Prior to grouting, each member was filled with fresh water to simulate any water-grout intermixing that might occur in an in-service member.

The grout mix used for all specimens is described in Table 2.2 and is similar to an API oil well "B" grout. The grout was supplied by a ready-mix concrete supplier in Bryan, Texas, and was pumped by an Austin, Texas, company. The pump used was a Mayco HD30 with a pumping pressure of 350 psi. A water/cement ratio of 0.40 was recommended by the concrete supplier to obtain a nominal 4000 psi compressive strength in 28 days or less. A superplasticizer was added to the grout to facilitate the pumping at this low water-to-cement ratio.

The amount of grout pumped into a specimen was approximately one and one-half times the internal volume of the specimen. This was done to insure that the specimen was completely filled with a "clean" grout. A "clean" grout at the outflow end is a grout that has the same appearance and properties as the grout at the inflow end. The outflow of grout was closely monitored to determine the proper time to terminate the grouting process. Standard grout cylinders (3-in. diameter x 6-in.) were taken at each end (inflow and outflow) to determine the compressive strength of the grout.

Although a superplasticizer was used in the mix, there were some difficulties in pumping some members until "clean" grout appeared at the outflow end. The superplasticizer used in the grout mix is very sensitive to mixing. As long as the grout mix remained agitated, it could be easily pumped. However, there are times when the pumping would have to stop. Pumping would

obviously stop when a specimen was full and the hose had to be transferred to another specimen. This also occurred several times when a small piece of coarse aggregate (inadvertently included in the mix) would become lodged in the pump hose or gate valve. When the pumping action stopped for more than a few minutes, the grout in the hoses and pump would lose its plasticity and could no longer be pumped. Pumping could not be resumed until all the hoses, hopper, and piston housing of the pump could be cleared. During the time that the pump and hoses were being cleared, the grout already placed in the specimen would also lose its plasticity.

In one instance this resulted in incomplete grouting of a specimen. A piece of coarse aggregate became lodged in the gate valve of specimen 07 just prior to observing "clean" grout at the outflow end. By the time the hoses and pump were cleared, it was not possible to move the grout "plug" that had formed inside the specimen. Therefore, the last 36-in. at the outflow end of specimen 07 did not contain grout that exhibited properties consistent with the remainder of the specimen.

Based on the experience of the authors, it is recommended that at least 3-in. diameter couples, nipples, ball valves, and pumping hose be used for all similar grouting operations. Using larger diameter hoses and valves will prevent pieces of coarse aggregate unmixed lumps of fine aggregate, etc., from clogging the system. It is also recommended that the pump hopper and piston housing be pumped "dry" before pumping is stopped to change the hose from one specimen to another. Again, the grout can lose its plasticity while this operation is being conducted and will clog the piston and the lines.

2.2.3 Component Instrumentation and Preparation. Approximately seven days after grouting the specimens were transported to Texas A&M University's main campus to perform all remaining tasks. Each test specimen was instrumented with thirty 350 Ohm strain gages. A set of six gages were mounted at five locations along the tubular member as shown in Figure 2.7. A set of gages was placed at a distance of three member diameters from each end. Another set was placed 2-ft. from midspan, towards end B to avoid the dent on the damaged specimens. The other two sets were placed at half the distance between the set near the dent and the set near the ends. At each location, six strain gages were mounted equally about the circumference of

the tubular member (as shown in Figure 2.7.). For consistency, the same five locations were used along the length of the undented specimens.

The locations of all strain gages were carefully documented for data reduction. This was done prior to the full-scale testing by measuring the circumferential distance from a reference chalk line on top of the member and the distance from end B of the member. These locations were then transformed to the x, y, and z coordinate system shown in Figure 2.8 by the program SGL and later used by the data reduction programs CURVE, CHANGE, and ECC.

Individual members were then placed in the load frame (described in the next section). The member was held in place by three clip angles spaced at 120 degrees to restrain lateral movement. The clip angle at the bottom was modified with wings to prevent the member from rotating out of the frame until the other two clip angles were secured. A schematic of these angles is shown in Figure 2.9. The jacks were elongated to push the specimen ends flush against the fixed tailstock and the moveable headstock. Due to the weight of the member which caused some small initial rotation at the ends, it was virtually impossible to have the specimens completely flush against the tailstock and headstock. Shimming was needed to achieve full contact between the specimen and the fixed tailstock and moving headstock. No other restraint was provided at the ends of the members.

2.3 Full-Scale Testing

2.3.1 Load Frame. The load frame used for the full-scale compression testing has a design capacity of 1.8 million pounds. A drawing and photograph of the load frame are shown in Figures 2.10 and 2.11 respectively. The frame consists of three W24X104 members that are 58-ft. in length. These legs are held in place by a fixed headstock and fixed tailstock. There are three, 300-ton jacks with a four foot stroke that apply the load. The jacks apply the load through the centroid of a moving headstock which transfers the load to the tubular member. The end with the moving headstock is designated as end A while the fixed tailstock is designated as end B.

2.3.2 Data Acquisition. The data acquisition system used was developed by Equipment Development, Houston, Texas, and was specifically designed for Texas A&M University. The basic components of the system include: 1) power supply, 2) high speed multiplexer, 3) the FASTBOX, and 4) PC (640 KB RAM) and printer. The multiplexer contains the bridge completion card for each channel of data and samples each channel (up to 64) to be stored in the FASTBOX. The FASTBOX stores the data in internal memory (1 MEG) until it can be downloaded in hexadecimal form to a standard 5-1/4-in. floppy disk where it can be converted to an ASCII file. A hard copy of all data is also printed at each data step. A photograph of the data acquisition system is shown in Figure 2.12.

2.3.3 Instrumentation. The 30 strain gages on the specimen, as previously mentioned, measure the normal strains that occur during the full-scale compression testing. In addition, the legs of the load frame contain strain gages that are used to measure the applied load. The locations of the strain gages on the test frame are shown in Figure 2.13. To negate any bending strains, the gages on diagonally opposite flanges were averaged. For example, the strain readings from gages 40 and 42 were averaged to obtain the axial strain in leg #2. The sum of strain averages in all three legs is used to compute the total load in the test frame and specimen. Note, gages 41, 44, and 47 were recorded but not used in the data reduction.

Three, string linear potentiometers (pots) were mounted on the moveable headstock. The string lines from each pot run the full length of the load frame and are connected to the fixed tailstock. The data from these pots provide data used to compute the chord shortening of the member and any rotation of the moveable headstock. Chord shortening is the change in longitudinal distance between the ends of the tubular member. To monitor the rotation of the ends of the specimen relative to the load frame, two dial gages were mounted on the specimen at the moving headstock and fixed tailstock. The gages are located 180 degrees apart so that the average displacement of the specimen relative to the moving headstock and fixed tailstock can be measured. An illustration of the dial gage location is shown in Figure 2.14. Dial gage readings taken at each load step are used to compute end rotations and corrections for the chord shortening computations during data reduction.

At three locations along the specimen there are two string pots mounted on the load frame. Two of these locations are next to the set of strain gages closest to the ends while the remaining location is near the set of strain gages closest to the middle of the specimen. At each location, one pot measures the horizontal (x) displacement while the other measures the vertical (y) displacement.

2.3.4 Test Procedure. A load approximately 10% of the estimated capacity of the specimen was initially applied to seat the specimen in the load frame and to check all instrumentation. The stroke of the jacks was then increased at timed increments by a hand controlled, electric hydraulic pump. At each load all data was displayed on the video monitor of the computer so that the load, strain, and displacement readings could be monitored. At each load step, the displacement of the member was allowed to stabilize, as monitored by the end-rotation dial gages, before any data was recorded. At the initial load steps this would take only a matter of seconds. At load steps beyond peak load when the specimen experienced large lateral deflections, this would take more than one minute. Three sets of load, chord shortening, strain, and displacement data were taken by the FASTBOX data acquisition system at each load step. The dial gage readings for end rotation were manually taken once per load step. The number of load steps used for each specimen varied depending on the behavior of the specimen. However, a minimum of 20 load steps was taken for each specimen. The specimens were subjected to increasing longitudinal deformation until either the lateral deformations became excessive ($>$ 12-in.) or continuation of the test posed a safety hazard.

2.3.5 Data Reduction. The data obtained during the full-scale tests was reduced using a series of data reduction programs. The programs are: COMPRESS, SGL, DISPLAC, CURVE, CHANGE, and ECC. The computer codes for these programs are presented in Appendix B. The programs were written as part of a previous research effort, but are applicable to this research, (Moehlman, 1990). The analytical basis for these programs is presented in Appendices C and D.

The program COMPRESS converts data from a hexadecimal format to a more useable ASCII format that is used by most software packages. The program SGL converts the strain gage

locations recorded in the lab to the x, y, and z coordinate system used in all remaining data reduction algorithms.

The program DISPLAC takes the raw chord shortening data, load data, horizontal and vertical string pot data, and end rotation data and converts them to total axial load, corrected chord shortening, and true horizontal and vertical displacement data. As previously discussed, the load in each leg was computed by multiplying the axial strain in diagonally opposite flange elements of the leg by the modulus (29,500 ksi) and cross-sectional area of the W24x104. The true chord shortening was computed by first taking the average value of the three equidistantly spaced string pot values and then applying the appropriate dial gage correction at each end due to the rotation.

The data obtained from the horizontal and vertical string pots are not true horizontal and vertical displacements because of the large displacements the specimen experiences during a test. The vertical string pot measurements include some horizontal components of displacement while the horizontal measurements include some vertical components of displacement. The two equations shown below were solved simultaneously to obtain, δ_h and δ_v:

$$(X_o + \delta_h)^2 = (X_o + \Delta X)^2 \qquad 2.1)$$

$$(Y_o + \delta_v)^2 = (Y_o + \Delta Y)^2 \qquad 2.2)$$

where:

X_o = original length of string extending from horizontal string pot,
Y_o = original length of string extending from vertical string pot,
ΔX = measured horizontal displacement,
ΔY = measured vertical displacement,
δ_h = true horizontal displacement, and
δ_v = true vertical displacement.

The program CURVE determines the effective length of the specimen using the displacement data (six channels) and strain gage data (thirty channels). The program utilizes a least squares fit algorithm as detailed in Appendix C. In addition, the program computes the eccentricity of

the applied load based on the displacement of the member at the points of inflection (zero moment). The output data from CURVE are input data for the program CHANGE. CHANGE simply arranges the data into files that are conveniently used as plot files.

The program ECC computes the eccentricity of the applied load based on the end moments as determined from the curvature data from CURVE and specimen section properties. The details of this calculation can be found in Appendix D.

2.4 Material Tests

2.4.1 Grout Compression Tests. Grout compression tests were conducted prior to and on the day of the full-scale tests. Six cylinders (3-in. diameter) were tested to obtain a mean value to be used in the analytical evaluation. It should be noted that the cylinders were cured under the same conditions as the grouted members. In order to achieve good loading surfaces, the cylindrical specimens were capped with plaster of paris.

2.4.2 Tensile Coupon Tests. The equipment used in these tests is manufactured by Soil Test and specifically designed for concrete/grout cylinder and cube testing. The specific piece of equipment was a Model #CT-6500 with a capacity of 675,000 pounds.

After the full-scale compression test was completed on a specimen, two 3-in. x 12-in. coupons were removed from an unyielded portion near the end of the specimen. The coupons were cut along the longitudinal (z) axis of the specimen. From these, the tensile coupons were machined to a final configuration as shown in Figure 2.15. This configuration conforms to ASTM E8-88 (ASTM, 1988). The final thickness, T, was determined based on the minimum amount of material to machine the specimen flat. The cross-sectional dimensions were measured and recorded for later use during the reduction of the tensile test data.

All tensile tests were conducted and all data were reduced according to the procedures of SSRC Technical Memorandum No. 7 (SSRC, 1988). The tensile coupons were tested using a standard 20 kip MTS extensiometer load frame in stroke control at a rate of 0.2-in. per minute. An MTS extensiometer, Model No. 632.11B-20, Serial No. 450, with a 1.00-in. gage length was used

to measure the axial deformations. The extensiometer was used such that the maximum range was 0.20-in.

Load (stress) and displacement (strain) data were taken at 0.5 second intervals over the duration of the test. Beyond the yield load, displacement (strain) was held constant at three strain measurements roughly corresponding to $F_y/E + 0.005$, $F_y/E + 0.010$ and $F_y/E + 0.015$. At each of these strains, the load was allowed to stabilize for approximately five minutes or until there was no further apparent decrease in the load. After the test was stopped for the third time, it was not stopped again until the specimen ruptured. The maximum "stroke" of the extensiometer (0.20-in.) was exceeded in all tests. The extensiometer was removed when this occurred, and no further-displacement (strain) data were taken. However, the load was still recorded at 0.5 second intervals (to obtain ultimate strength) until rupture occurred. The 0.20-in. displacement (corresponding to a strain of 0.20) is well beyond the range required to obtain the data needed from this test.

All data from these tests were recorded on standard 5 1/4-in. floppy disks and later input into a commonly used spreadsheet program. The load/displacement data were converted and plotted as stress/strain data. The static yield strength, dynamic yield strength, and ultimate strength were determined for each specimen, as described in the next chapter.

Figure 2.1. TYPICAL DENT CROSS–SECTION AT MAXIMUM DEPTH

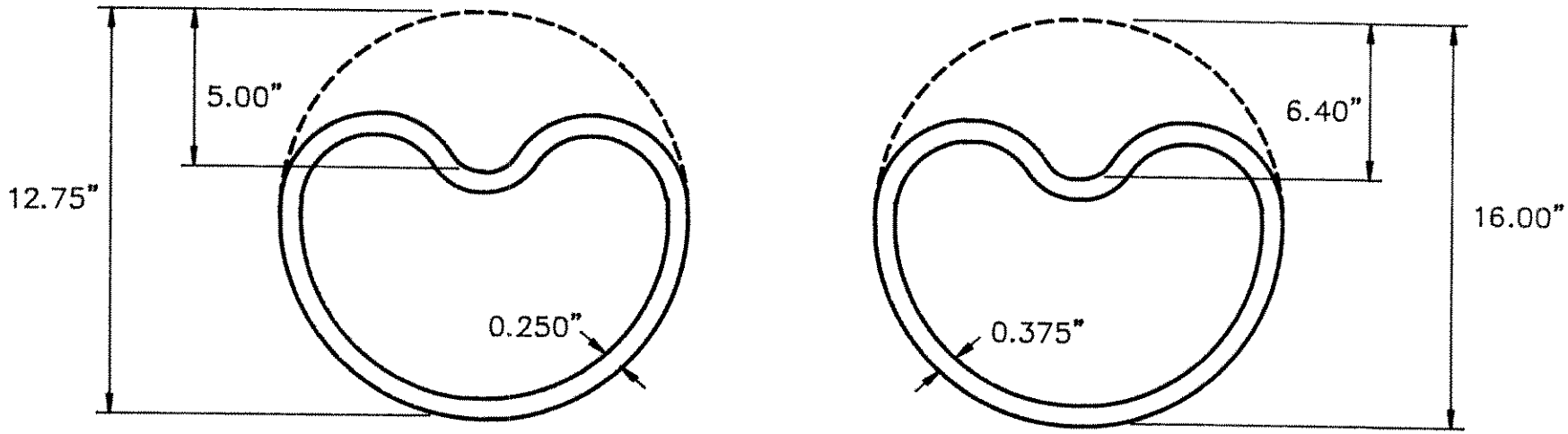

SPECIMENS 01–08

SPECIMENS 09–12

Figure 2.2. TYPICAL LONGITUDINAL DENT PROFILE AT MAXIMUM DENT DEPTH

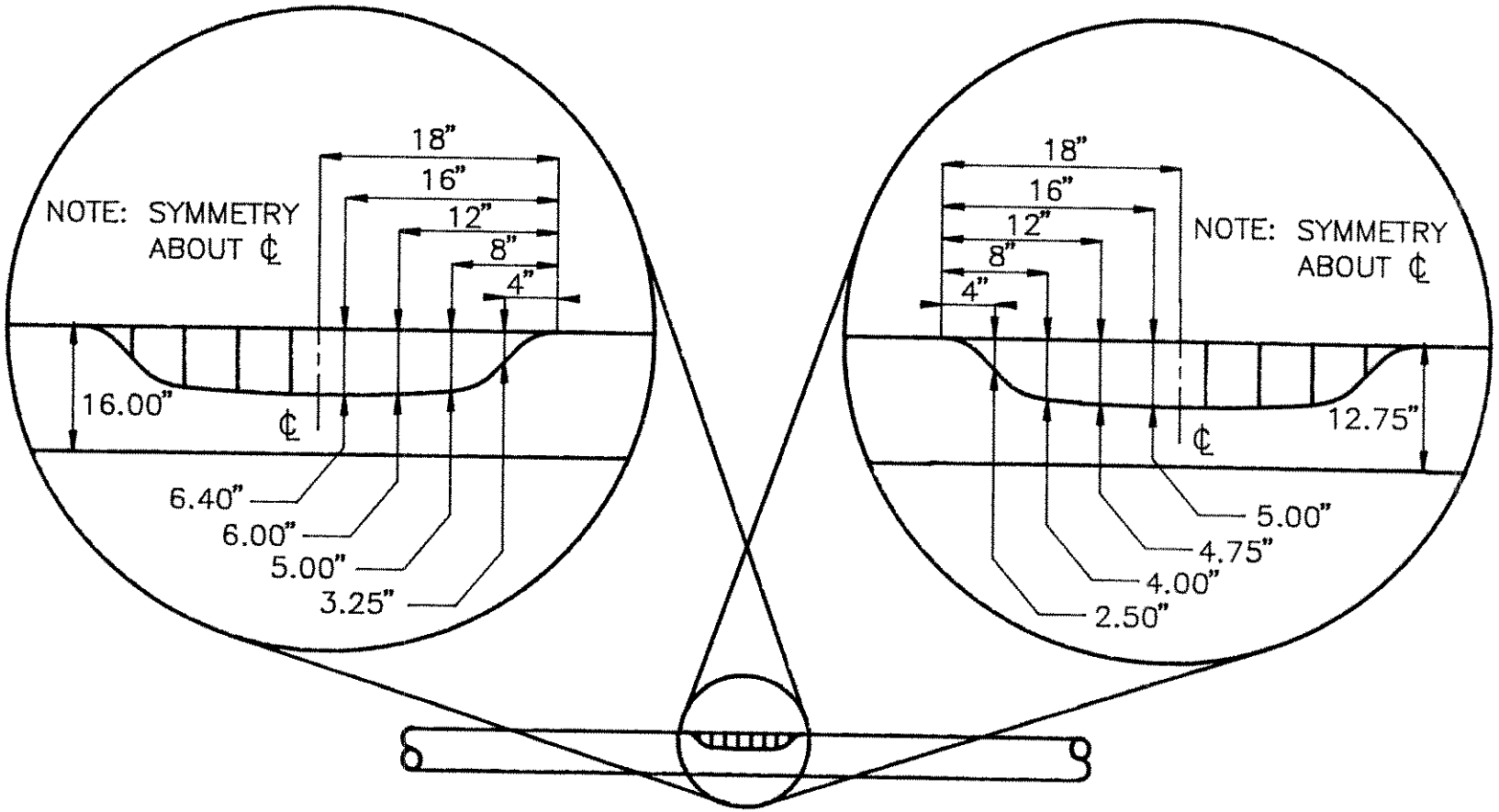

Figure 2.3. Indentor Frame and Cradle

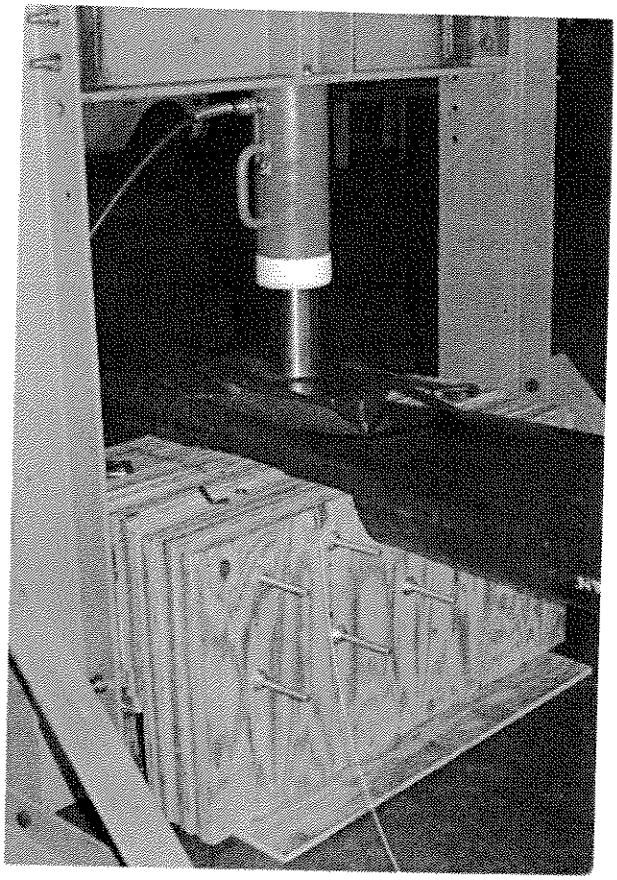

Figure 2.4. Indentor Head and Typical Dent for 12.75 in. Specimens

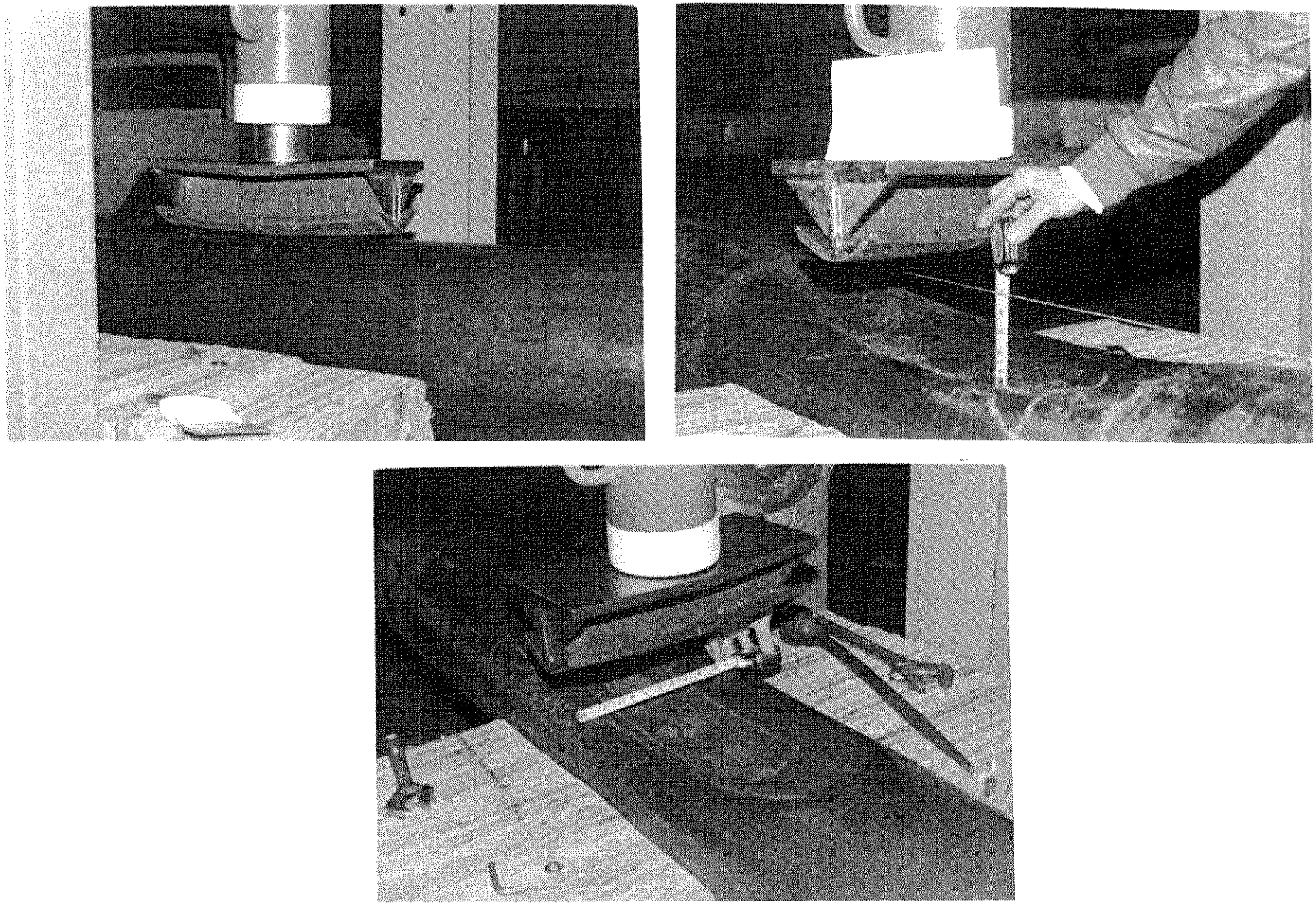

Figure 2.5. Inflow Apparatus for Grouting

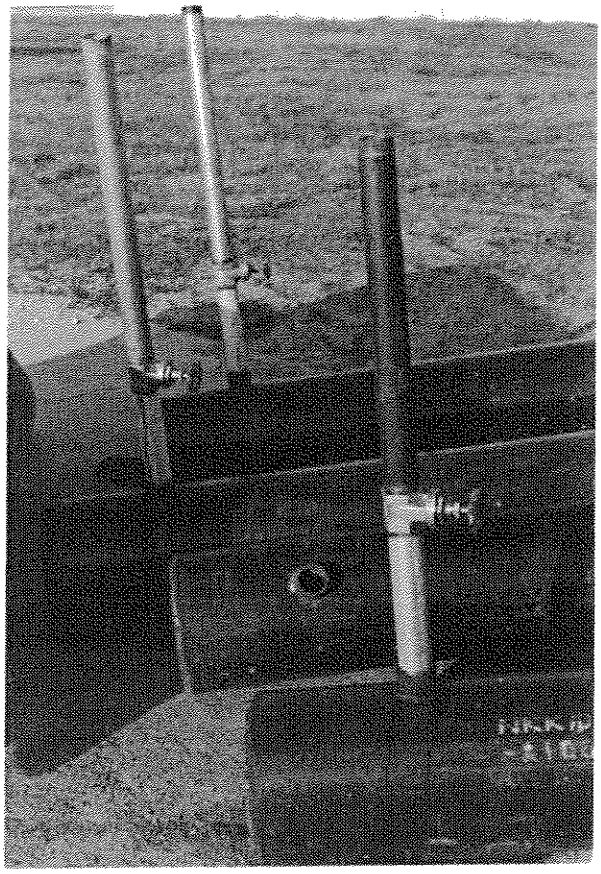

Figure 2.6. Orientation of Members for Grouting

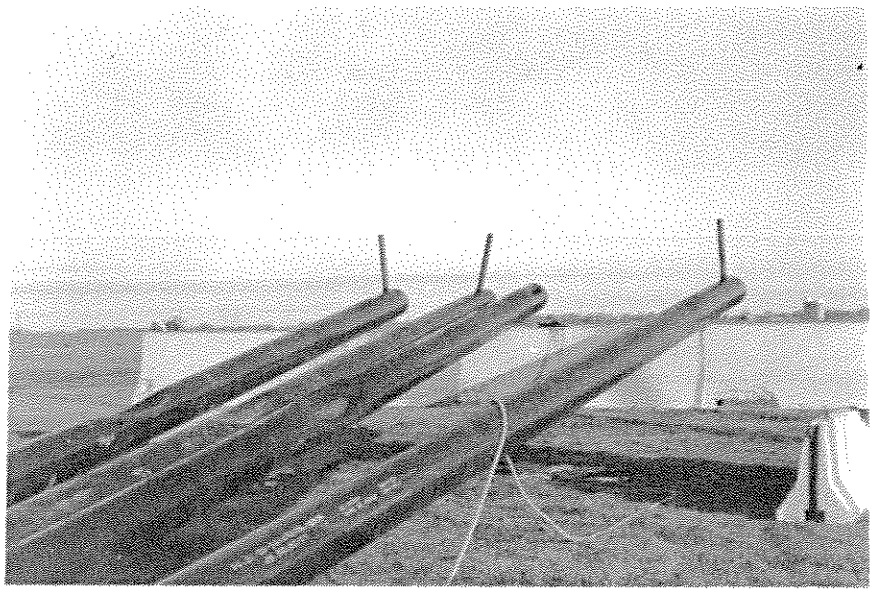

Figure 2.7. STRAIN GAGE LOCATIONS

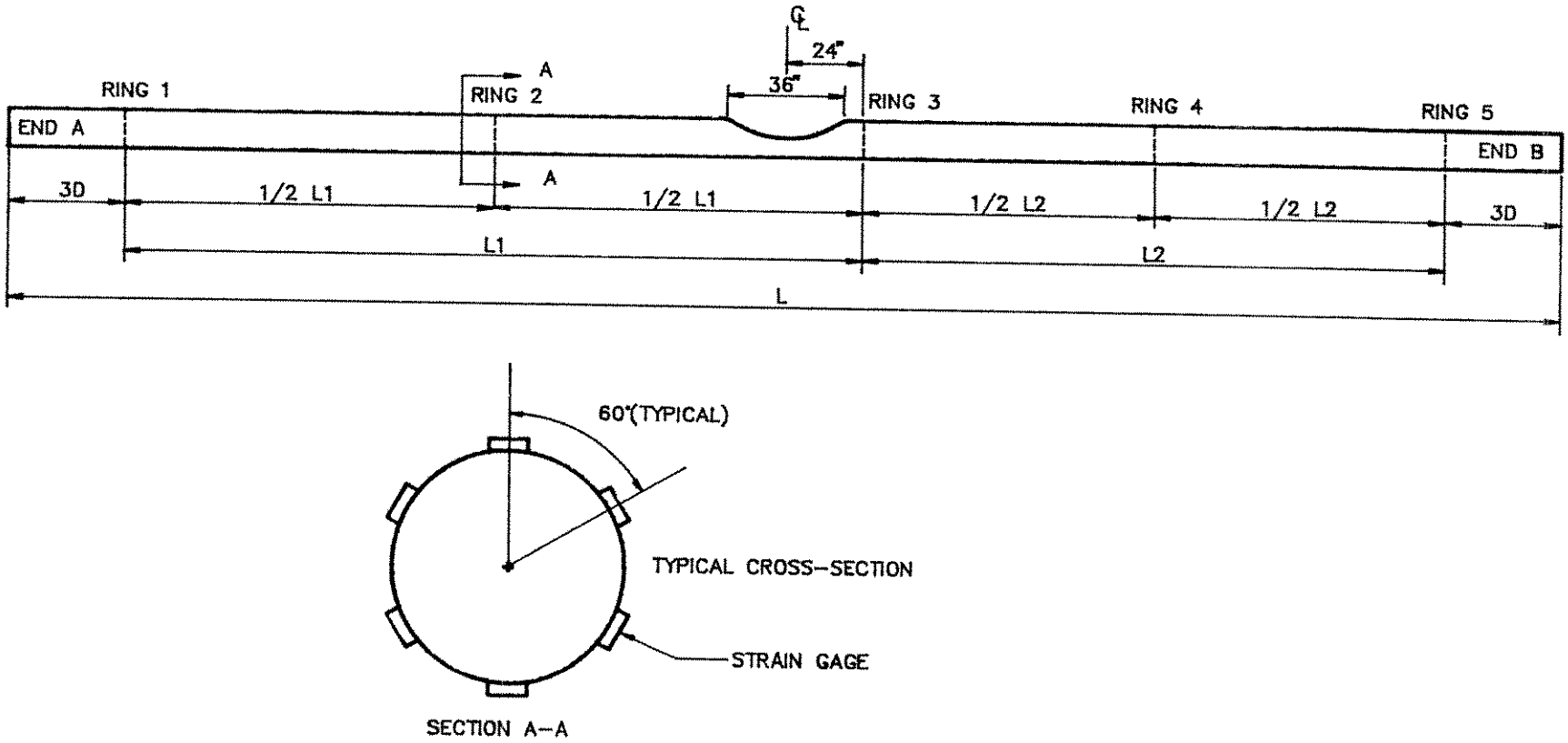

Figure 2.8. COORDINATE SYSTEM FOR DATA REDUCTION PROGRAMS

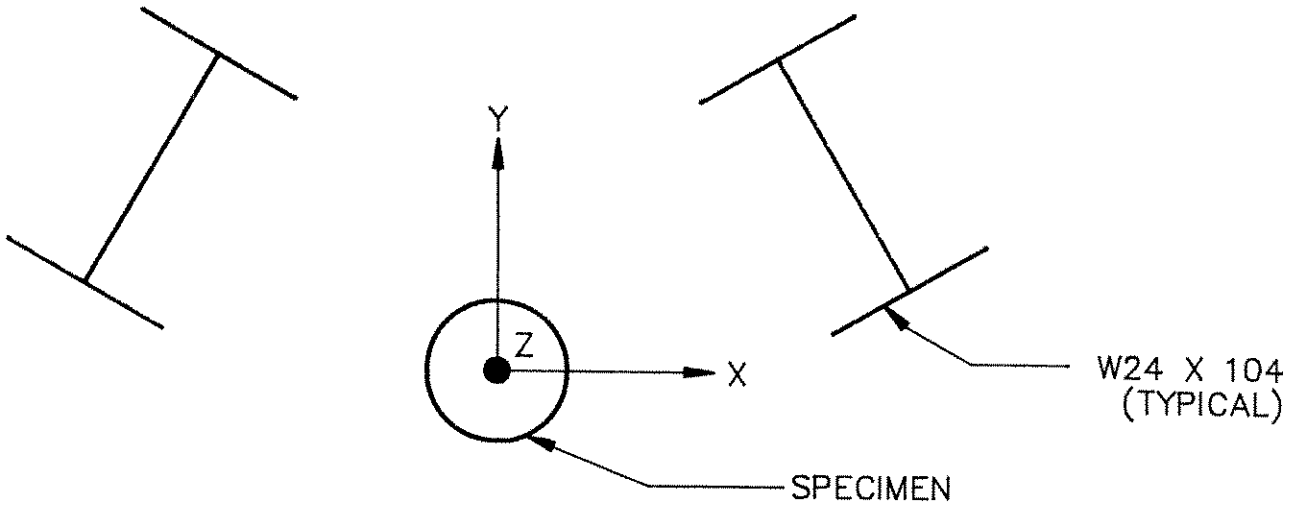

NOTE: Z=0 AT END A

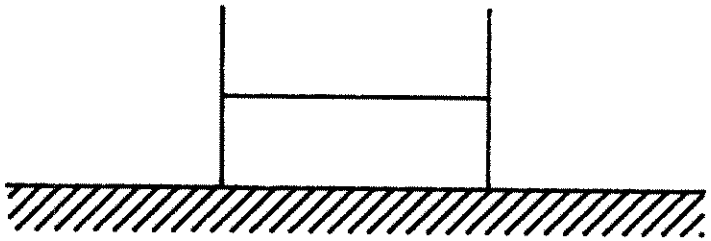

LOOKING TOWARDS END B

Figure 2.9. END RESTRAINT CLIP ANGLES

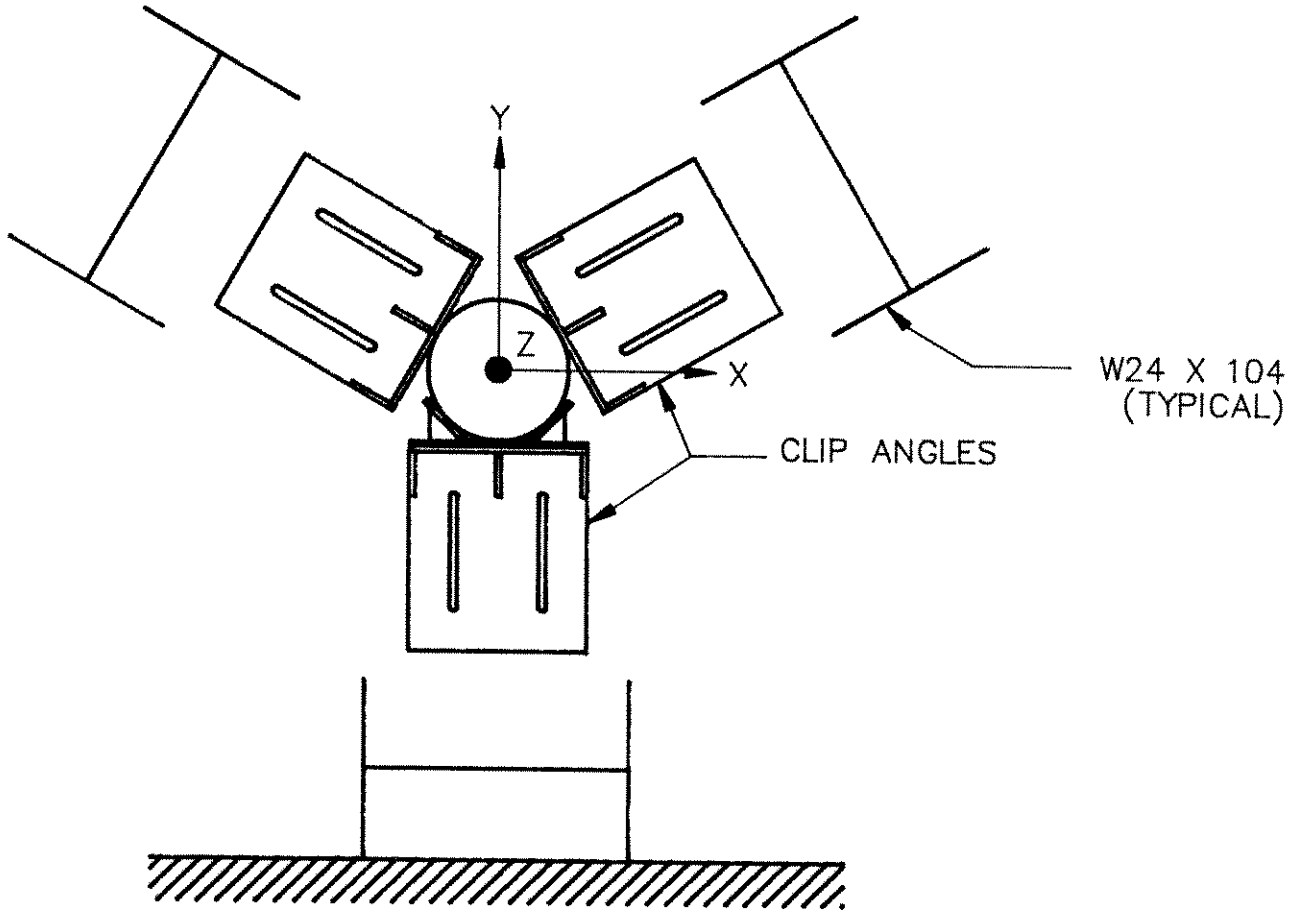

LOOKING TOWARDS END B

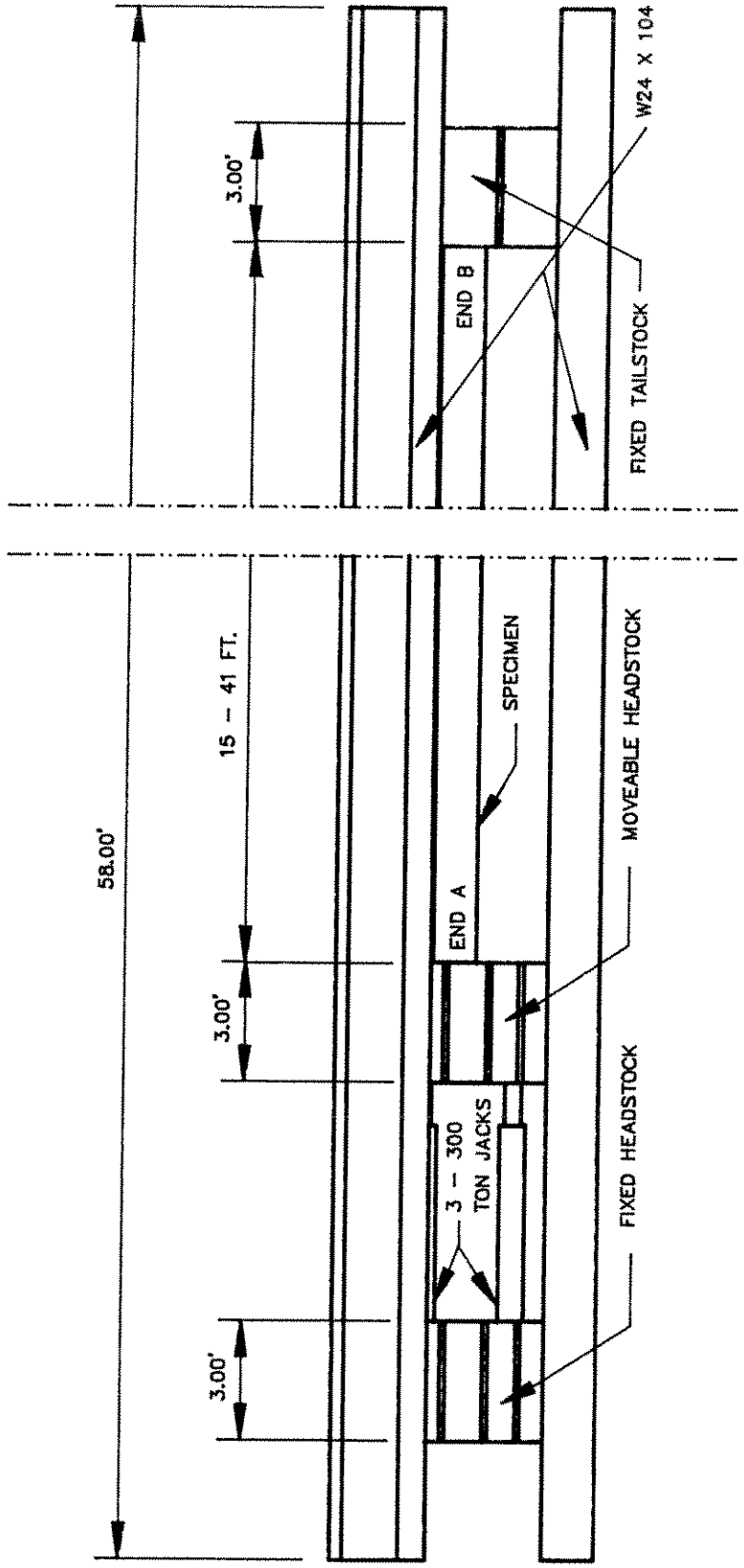

Figure 2.10. SCHEMATIC OF 1800 KIP LOAD FRAME

Figure 2.11. 1800 kip Load Frame

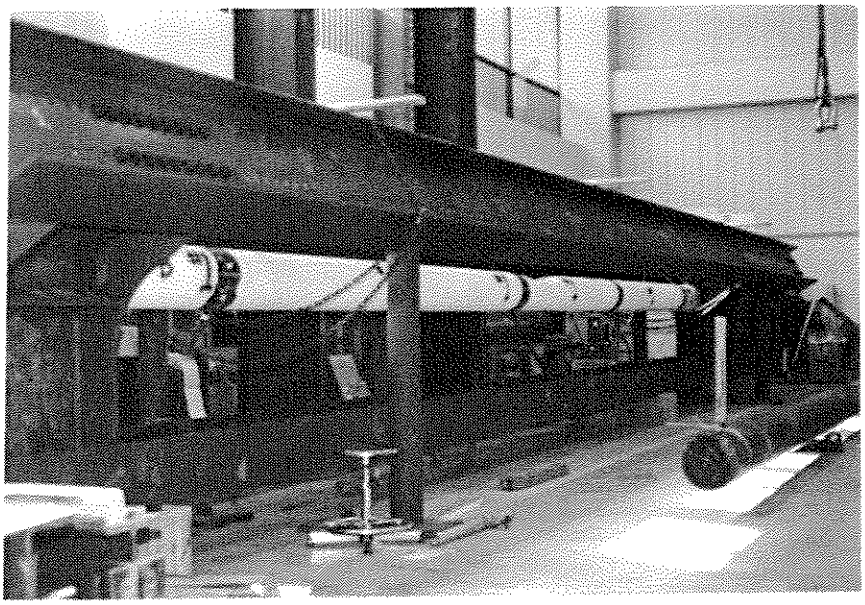

a) Fixed tailstock looking towards end A

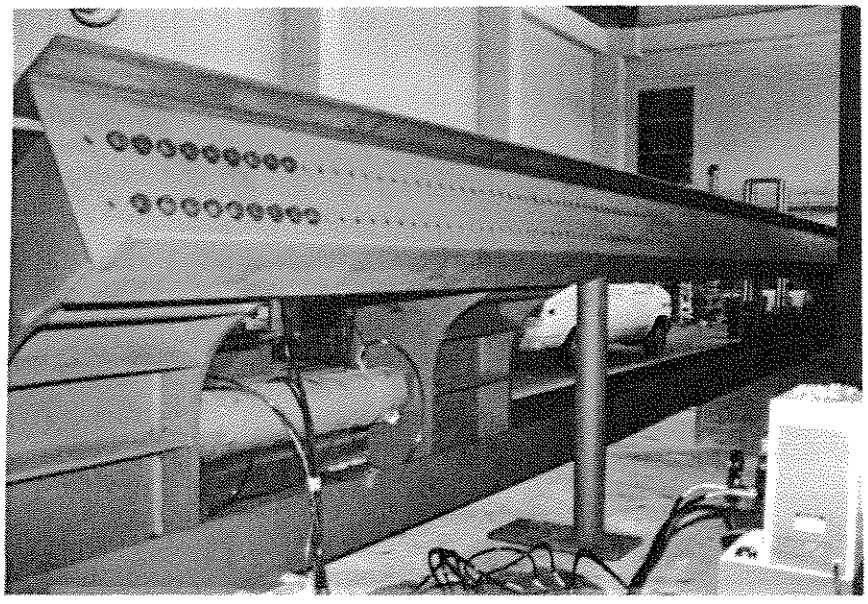

b) Moveable and fixed headstocks looking towards end B

Figure 2.12. FASTBOX Data Acquisition System

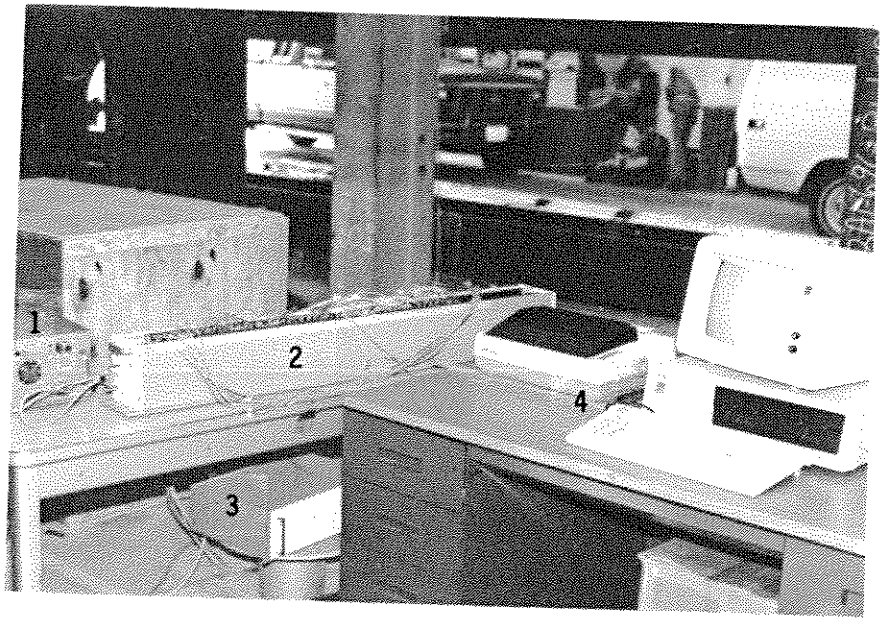

1) FASTBOX
2) Front end box (multiplexer)
3) Power supply
4) PC and printer

Figure 2.13. STRAIN GAGE LOCATIONS ON TEST FRAME

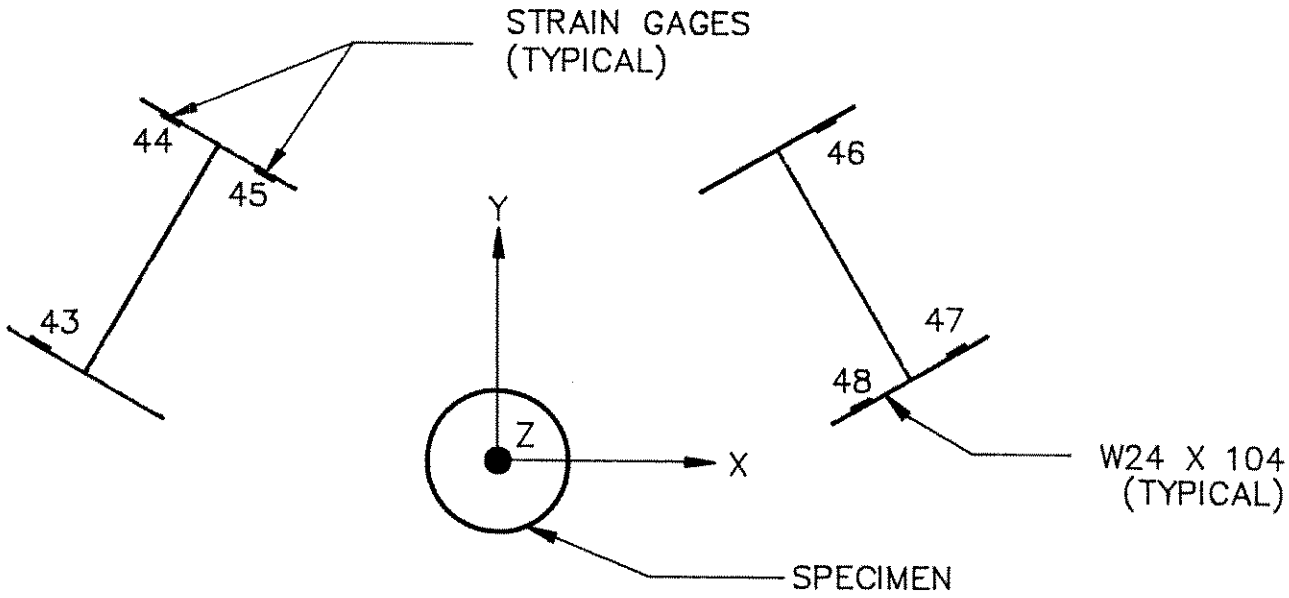

NOTE: Z=29'

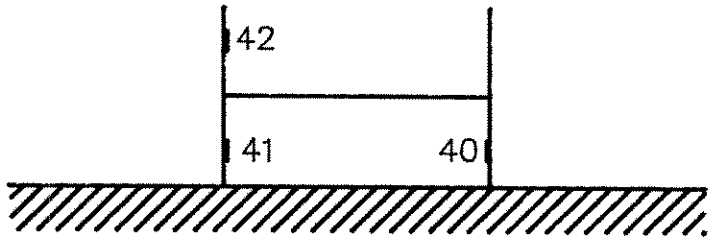

LOOKING TOWARDS END B

Figure 2.14. LOCATION OF DIAL GAGES

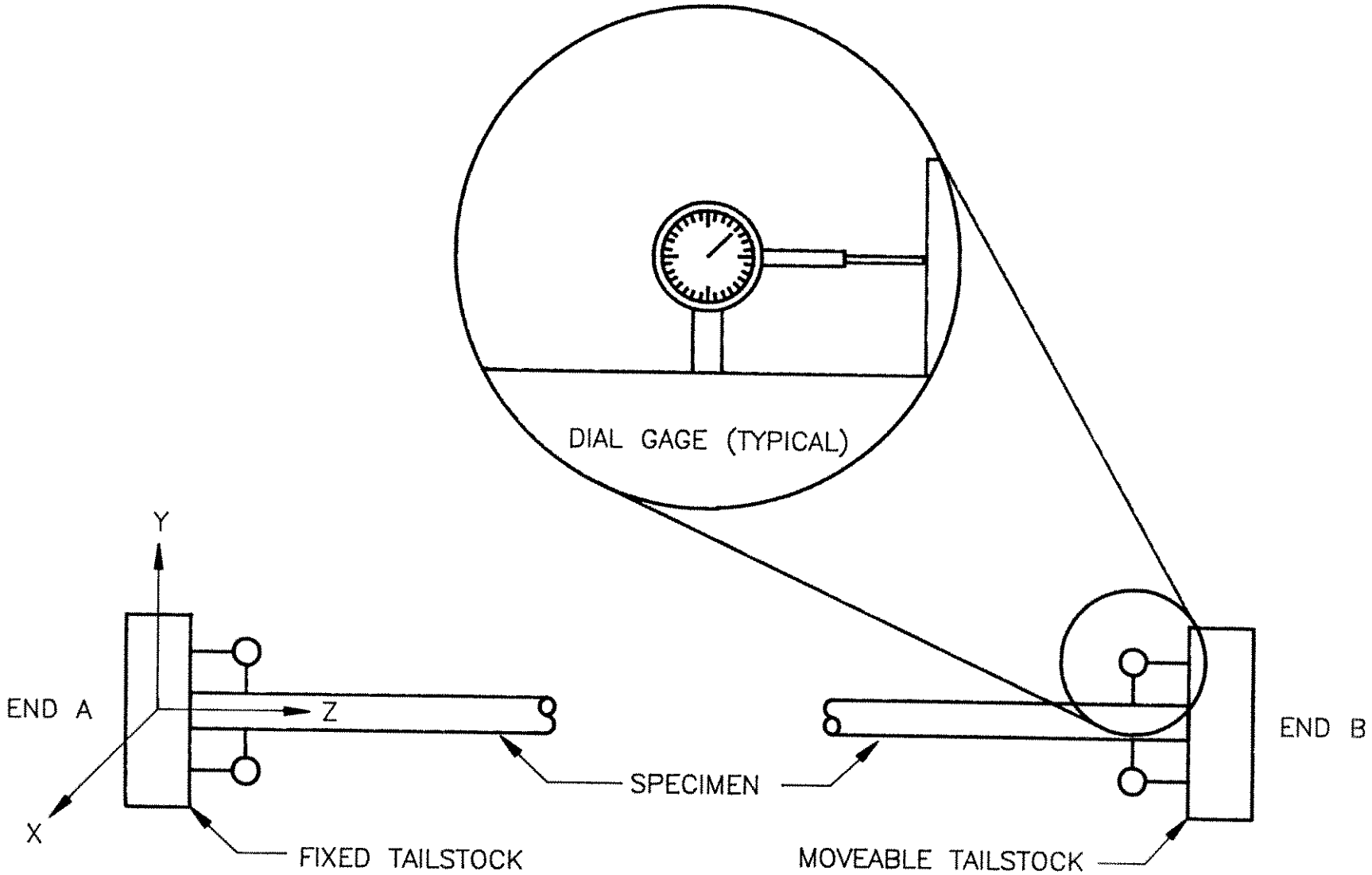

Figure 2.15. TENSILE COUPON SPECIMEN

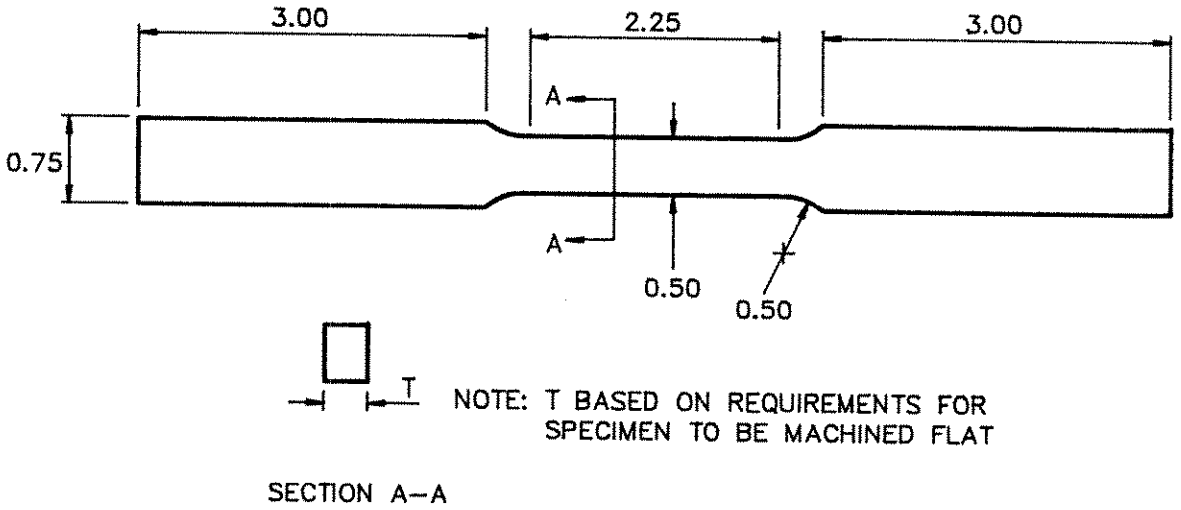

Table 2.1. Test Matrix for Full-Scale Compression Tests

Specimen No.	Length (ft.)	Outside Diameter (in.)	Wall Thickness (in.)	d/D	Grout	δ/L [5]	D/t	(kL/r)
01	40.19	12.75	0.375	0.39	No	0.0000	34.0	55.07
02	40.19	12.75	0.375	0.00	Yes	0.0000	34.0	85.91
03	40.15	12.75	0.375	0.39	Yes	0.0027	34.0	59.48
04	40.15	12.75	0.250	0.39	Yes	0.0042	51.0	60.00
05	40.27	12.75	0.375	0.00	Yes	0.0000	34.0	68.40
06	40.25	12.75	0.375	0.39	Yes	N.A. [4]	34.0	55.14
07	40.21	12.75	0.250	0.00	Yes	0.0000	51.0	64.48
08	40.19	12.75	0.250	0.39	Yes	0.0043	51.0	55.56
09	40.06	16.00	0.375	0.00	Yes	0.0000	42.7	57.42
10	39.96	16.00	0.375	0.40	No	0.0036	42.7	43.39
11	39.96	16.00	0.375	0.40	Yes	0.0095	42.7	57.27
12	40.00	16.00	0.375	0.00	No	0.0000	42.7	52.12

Notes: 1) Dent Length = 36 in. for all dented members
Dent Width = 10.2 in. for all dented members
2) All specimens API 5L grade B steel
3) Specimens 02, 03, 04: $f_c' = 4140$ psi
Specimen 05: $f_c' = 4020$ psi
Specimens 06, 07, 08: $f_c' = 4210$ psi
Specimens 09, 11: $f_c' = 5070$ psi
4) The out-of-straightness for specimen 06 was not measured.
5) The out-of-straightness was determined after grouting and with the specimen horizontally positioned.
6) Specimen diameter and wall thickness are specified nominal values (i.e., not measured).

Table 2.2. Grout Mix

CONTENTS	MIX
CEMENT	846 POUNDS
SAND	2600 POUNDS
WATER	300 POUNDS
SUPERPLASTICIZER	6.75 POUNDS

Notes:
1) Quantities are per cubic yard.
2) Superplasticizer used is Rheobuild 1000 made by Masterbuilder.
3) Water to cement ratio is 0.40.

3.0 TEST RESULTS

The data collected from the full-scale compression tests described in the previous chapter were analyzed and presented in graphical form. A complete set of graphs for all specimens is presented in Appendix A. A summary of these results and a detailed description of the results from a typical test will be presented in this chapter.

3.1 Typical Test Results

Specimen 04 is considered a "typical" specimen and will be used to present "typical" results. Specimen 04 was 40.15-ft. in length with a 12.75-in. outside diameter and a 0.25-in. wall thickness. The specimen had a 5.0 x 10.2 x 36-in. dent at midspan and was fully grouted with a grout having a compressive strength of 4140 psi. The static and dynamic yield strength of the steel were 51.8 ksi and 55.1 ksi respectively, while the ultimate strength was 75.0 ksi. The peak load measured during the full-scale compression test was 411 kips.

3.1.1 Full-Scale Tests. The full-scale compression tests provided data used to determine the pre-ultimate and post-ultimate behavior of all specimens. From these tests, load, effective length, chord shortening, horizontal and vertical displacements, load eccentricities, and end rotation were either measured directly or computed from data taken during the test.

The results obtained from the full-scale compression tests were summarized in ten graphs for each specimen. These graphs are:

(1) Load and Normalized Midspan Deflection vs. Load Step
(2) Effective Length vs. Load Step
(3) Load vs. Chord Shortening
(4) Horizontal Displacements
(5) Vertical Displacements
(6) x - Eccentricities based on Inflection Points
(7) y - Eccentricities based on Inflection Points
(8) x - Eccentricities based on End Moments
(9) y - Eccentricities based on End Moments
(10) End Rotation and Load vs. Load Step

The effective length graph shows the results from the least-squares error analysis of the full-scale strain and displacement data. The derivation and the discussion of this formulation can be found in Appendix C. The effective length, "kL," is a critical parameter used to calculate the buckling capacity of members loaded in axial compression. It is dependent on the end conditions and the behavior of the specimen during the full-scale test. More discussion on the effective length will be presented in Section 3.1.2.

Shown in Figure 3.1 are the load and normalized deflection versus load step. The normalized deflection is the resultant (from vertical and horizontal components) midspan deflection divided by the initial length of the specimen. Using Figure 3.1, a horizontal line is drawn from the normalized resultant deflection of 0.007 to determine the load step at which buckling occurred. The value of 0.007 is an accepted value that has been used in previous research to define the condition of "buckling" (Moehlman, 1990). Based on this, "buckling" occurred at load step 72. Shown in Figure 3.2 is the graph of effective length-versus-load step. The load step (72), as determined from Figure 3.1, is used in this figure to determine the effective length factor, K, at the point of buckling. The K value was determined to be 0.54 for this specimen (04).

Figure 3.3 is the load versus chord shortening relationship for specimen 04. This plot is used to distinguish between the pre-buckling and the post-buckling behavior of the specimen. The portion of the graph before maximum axial load is the pre-buckling region and is generally linear. The portion of the graph after the maximum axial load is the post-buckling region where the chord shortening increases while the load decreases. The behavior shown in Figure 3.3 is typical of axially loaded specimens in the pre- and post-buckled region.

At the initial loads shown in Figure 3.3, there appears to be a region of negative chord shortening. This implies that the specimen increased in length as the compressive load increased. Obviously, this cannot occur. This contradiction in behavior could have been caused by the ends of the specimen not being flush against the fixed tailstock or the moving headstock during the initial load steps of the test. In computing the "corrected" chord shortening, the dial gage correction factor at each end, which is calculated from the dial gage data, is subtracted from the chord shortening data taken from the headstock string pots. If the specimen is not flush

with the fixed tailstock and moving headstock, the dial gage correction is larger than the string pot displacements. This would then result in negative chord shortening (or chord lengthening) values.

The horizontal (x) displacements at three locations along the member are plotted in Figure 3.4 for specimen 04. Locations 1, 2, and 3 refer to the locations 4.00-ft., 22.25-ft., and 36.40-ft. from end A, respectively. The displacements shown are small (<0.5-in.) prior to peak load. Beyond peak load the specimen begins to deflect with the maximum horizontal deflection of -1.60-in. occurring at location 2 (near midspan) at the final load step. As expected, the horizontal deflections are relatively small when compared to the vertical (y) deflections shown in Figure 3.5.

In Figure 3.5, the vertical (y) deflections are plotted versus the load for specimen 04. The locations are the same as those for the horizontal deflections. The maximum vertical deflection was -13.75-in. and occurred near the midspan (location 2) at the last load step. This behavior was expected considering the location and orientation of the dent. Also as expected, the deflections near midspan (location 2) were relatively large compared to those at the locations nearer the ends (1 and 3).

All specimens were to be centrically loaded. However, eccentricities are invariably introduced by the end reactions (headstock and tailstock). These eccentricities were calculated based on two different methods. Both methods utilize the data from the curve fit algorithm described in Appendix C. One method is based on lateral displacement at the points of inflection, and the other is based on the moments at the end of the member. The two methods are used so that a comparison can be made between the computed values.

Method 1 is based on inflection point data. Since an inflection point is a location of zero moment, the resultant load must pass through the centroid of the cross-section at that point. Thus, the eccentricity of the resultant load is equal to the lateral deflection (x and y) of the member at the location of the inflection points. The locations of the two inflection points were

determined in the program CURVE. The x and y deflections were computed at these locations and used as the eccentricity of the applied load.

Method 2 is based on end moment data. A summary of this formulation can be found in Appendix D. The end moments were computed at each data step by multiplying the x and y curvature at each end from the CURVE algorithm by the modulus of elasticity and the moment of inertia of the specimen. These end moments were then divided by the measured load to compute the eccentricity of the load. This calculation was performed by the program ECC.

The eccentricities of the applied load as computed from the inflection points are plotted in Figures 3.6 and 3.7 for specimen 04. Figure 3.6 contains the eccentricities in the x direction, while Figure 3.7 contains the eccentricities in the y direction. These graphs indicate that the y eccentricity increased very slightly prior to peak load and then increased rapidly beyond peak load. This was due to the rotation of the ends away from the headstock and tailstock as the specimen deflected downward (negative y). Thus, the line of action of the resultant load was located below the centroid (negative y) of the cross-section. As expected, the x eccentricities were very small prior to peak load and less than 1-in. beyond peak load.

The eccentricities of the applied load as computed from the calculated end moments are presented in Figures 3.8 and 3.9 for specimen 04. Figure 3.8 contains the eccentricities in the x direction, and Figure 3.9 contains the eccentricities in the y direction. As shown in these figures, the y eccentricities are much greater than the x eccentricities due to the fact that the displacement in the y direction is much greater than that in the x direction. This is consistent with the behavior and eccentricities as determined by the inflection points. In Figure 3.9, the y eccentricity (computed from end moments) is greater than 6.375-in. near the end of the test. This would indicate that the load is applied outside the radius of the specimen. In addition, the eccentricity at the initial load step is approximately 1.00-in. Both of these observations can be attributed to the initial deflection, end rotation, and end moment created by the dead load of the member.

Figure 3.10 presents the end rotation and load versus the load step for specimen 04. This figure indicates that the end rotations of end A and end B are similar in magnitude but with different signs. The difference in sign is consistent with the coordinate system. The end rotations at end A are negative while the end rotations at end B are positive as the specimen deflects downward (negative y) and the top of the specimen rotates away from the headstock and tailstock. There is very little end rotation prior to peak load. At peak load the rotation is 0.81 degrees at end A and 0.41 degrees at end B. Beyond peak load when deflections are increasing, the end rotations, as expected, also increase. The rotations observed at peak load seem to be consistent with the "k" value (0.54) computed for specimen 04.

3.1.2 Discussion of End Conditions and Effective Length. The effective length factor, k, is a critical parameter in any analytical method used to determine the ultimate capacity of a compression member. This parameter is dependent on the restraint at the ends of the member. For a member braced against end translation, the theoretical values of k range from 0.5 to 1.0. If both ends of the member are fully unrestrained against rotation, the k value is 1.0. However, if both ends are fully restrained against rotation, the k value is 0.5.

In any experimental program it is necessary to determine k so that comparisons can be made with analytical models. Historically, researchers have used load frames with "ideal," "pinned," or "fixed" end conditions and assumed k values of either 1.0 or 0.5. However, it is a well-known fact that even under laboratory conditions, it is impossible to produce such idealized end conditions. Therefore, it is necessary to determine the effective length (kL) of the compressive test specimen for the "as-built" end conditions.

To prevent lateral displacement of ends A and B, clip angles were spaced at 120 degrees around the circumference of the member as shown in Figure 2.9. The ends of the member were butted tight against the face of the headstock and tailstock. Shims were also used to keep the tubular member flush against the headstock and tailstock. The member ends were not attached in any other manner to the load frame.

3.1.2.1 Experimental Determination of Effective Length. As previously discussed, the effective length factor, k, was determined by the use of the algorithm in the program, CURVE. The limits used for k in this program were set at 0.32 and 2.00 so that the theoretical limits of 0.50 and 1.0 were not imposed on the member. A summary of the values obtained for k at peak load are presented in Table 3.1. These values are determined at the load step where the normalized midspan deflection is 0.007 (see Figures 3.1 and 3.2). The values for k varied from 0.5 to 0.78, however all but specimen 02 had a k value less than 0.66.

For specimen 02, a grouted, undented tubular member, the calculated effective length was significantly larger than the other specimens. For specimens 01-04, the end cap was welded to the inside wall of the member with approximately 1/4-in. of the cap protruding from the end of the specimen. This resulted in the load being applied through the end caps, through the weld, to the wall rather than being directly applied to the wall through bearing of the end cap. In specimen 02, the weld connecting the end cap to the specimen wall failed prior to peak load. This failure occurred on the bottom portion of the specimen, which concentrated the loading at the upper portion of the end of the member. The increased loading resulted in some local yielding in the wall known as "elephant footing," near the end of the specimen. This resulted in increased rotations at end B, thus creating an end condition indicative of a pinned end condition. The weld at end A did not fail, thus producing a near fixed condition at that end. Thus, the k value of 0.78 seems consistent with the behavior of fixed-pinned ends.

With the exception of specimen 02, the other specimens had effective length factors between 0.5 and 0.66 indicating nearly ideal fixed end conditions. The ends of these specimens rotated less than 1 degree prior to ultimate capacity as monitored by the dial gage readings and chord shortening data. The k values are directly related to the end rotations exhibited by the specimen. These end rotations prior to peak load are consistent with the k values obtained for all specimens.

3.1.2.2. Analytical Determination of Effective Length. To verify the effective length factors presented in Table 3.1 that were computed from the experimental data by the program CURVE, a closed form analytical solution was developed to compute k for a compression member with

non-ideal end conditions. This section contains a brief discussion of the formulation and a summary of computed k values from the method. The reader is referred to the work by Marek (1993) for a more complete presentation of this method.

The clip angles at ends A and B of the load frame shown in Figure 2.9 prevent any lateral displacement. The ends of the member were butted and shimmed tight against the headstock and tailstock but were not attached in any other manner to the load frame. Thus, the load frame ends can be idealized as nontranslating ends with elastic restraints as shown below:

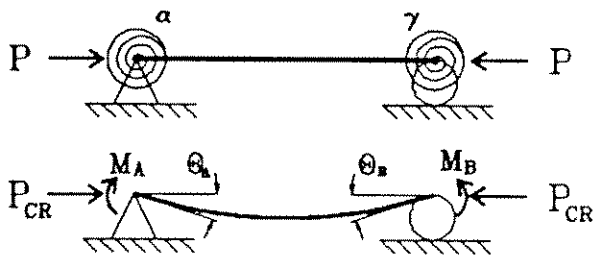

The rotational stiffness at each end can then be defined by end moments and rotations as:

$$\alpha = \frac{-M_A}{\theta_A} = \frac{Pe_A}{\theta_A} \qquad \gamma = \frac{-M_B}{\theta_B} = \frac{Pe_B}{\theta_B} \qquad (3.1)$$

where:

α,γ = rotational stiffness at ends A and B, respectively (k-in./rad),
M_A,M_B = moment at ends A and B, respectively (k-in.),
P = axial compressive load (kips),
$e_A = e_B$ = eccentricity of load at ends A and B, respectively (in.), and
θ_A,θ_B = rotation at ends A and B, respectively (rad).

Timoshenko and Gere (1961) have developed a solution for a symmetrical member (i.e., equal rotational stiffness at the ends, $\alpha = \gamma$). The transcendental equation for this problem is:

$$\tan(u) + 2\epsilon = 0 \qquad (3.2)$$

where: $u = \frac{\beta L}{2}$ (rad),

$\beta = \sqrt{\frac{P_{cr}}{EI}}$ (in.$^{-1}$),

$L =$ member length (in.),

$\epsilon = \left[\frac{(EI/L)}{\alpha}\right]$ (dimensionless),

$\frac{EI}{L} =$ flexural stiffness of compression member (k-in.),

$\alpha =$ rotational stiffness of <u>both</u> ends (k-in.), and

$\alpha = \frac{M}{\theta}$.

The value for u that satisfies Eqn. 3.2 is the critical value, u_{CRIT}, and defines buckling in the compression member. Now, the critical (buckling) load for a member can be defined by:

$$P_{CR} = \frac{P_E}{k^2} \qquad 3.3)$$

where: $P_E = \frac{\pi^2 EI}{L^2}$ = Euler buckling load (kips)

Substituting Eqn. 3.3, β, and ϵ into Eqn. 3.2, the effective length factor k can be found:

$$k = \frac{\pi}{2u_{CRIT}} \qquad 3.4)$$

where: u_{CRIT} is the solution to Eqn. 3.2.

The procedure to compute k based on this method is:

1) Compute ϵ based on EI/L of the compression number and $\alpha = Pe/\theta$ for the load frame.

2) Solve Eqn. 3.2 for u_{CRIT}.

3) Solve Eqn. 3.4 for k.

The difficulty in implementing this procedure occurs in Step 1. To compute ϵ, EI of the compression member must be computed. In the case of a dent-damaged/grouted member, four possibilities exist. EI can be based on the dented or undented cross section assuming either composite or noncomposite behavior for the steel tube and grout core. In addition, ϵ and θ must be determined at the critical load, P_{cr}. The question arises as to whether the values of ϵ and θ should be measured at the peak load, P_{max}, or at the load in which the normalized midspan deflection is 0.007, $P_{0.007}$. To complicate the procedure further, the load frame used in this research did not have equal rotational stiffness at ends A and B (i.e., $\alpha \neq \gamma$).

The following assumptions were made to compute ϵ, and hence the theoretical effective length factor, K_{THEO}:

1) An average end rotational stiffness was computed using the load, rotation, and eccentricities at the load in which the normalized resultant deflection at midspan was 0.007:

$$\gamma_{AVE} = P_{0.007}\left[\frac{\frac{e_A + e_B}{2}}{\frac{\theta_A + \theta_B}{2}}\right] = P_{0.007}\left[\frac{e_{AVE}}{\theta_{AVE}}\right]$$

2) Composite behavior was assumed for all grouted members. Dented section properties were used for all damaged members and undented section properties were used for all undamaged members. The modulus of elasticity used for each material:

E_{STEEL} = 29,000 ksi, and

E_{GROUT} = $57\sqrt{f_c'}$ (ksi),

where: f_c' = compressive strength of the grout (psi).

The values used to compute k_{THEO} are summarized in Table 3.2. Table 3.3 contains a summary of k_{THEO}, k_{EXP}, and the percent error between the two values. In all specimens the theoretical effective length factor exceeds the experimentally measured effective length factor

($k_{THEO} > k_{EXP}$). On the average, k_{THEO} exceeded k_{EXP} by 22%. There are several reasons which might explain why this occurred. First, using an average end stiffness, γ_{AVE}, may underpredict the effective true end stiffnesses of ends A and B (γ_A and γ_B). Secondly, numerous assumptions had to be made for the values used for P, ϕ, e, and I when computing ϵ. Changing these assumptions can significantly change ϵ and the resulting k_{THEO}. Finally, the dead weight of the member was not considered in the theoretical formulation. The weight of the member would result in a reduced effective flexural stiffness of the specimen which would result in lower k_{THEO} values.

3.1.3 Tensile Coupon Tests. Tensile tests were conducted to determine the static and dynamic yield stress of each specimen. The final value for each specimen was obtained by averaging the values from two coupon tests. The modulus of elasticity was not determined since the extensiometer used did not have the sensitivity required to make this calculation. An accepted value of the modulus of elasticity for steel (29,500 or 29,000 ksi) was used in all data reduction calculations.

Figure 3.11 shows the entire stress-strain curve for specimen 04-2 (specimen 04, tensile coupon 2) while Figure 3.12 shows the initial portion of the curve used to determine the static and dynamic yield stresses. The dynamic yield stress is determined by using the standard 0.2% offset method. The static yield strength was determined according to the procedure presented in the SSRC Technical Memorandum No.7 (SSRC, 1988). As previously mentioned, these tests were performed using standard MTS equipment in a stroke control mode. The tests were stopped three times at designated strains beyond the yield strain. The strain was held constant while the load relaxed during these pauses. The testing was first stopped at approximately the 0.2% offset strain. The last two stopping periods occurred at strain levels of approximately 0.007 and 0.012 (prior to strain hardening). These periods were approximately three minutes in length or until the load stabilized. After the third stopping period, the test was resumed and continued until the tensile coupon ruptured. As shown in Figure 3.12, the static yield stress was determined by drawing a line through the minimum stress values in the stress-strain curve beyond the point of yield. Where this line intersects, the 0.2% offset line defines the static yield

stress. The static yield stress and dynamic yield stress were 52.7 and 55.5 ksi respectively for this tensile coupon.

Rockwell "B" hardness values were taken on the tensile coupons for specimens 01-08. These results will be discussed later in this chapter.

3.2 Summary of Test Results

Table 3.4 contains a brief summary of the data obtained from the full-scale compression tests. These data include the peak load, the chord shortening, the horizontal and vertical displacements, and the effective length. More data are presented in Chapter 4 and Appendix A.

Table 3.5 contains a summary of all material properties obtained from tensile and Rockwell hardness testing. Note that the values presented in this table are based on the results of two tensile coupon tests. All specimens with a 0.375-in. wall thickness (specimen nos. 01, 02, 03, 05, 06, 09, 10, 11, and 12) had static yield strengths consistent with API 5L grade B steel (36.1 to 48.6 ksi). However, the thin-walled (t=0.250-in.) specimens (nos. 04, 07, and 08) had significantly higher static yield strengths (51.8 to 74.2 ksi) than expected. To verify the tensile coupon results, Rockwell "B" hardness data were taken on the coupons for specimens 01-08. Figure 3.13 is a plot of the static yield strength versus the Rockwell hardness value for each specimen. As shown in this figure, the Rockwell hardness values are consistent with the yield strength values. Using a linear, least squares regression analysis, the equation of the "best fit" line is:

$$F_y = 2.12 \times RH - 129 \qquad 3.5)$$

where:

F_y = static yield strength (ksi)

and RH = Rockwell B hardness value (no units).

3.3 Discussion of Specimen Behavior - Full-Scale Tests

3.3.1 Common Behavior. All twelve specimens failed in a global buckling mode. Specimen 02 was the only member that exhibited any local buckling. This occurred at the end where the end cap weld failed. A photograph of typical global buckling is shown in Figure 3.14. The

undamaged members generally buckled along the entire length of the specimen. Also, the dented members failed after a hinge had formed in the dent at a load step beyond which peak load occurred.

All specimens generally exhibited the same behavior prior to peak load. This is shown in the normalized deflection and end rotation graphs for each specimen (Appendix A). Prior to peak load the normalized deflection was less than 0.01 and the end rotation was less than 1 degree for all specimens except specimen no. 02. Again, specimen 02 exhibited unique behavior due to failure of the welded end caps that is described in the next section.

All specimens exhibited large vertical deflections and relatively small horizontal deflections beyond peak load. This was caused by the self weight of the member/grout for all members and the orientation of the dent for damaged members. In addition, specimens 03, 04, 05, 06, 08, and 09 exhibited classical "snap-through" buckling behavior at peak load. That is, the specimen exhibited large midspan deflections at a load step just beyond the peak load step. This behavior is shown in the normalized deflection plots for these specimens in Appendix A.

3.3.2 Unique Behavior. Specimen 02 exhibited unique behavior in that the deflections and end rotations at ends A and B that were considerably larger than that of the other specimens at peak load. The weld seam at end B failed in the lower portion of the tube, which resulted in additional rotation at the end and an overall increase in the vertical deflection. Figure 3.15 shows the failed weld seam in specimen 02. After the end cap weld failed, the load was transmitted from the tailstock to the wall of the specimen by direct bearing and was not uniformly distributed over the end of the specimen. Thus, the lower portion of the end (negative y) of the specimen carried significantly more load than other regions, which resulted in some local yielding at end B. This phenomenon is termed "elephant footing" because of the bulged shape of the specimen end after this yielding occurs. Beyond peak load, a region approximately 10-in. in length (measured circumferentially) and within 4-in. of the end of the specimen "bulged" approximately 1-in. laterally beyond peak load. The "elephant footing" may have had some effect on the post-ultimate behavior of the specimen but had no effect on the pre-ultimate behavior or ultimate capacity.

Specimen 07, an undented/grouted member, exhibited unique behavior during full-scale testing prior to peak load. At 450 kips, there was a bond failure between the grout and the steel. This resulted in an extremely loud "pop" and an immediate 110 kip loss in load. In the load steps immediately after this event, the specimen began to carry additional load. The specimen obtained a second peak load of 543 kips before failing in a "snap-through" global buckling mode. Figure 3.16 is a graph of the load versus normalized midspan behavior. From this graph it can be seen that the 110 kip loss in load was not due to global buckling because the normalized midspan deflection was extremely small (<0.001). However, it is unlikely that this bond failure affected the ultimate capacity of the member. More importantly is the fact that the member did not have "clean" grout over the entire length of the member.

As previously discussed, there were several problems encountered during the grouting of specimen 07. The specimen did not receive a good "clean" grout over the entire length as a result of these problems. A destructive examination of the specimen after full-scale testing showed that the last 3-ft. of the specimen at end B contained either no grout or an inferior "chalk-like" grout with little or no compressive strength. Figure 3.17 is a photograph of specimens 05, 07, and 08 at end B. This figure clearly shows the grouting problem for specimen 07 when compared to the other two specimens.

This void had two major effects on the pre- and post-ultimate load behavior. First, it is believed that the void was the origin of the bond failure between the grout and the steel prior to peak load. In the region where there is a transition from grout and steel to steel only, the stresses in the grout would be considerably higher than the normal stress due to an abrupt change in axial stiffness in this region. The void also provided space to accommodate the displaced grout core after the bond failure. Again, destructive examination of the specimen indicated that there was some relative longitudinal displacement between the steel and the grout. This relative displacement was more likely to occur because there was no dent damage. The presence of a dent would have had a restraining effect on the relative longitudinal displacement between the grout and the steel.

Secondly, the void resulted in higher stresses in the steel at end B. In addition, there was not enough grout to support the walls of the specimen in this region. This resulted in significant "elephant-footing" at end B beyond peak load near the end of the test. The primary objective of testing specimen 07 was to determine the increase in strength that can be obtained by grouting an undamaged specimen. The behavior of specimen 07 is significant because it emphasizes the importance of grouting the full length of an undamaged member. Although there was some increase in strength (discussed in next chapter), this increase was not as large as expected due to the bond failure and local buckling effects caused by the void at end B.

3.3.3 Post-Test Examination of Grouted Members. The grouted specimens (02, 03, 04, 05, 06, 07, 08, 09, and 11) were destructively examined after the full-scale tests were completed. One, and in most cases, both end caps were removed so that the condition of the grout could be determined. Portions of the tube wall were removed along the length of specimens 07 and 08 so that the grout could be further examined.

Shown in Table 3.6 is a summary of the data taken during these destructive examinations. The % A_{grout} is the percentage of the total possible area of the end that was filled with quality grout. Quality grout is defined as grout that, by visual examination, has the proper mixture of cement and fines. In addition, the grout could not be easily removed when scraped by a knife. A void is defined as any area not filled with quality grout.

As can be seen from the data in Table 3.6, there were significant void areas in several of the specimens. In general, end A did not have air voids but had a significant area in which the cement had been washed from the fines. In these areas the "grout" could be easily removed by scraping. End B generally had a significant air void due to water bleed and the resulting shrinkage of the grout.

It should be noted that specimen 07 had very poor quality grout at both ends. However, examination of the grout along the length of the member revealed a much better quality than at the ends. This examination also revealed a significant gap ($> 1/16$ in.) between the walls of the

tube and surface of the grout core due to shrinkage. Examination of specimen 08 also revealed a gap between the grout and the walls of the tube.

The ends of specimens 09 and 11 were completely filled with quality grout (% A_{grout} = 100). These 16 in. O.D. specimens were filled using 3-in. diameter nipples rather than the 2-in. nipples used for the other specimens. It is believed that the high quality of grout obtained in these specimens was due to the fact that each specimen was pumped full of grout without interruption. In all other specimens, pumping of the grout was interrupted, then resumed, until the member was filled with grout. These members generally contained air voids at end B and areas of poor quality grout at end A.

Figure 3.1. LOAD AND DEFLECTION VS. LOAD STEP
SPECIMEN 04

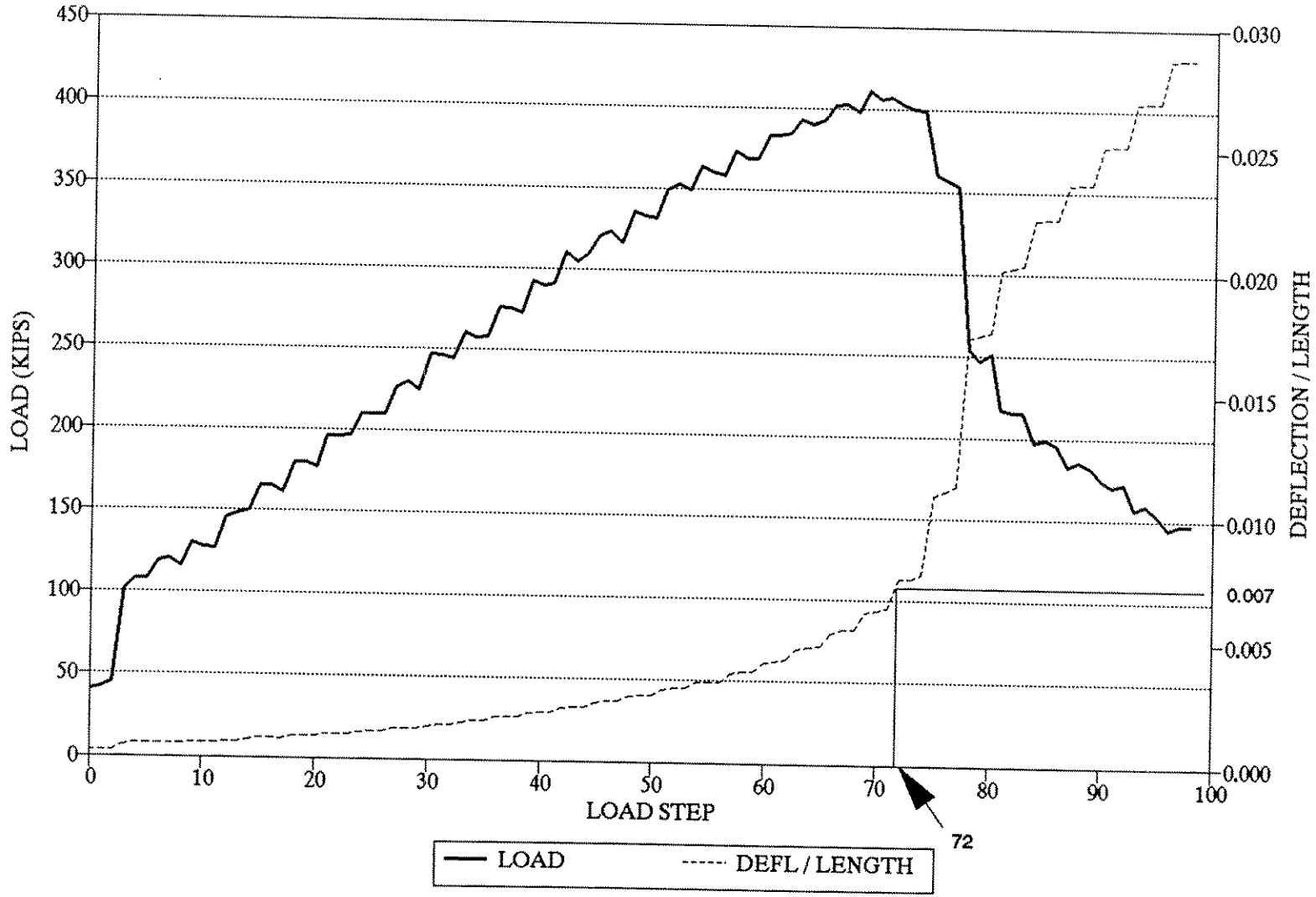

Figure 3.2. EFFECTIVE LENGTH VS. LOAD STEP
SPECIMEN 04

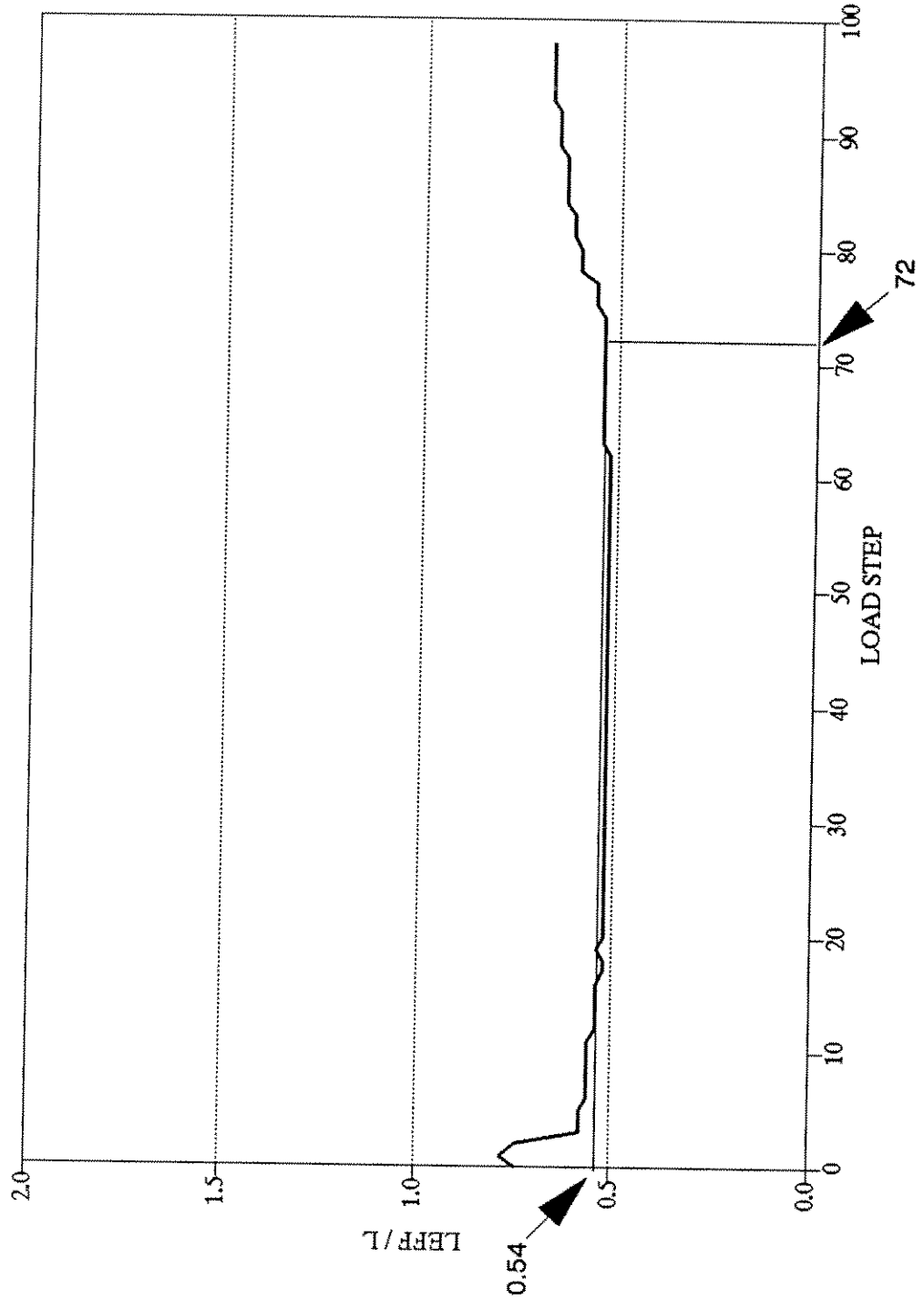

Figure 3.3. LOAD VS. CHORD SHORTENING
SPECIMEN 04

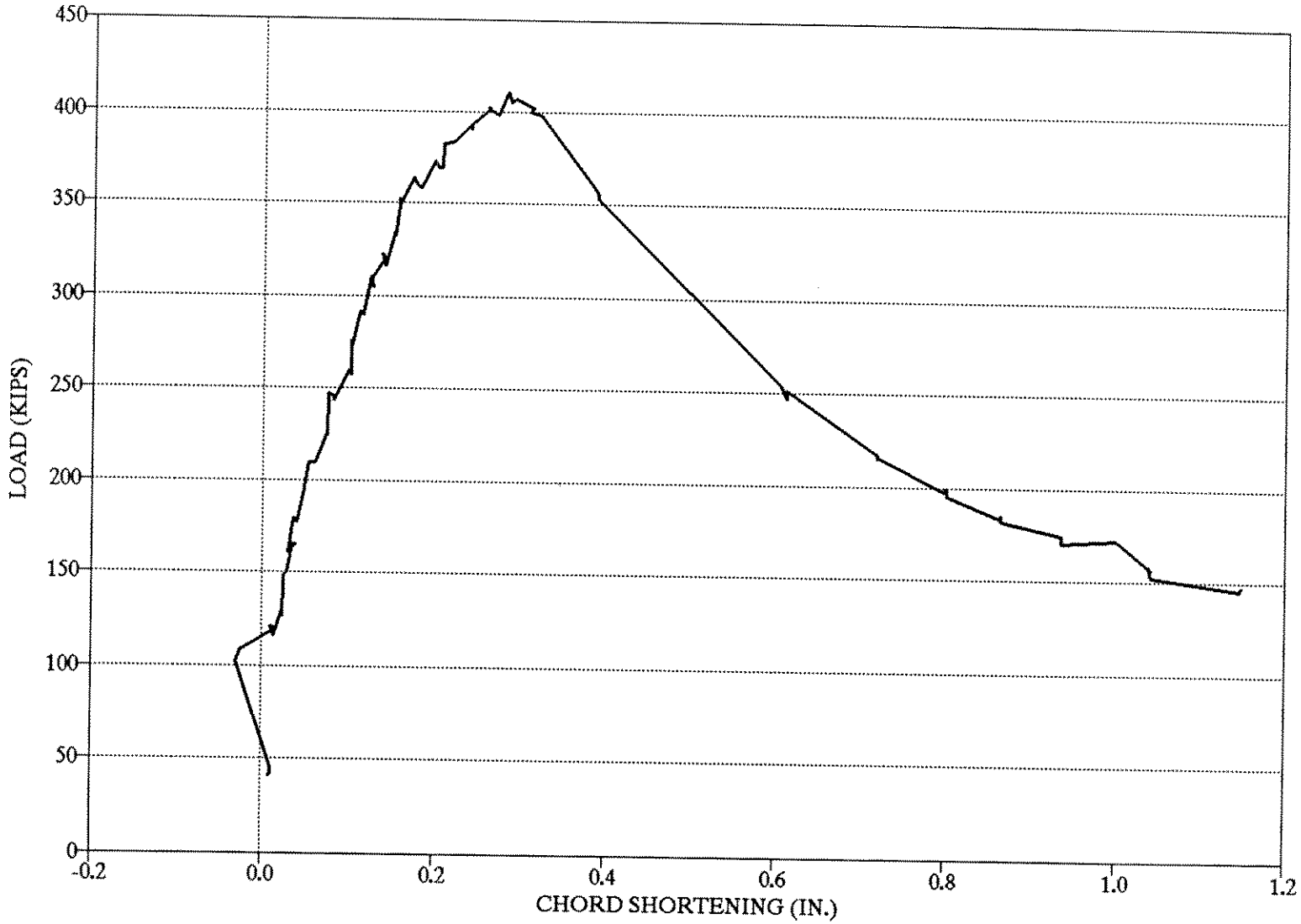

Figure 3.4. HORIZONTAL DISPLACEMENTS
SPECIMEN 04

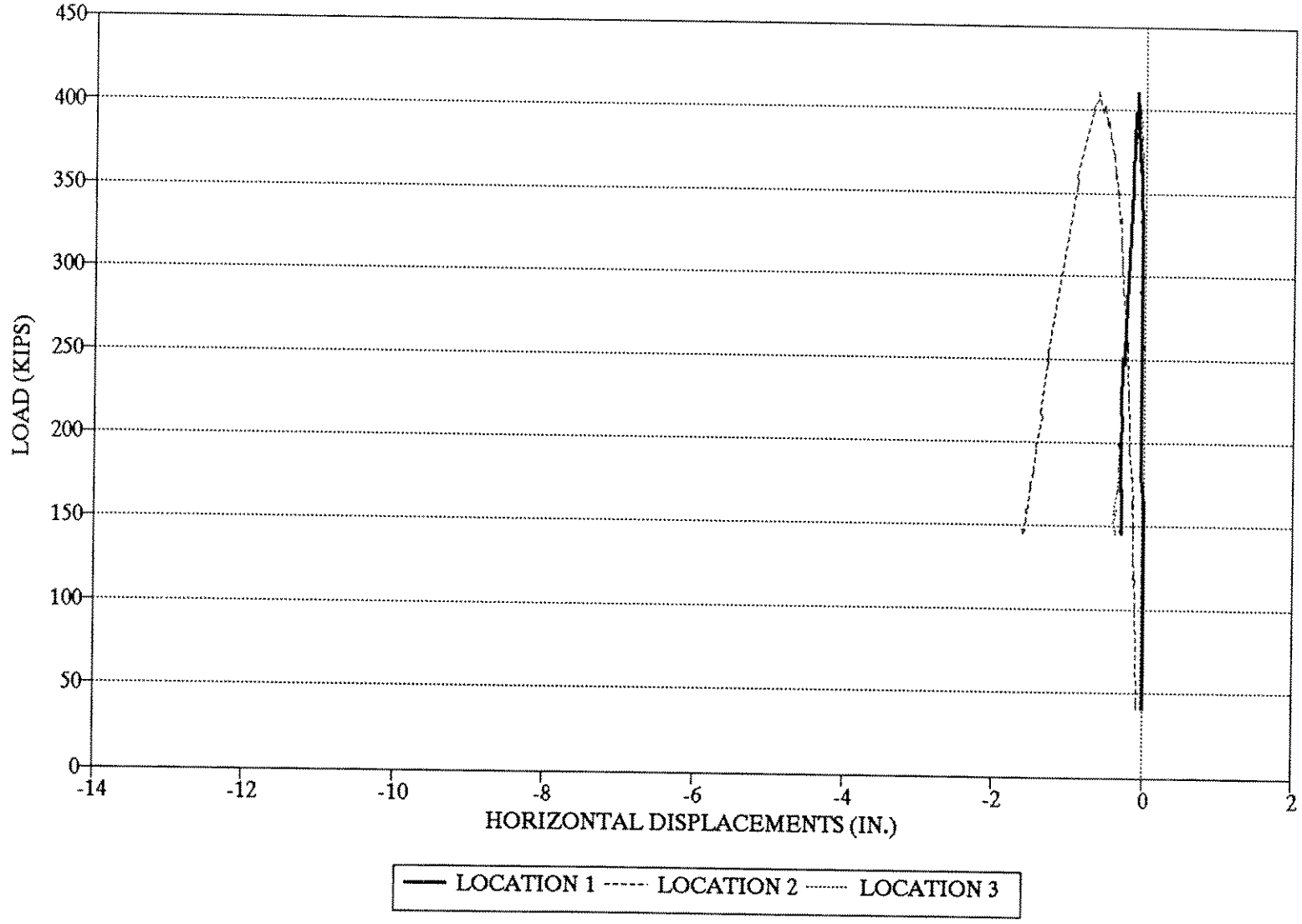

Figure 3.5. VERTICAL DISPLACEMENTS
SPECIMEN 04

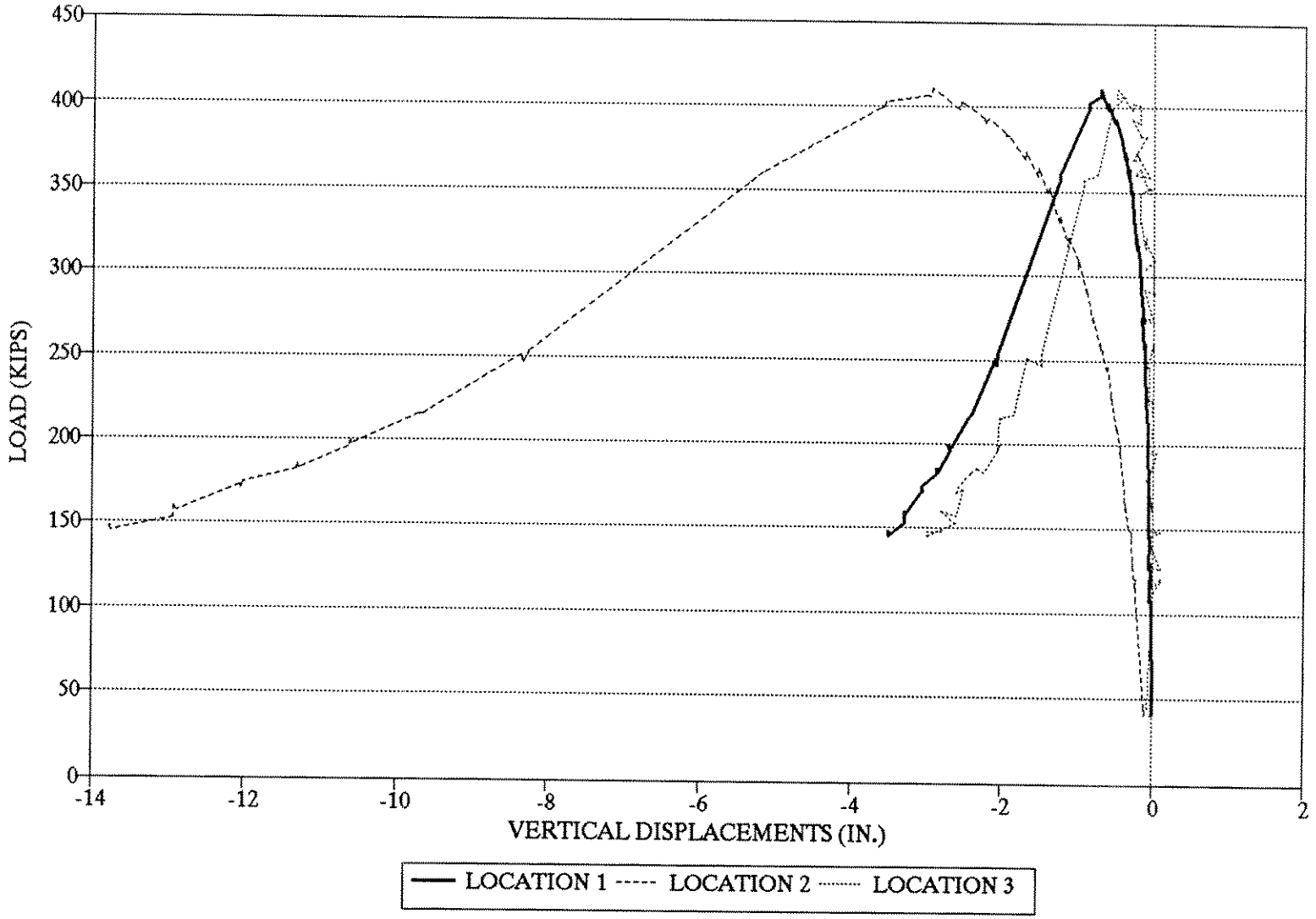

Figure 3.6. LOAD AND ECCENTRICITY VS. LOAD STEP

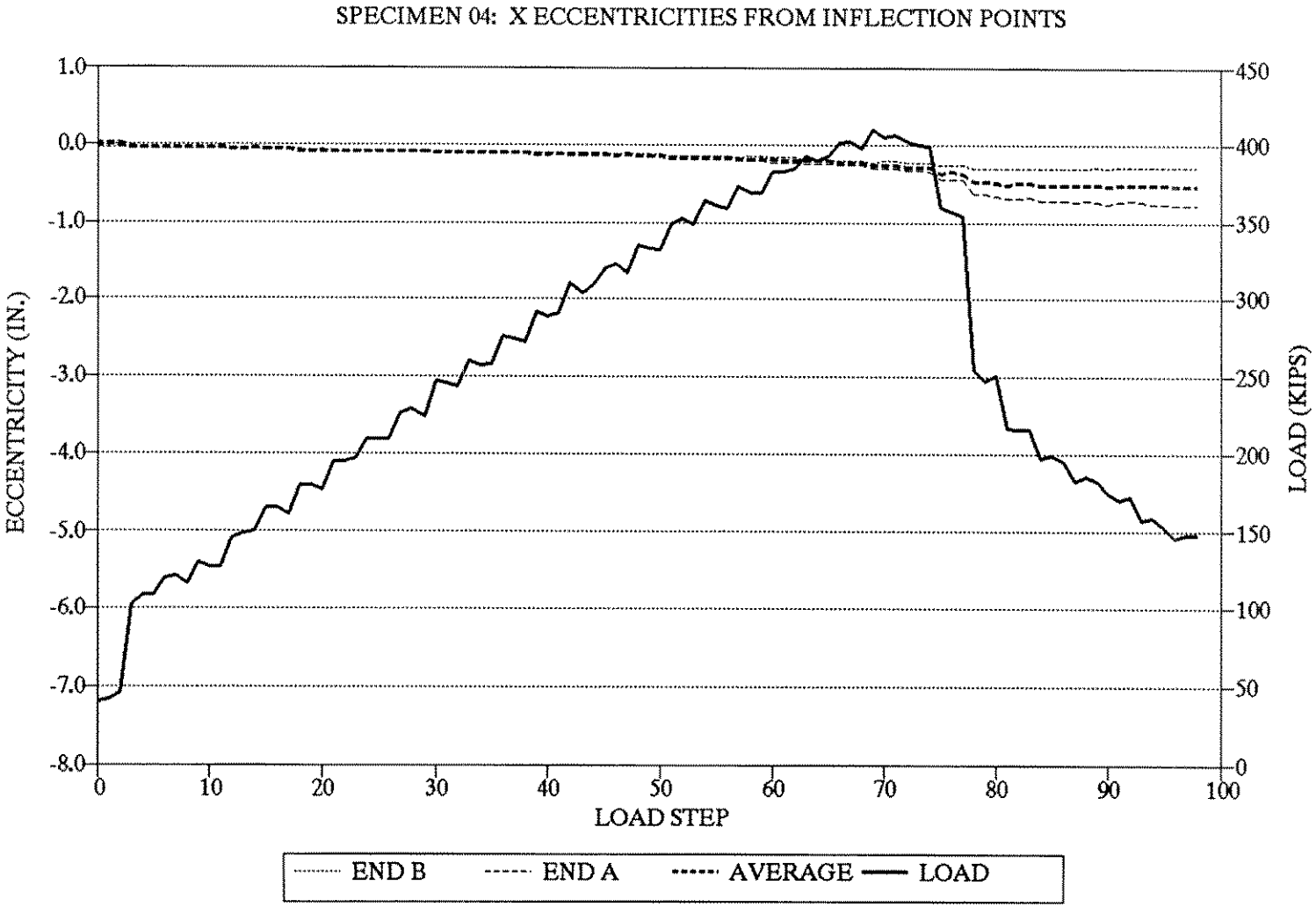

Figure 3.7. LOAD AND ECCENTRICITY VS. LOAD STEP

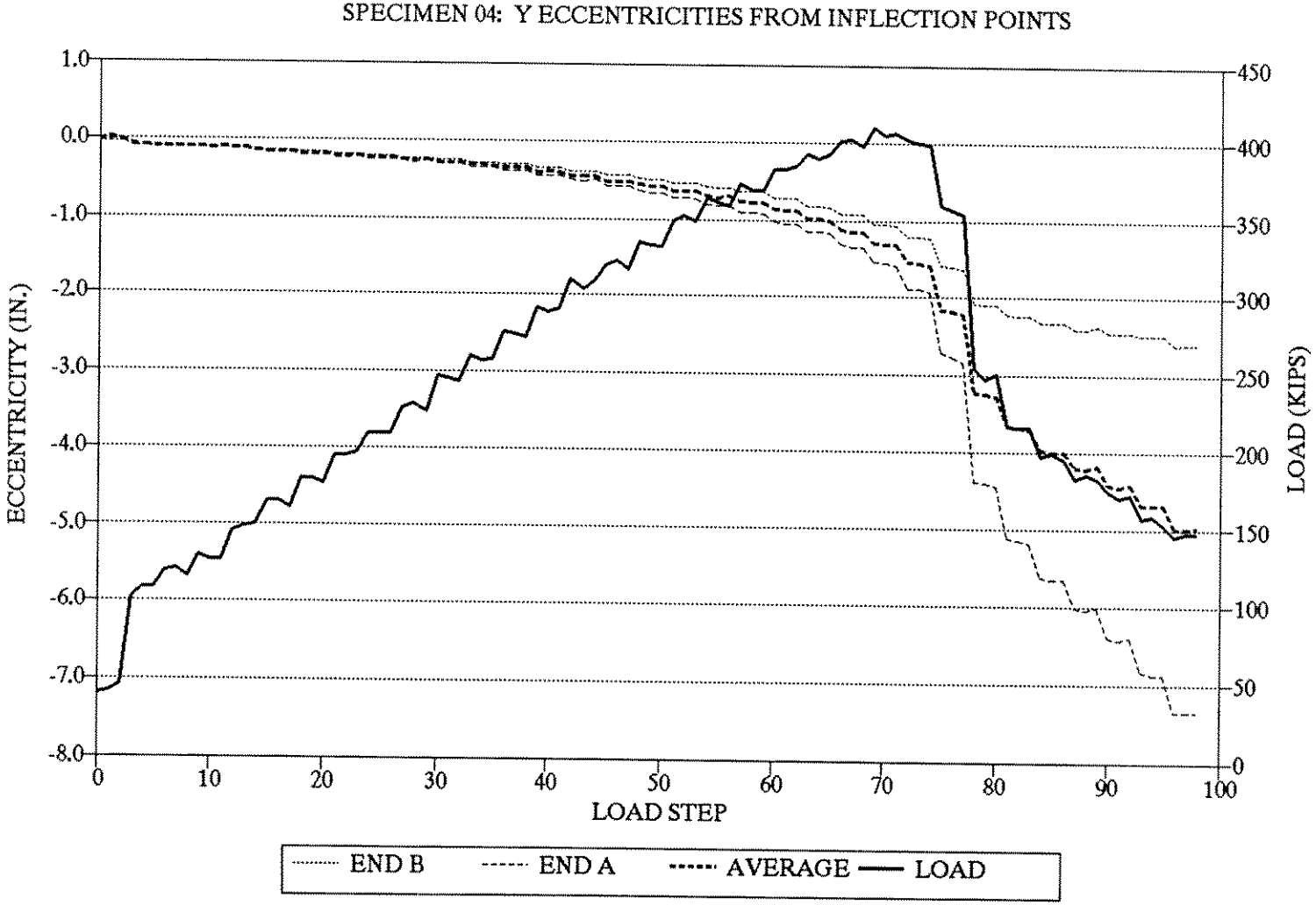

Figure 3.8. LOAD AND ECCENTRICITY VS. LOAD STEP

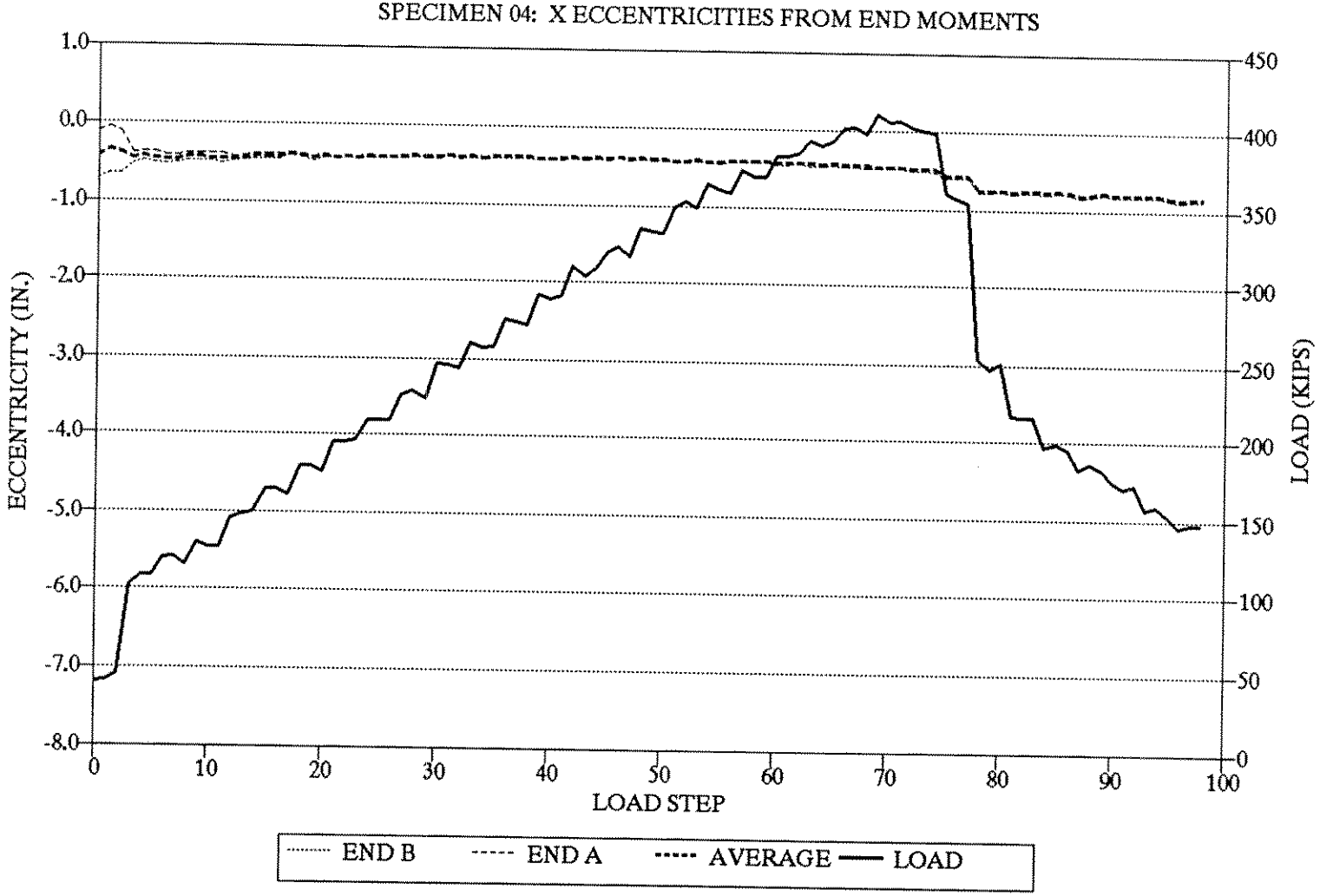

Figure 3.9. LOAD AND ECCENTRICITY VS. LOAD STEP

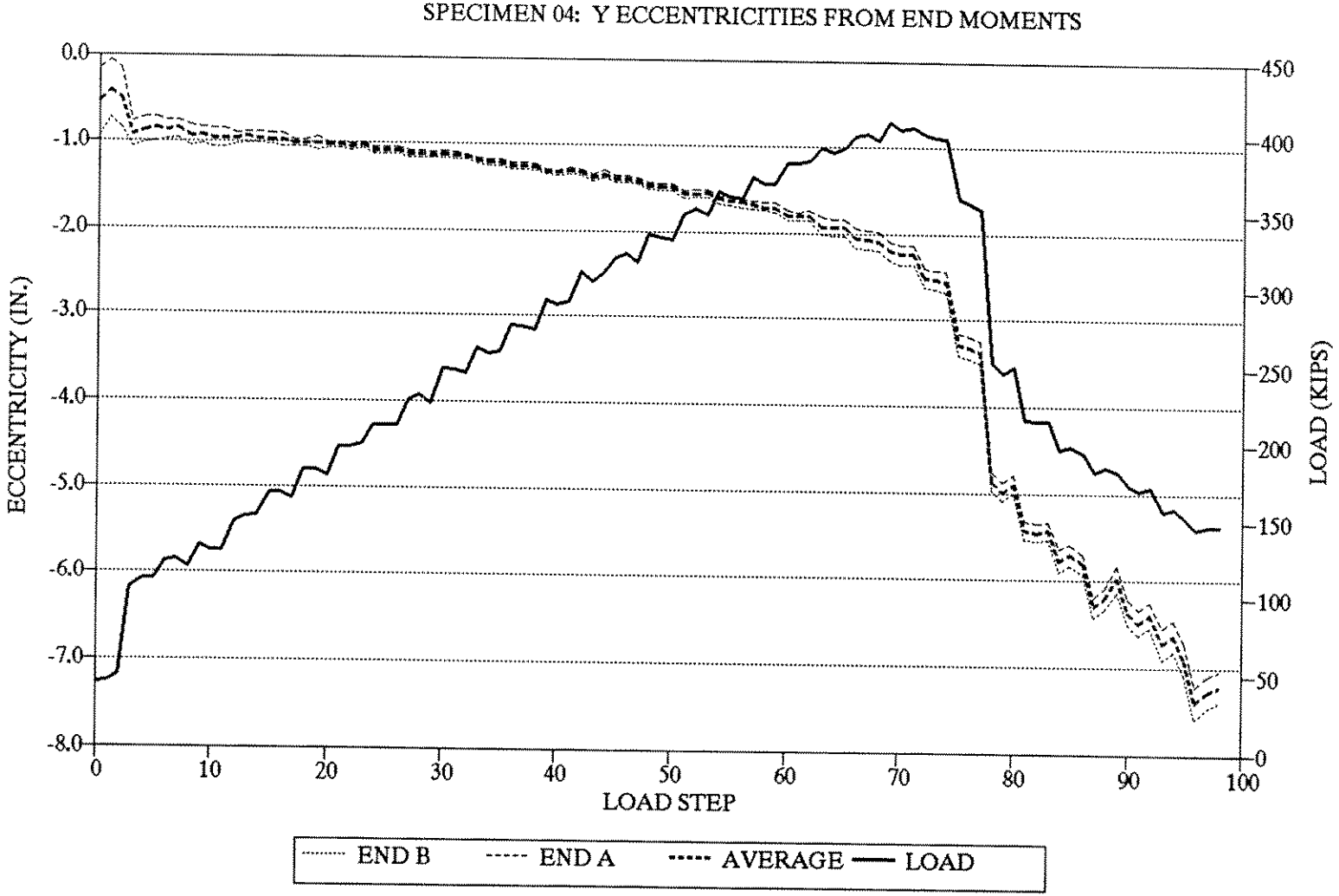

Figure 3.10. END ROTATION AND LOAD VS. LOAD STEP
SPECIMEN 04

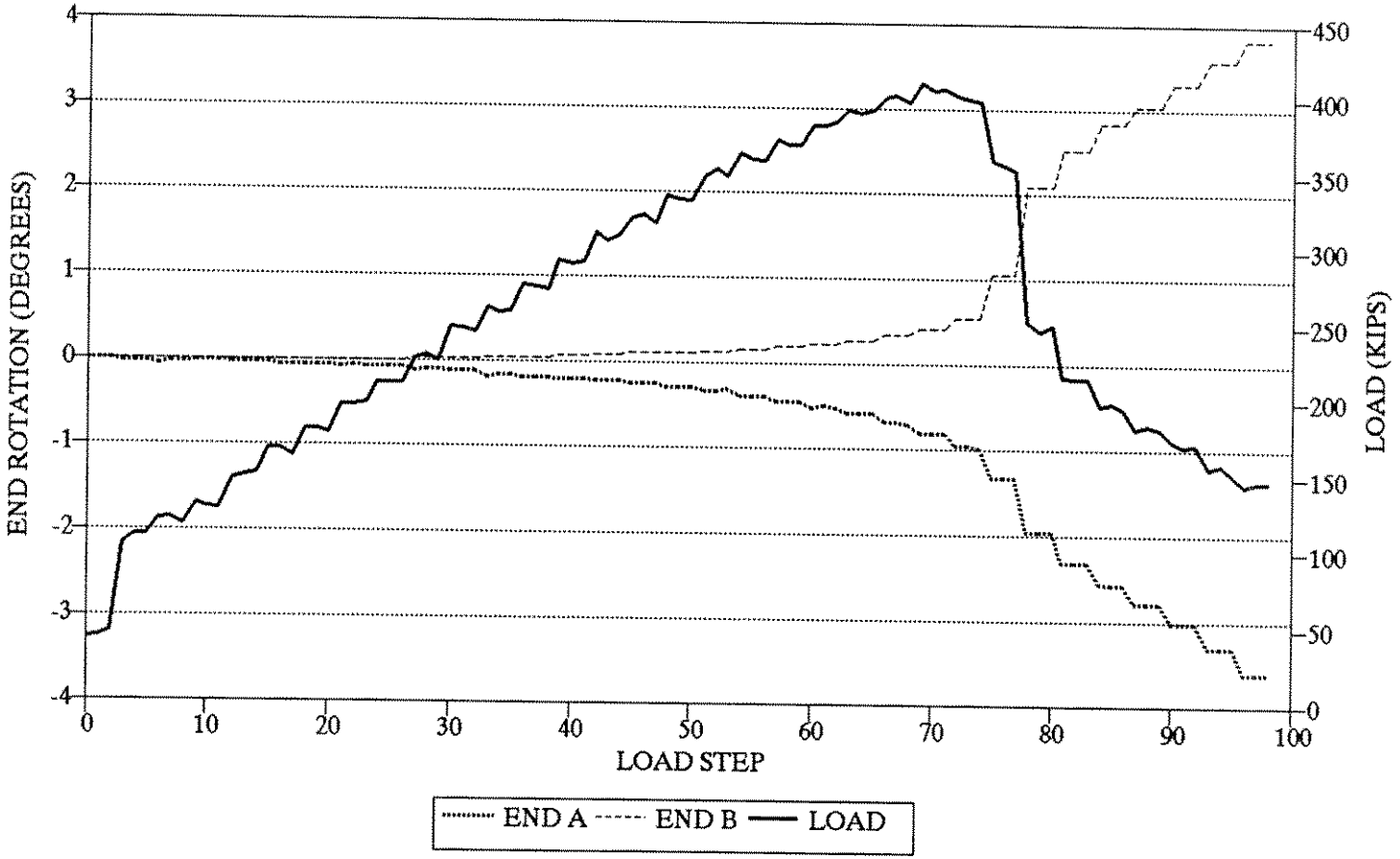

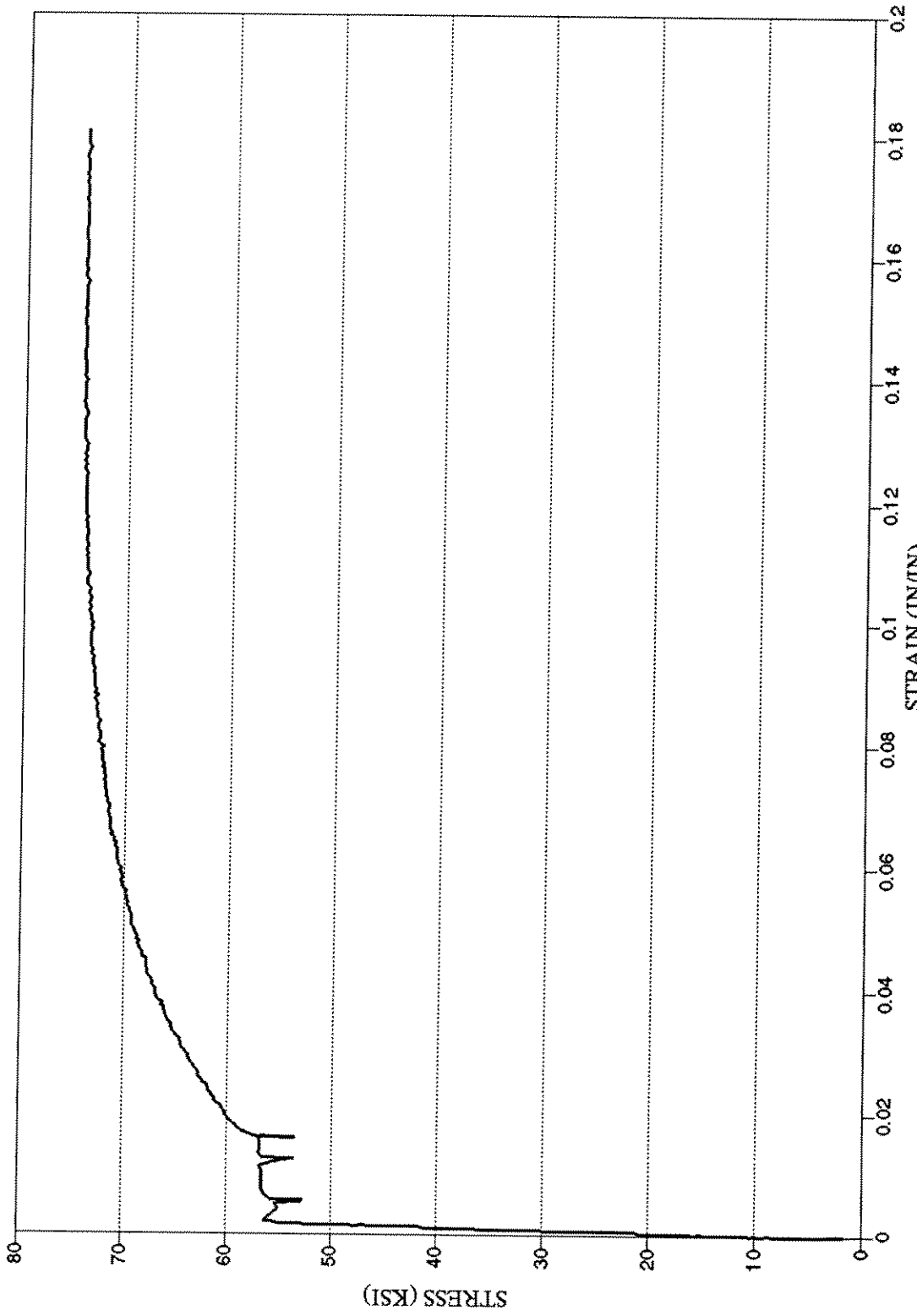
TENSILE COUPON DATA
SPECIMEN 04-2
STRESS (KSI)
80
70
60
50
40
30
20
10
0
0
0.02
0.04
0.06
0.08
0.1
0.12
0.14
0.16
0.18
0.2
STRAIN (IN/IN)

Figure 3.11.

Figure 3.12. TENSILE COUPON DATA
SPECIMEN 04-2

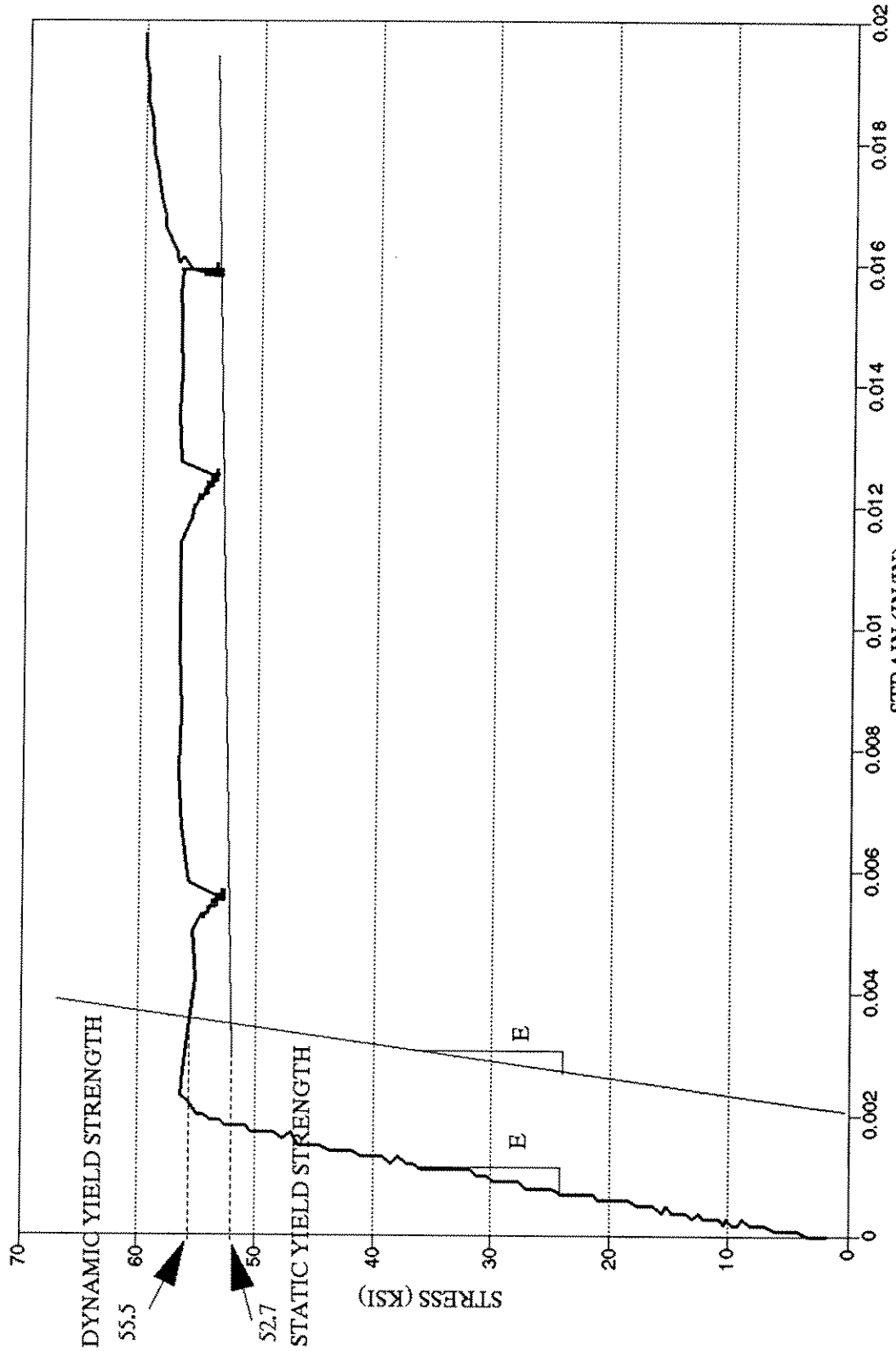

Figure 3.13. STATIC YIELD STRENGTH/ROCKWELL HARDNESS
for API 5L Gr. B (Specimens 01-08)

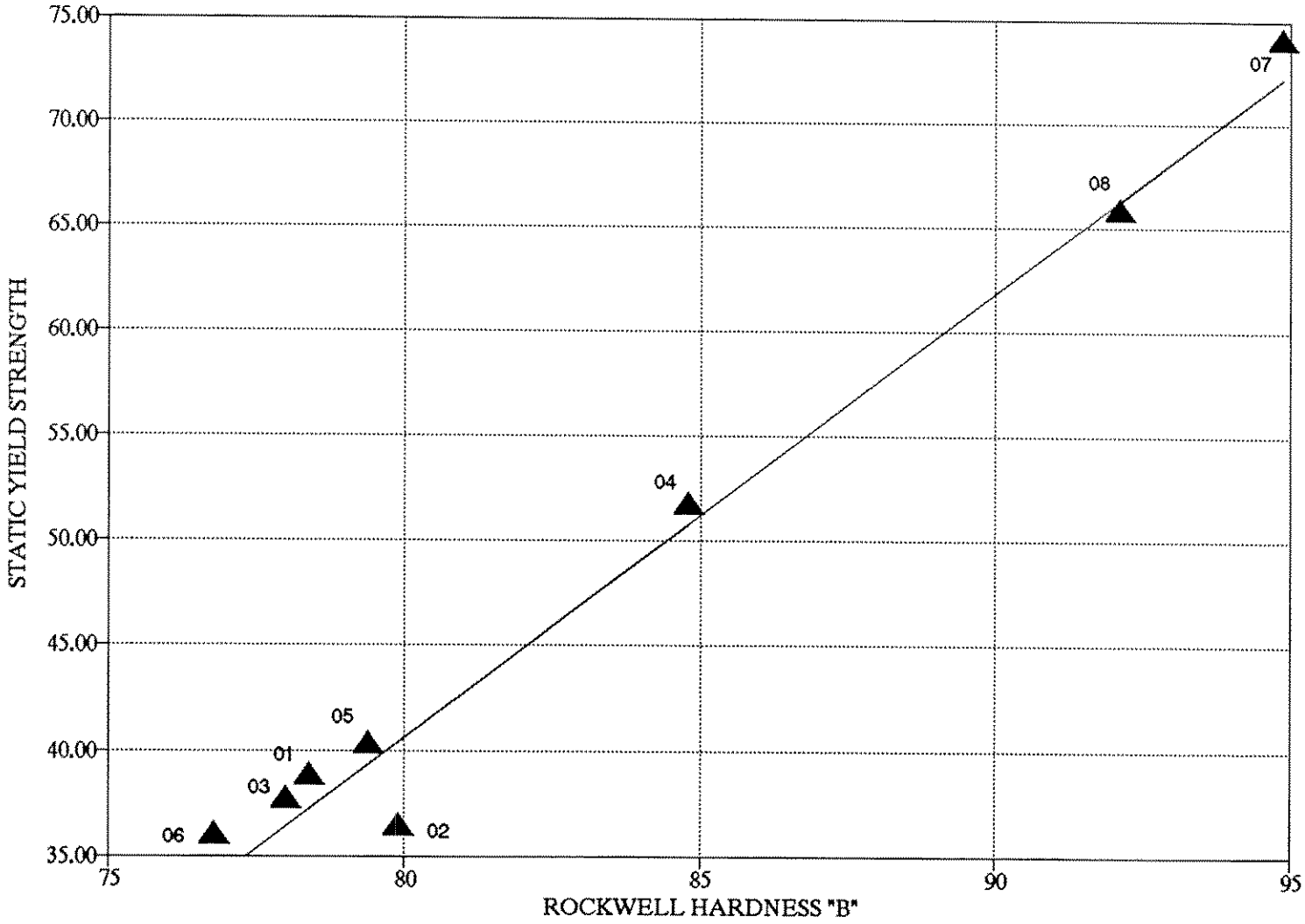

Figure 3.14. Typical Global Buckling

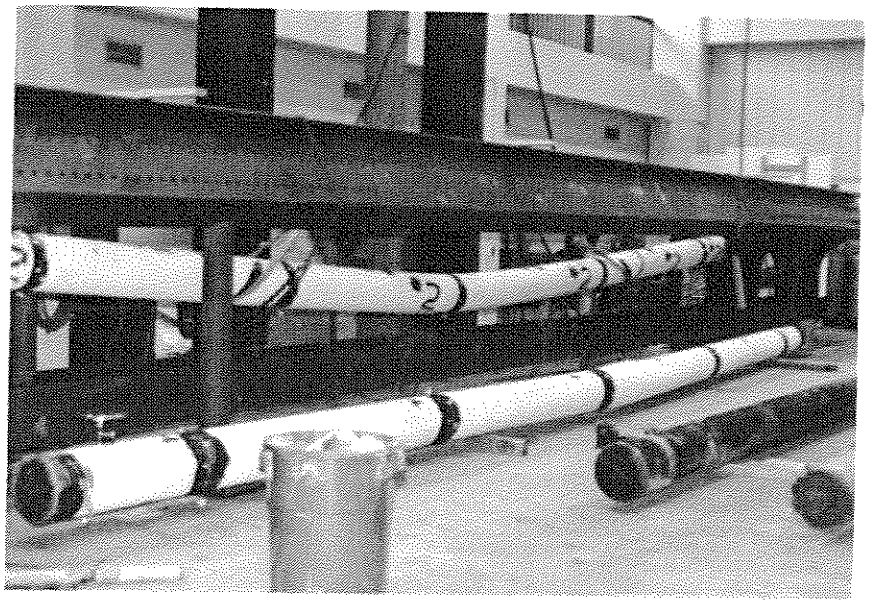

Figure 3.15. Failed Weld for Specimen 02

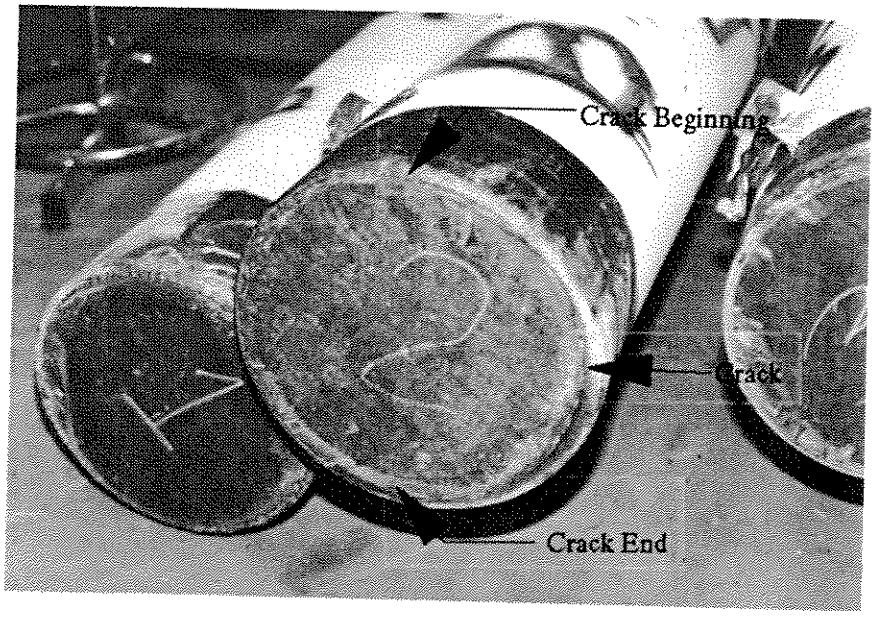

Figure 3.16. LOAD AND DEFLECTION VS. LOAD STEP
SPECIMEN 07

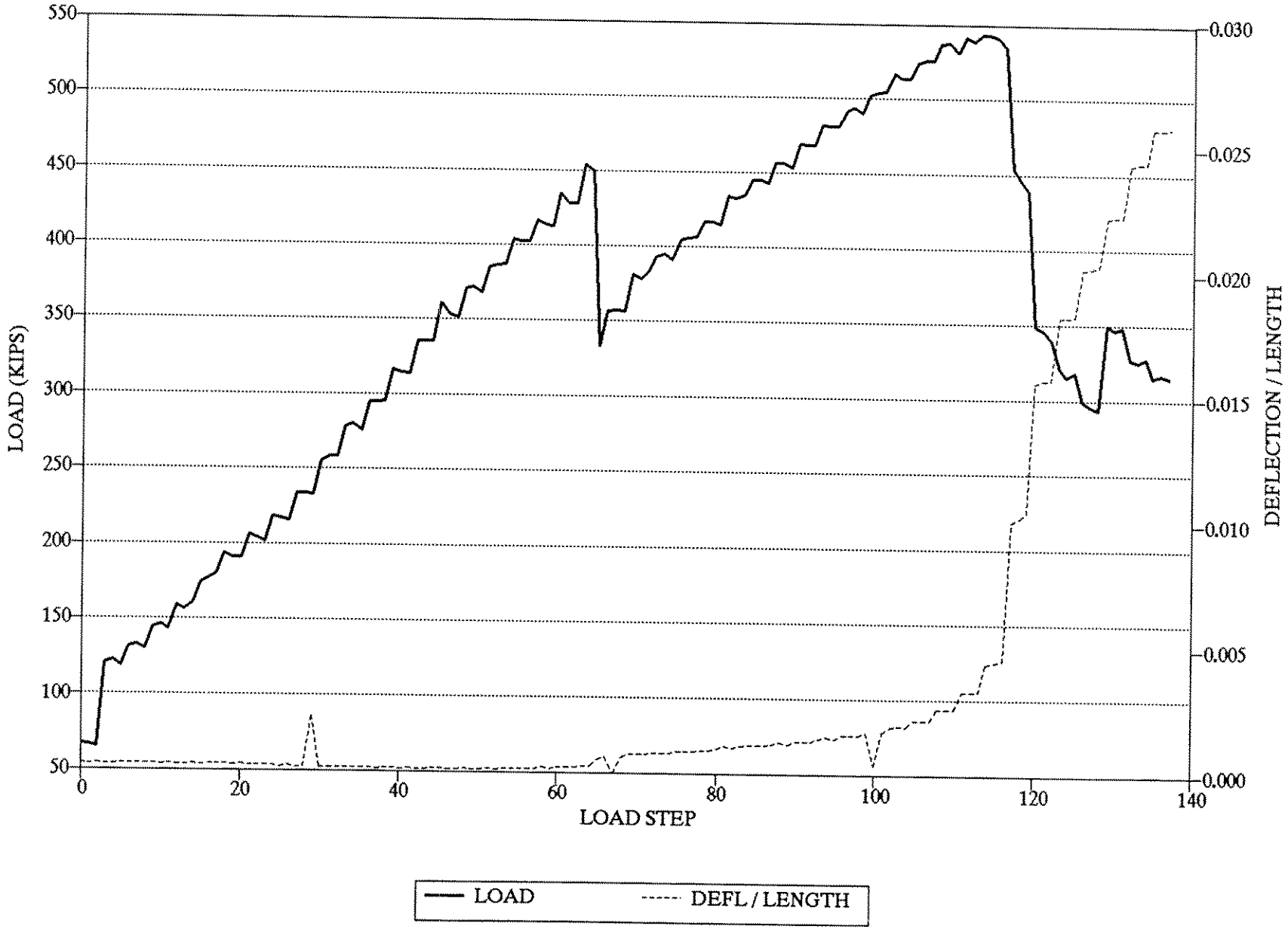

Figure 3.17. End B of Specimens 05, 07, and 08

Table 3.1. Effective Length Factor, k.

Specimen No.	k Value [1)]
01	0.50
02	0.78
03	0.54
04	0.54
05	0.62
06	0.50
07	0.58
08	0.50
09	0.66
10	0.50
11	0.66
12	0.60

1) Determined at load step for normalized midspan deflection of 0.007.

Table 3.2. Summary of Values Used to Compute k_{THEO}

Specimen No.	$P_{0.007}$ (kips)	e_{AVE} (in.)	θ_{AVE} (rad.)	EI (k-in.^{2})	α (k-in.)	ϵ (No units)
1	295	1.30	0.0087	3,741,000	44,080	0.1760
2	480	1.30	0.0227	11,774,000	27,489	0.8882
3	530	1.80	0.0122	8,352,000	78,197	0.2217
4	400	2.50	0.0131	7,482,000	76,336	0.2035
5	630	1.20	0.0131	11,774,000	57,710	0.4222
6	470	2.10	0.0070	8,352,000	141,000	0.1226
7	530	1.20	0.0242	9,541,000	26,281	0.7528
8	450	2.50	0.0074	7,482,000	152,027	0.1021
9	1140	1.10	0.0057	27,028,000	220,000	0.2559
10	430	2.30	0.0131	7,656,000	75,496	0.2113
11	600	1.60	0.0114	21,054,000	84,211	0.5209
12	650	0.50	0.0044	16,298,000	73,864	0.4597

Table 3.3. Theoretical and Experimental Effective Length Factors

Specimen No.	k_{THEO}	k_{EXP}	% Error
1	0.65	0.50	+30.0
2	0.84	0.78	+ 7.7
3	0.67	0.54	+24.1
4	0.66	0.54	+22.2
5	0.75	0.62	+21.0
6	0.60	0.50	+20.0
7	0.82	0.58	+41.4
8	0.59	0.50	+18.0
9	0.69	0.66	+ 4.5
10	0.66	0.50	+32.0
11	0.78	0.66	+18.2
12	0.76	0.60	+26.7
Ave. % Error			22.2 (s = 10.1)

$$\% \text{ Error} = \frac{k_{THEO} - k_{EXP}}{k_{EXP}} \times 100\%$$

Table 3.4. Summary of Results from Full-Scale Tests

Specimen No.	P_{max} (kips)	k Value	Chord Shortening at P_{max} (in.)	Vertical Displacements at P_{max} (in.)	Horizontal Displacements at P_{max} (in.)
01	324	0.50	0.37	-1.43	0.11
02	506	0.78	0.50	-4.81	-0.55
03	538	0.54	0.22	-2.93	0.33
04	411	0.54	0.30	-2.91	-0.63
05	677	0.62	0.41	-1.80	-0.05
06	496	0.50	0.51	-2.15	0.99
07	543	0.58	0.75	-2.10	0.29
08	458	0.50	0.28	-2.85	-0.30
09	1479	0.66	0.65	-0.95	1.13
10	443	0.50	0.47	-2.59	-0.34
11	598	0.66	0.32	-3.70	0.60
12	772	0.60	0.61	-0.49	1.26

Table 3.5. Summary of Specimen Material Properties

Specimen No.	Static Yield[1] Strength (ksi)	Dynamic Yield[1] Strength (ksi)	Ultimate Strength[1] (ksi)	Rockwell Hardness
01	38.9	42.1	64.7	78.4
02	36.5	40.1	65.4	79.9
03	37.8	41.2	66.7	78.0
04	51.8	55.1	75.0	84.8
05	40.4	43.7	65.6	79.4
06	36.1	39.6	62.9	76.8
07	74.2	77.9	94.1	94.9
08	65.9	69.7	85.2	92.1
09	44.0	48.0	68.3	NT
10	42.7	46.2	69.0	NT
11	40.8	45.2	67.1	NT
12	46.1	48.6	69.7	NT

Notes:
1) Average value based on the results of two tensile coupon specimens.
2) NT - Rockwell test not conducted on these specimens.

Table 3.6. Summary of Grout Quality at Specimen Ends

Specimen No.	End A		End B	
	$\%A_{grout}$	Void Type	$\%A_{grout}$	Void Type
02	95	A	100	-
03	74	PG	76	A,PG
04	80	PG	77	A,PG
05	83	PG	100	-
06	87	PG	94	A
07	0	S	29	A
08	100	-	87	A
09	100	-	100	-
11	100	-	100	-

Notes: 1) End A is the end at which the grout entered while end B is the end at which the grout exited during the pumping operation.

2) $\%A_{grout} = \frac{A_{core} - A_{void}}{A_{core}} \times 100\%$

where: $A_{core} = \frac{\pi}{4}(ID)^2$,

ID = inside diameter of specimen,

A_{void} = area not filled with quality grout.

3) Void is the area not containing quality grout.

Void types : A = air

S = sand

PG = poor quality grout

4) Air void at end A of specimen 02 extends inward 7 in.

5) Voids at end B generally extend inward 8-12 in. from the end. Exceptions: Void in specimens 07 and 08 extend 48 in. and 36 in., respectively.

4.0 ANALYSIS OF RESULTS

The analysis of the data is divided into two tasks. First, the experimental ultimate capacity of all members is compared to the capacity of ungrouted, undamaged tubular members with the same physical and material properties. This is done to determine: 1) if grout can restore the strength of the damaged member to the design capacity of the ungrouted, undamaged member and 2) the increase in strength that can be obtained by grouting an undamaged member. Secondly, the experimental ultimate capacity of all members is compared to the capacity predicted by different analytical methods. This is done to determine how accurate each analytical method is in predicting the capacity of the various members.

4.1 Comparison of Experimental Ultimate Capacities with Predicted Ultimate Capacities

The ultimate capacities for all the members tested in the experimental program were calculated using the Cox-LRFD method with and without the correction for bending moment. The Cox-LRFD formula is used for comparison purposes because it was developed specifically for steel tubular members and is a widely accepted method for determining the buckling capacity of undamaged, ungrouted steel tubular members. Thus, the capacities calculated using the Cox formula is assumed to best represent the initial design capacity of undamaged, ungrouted members. The various methods used in this research for determining the analytical ultimate capacities for the test specimens are summarized in Table 4.1.

All the analytical methods shown in Table 4.1 require input of general geometric and material properties such as: length, diameter, wall thickness, effective length, yield strength and modulus of elasticity for steel, and compressive strength and modulus of elasticity for grout (when applicable). The analytical methods for dented members also require input of dent depth and length (when applicable). A summary of all properties used in the various analytical models is presented in Table 4.2.

4.1.1 Discussion of the Analytical Formulations. In the following discussion of the various analytical models, all factors of safety, resistance factors, etc., have been assumed to be 1.0 since the ultimate capacity is the value of interest. The reader should refer to the reference given for each method to obtain the appropriate reduction factor(s) and design strengths.

4.1.1.1 Cox-LRFD Equation. The Cox-LRFD equation was developed to determine the ultimate capacity of undamaged, ungrouted members assuming that they are subjected only to axial load. The equation was developed by John W. Cox at TERA, Inc., as part of a project for the American Petroleum Institute. The equation is an empirical formula based on the results of 17 pipe column tests (Cox, 1987). It is currently being adopted into the latest API standard practice for offshore platforms, API RP 2A. The ultimate capacity is determined by:

$$P_u = (1.03 - 0.24\lambda^2)P_y \qquad 4.1)$$

where λ = slenderness parameter

$$= \frac{kL}{r\pi}\sqrt{\frac{F_y}{E}}$$

$P_y = F_y A_g$

where A_g = the cross-sectional area

F_y = yield strength of steel

E = modulus of elasticity for steel (29,000 ksi)

kL = effective length of member

r = radius of gyration

The formula includes the effects of all geometric properties, (L, r, A), material properties, (Fy, E), and end conditions, (k). Therefore, it is a formula that can be used to compare the experimental capacity of members with different end conditions, geometric properties, and material properties. Again, the Cox formula is valid for pure axial loadings only (i.e., no bending moment).

All specimens in this research were tested in a horizontal position. Thus, moment was created due to the self weight of the member. In the grouted members, this moment is quite significant. In addition, moment due to the eccentricity of the applied load was also present in all members tested. To determine the capacity of the members with the reduction caused by these moments, the LRFD-Cox equation was used in conjunction with the AISC-LRFD interaction formula (AISC, 1986). The ultimate capacity was determined by solving Eqn. 4.2 iteratively for P_u.

$$\frac{P_u}{P_n} + \frac{8}{9}\frac{M_{ux}}{M_{nx}} \leq 1.00 \qquad 4.2)$$

where P_u = ultimate capacity corrected for the effects of bending

where $P_n = (1.03 - 0.24\lambda^2)F_y A_g$ 4.3)

= ultimate capacity neglecting the effects of bending

$$\lambda = \frac{kL}{r\pi}\sqrt{\frac{F_y}{E}}$$

$M_{nx} = F_y Z$ 4.4)

= full plastic moment capacity

$M_{ux} = B_1(M_{uDEAD} + M_{uECC})$ 4.5)

M_{uECC} = end moment caused by eccentricity of load

M_{uDEAD} = moment due to member weight

$$B_1 = \frac{C_m}{1 - \frac{P_u}{P_e}}$$

where $C_m = 1.0$

$$P_e = \frac{A_g F_y}{\lambda^2}$$

$$M_{uECC} = P_{Exp} e_{END}$$

where P_{Exp} = experimentally measured peak load

$$e_{END} = \frac{e_A + e_B}{2}$$

e_A = eccentricity of load at end A

e_B = eccentricity of load at end B

$$M_{uDEAD} = \frac{w_{DEAD} L^2}{8}$$

w_{DEAD} = member weight per unit length

The ultimate capacity for all members was computed based on the Cox formula with (Eqn. 4.2 and without (Eqn. 4.1) correction for bending moment. These capacities were used to "normalize" the experimental capacities (i.e., account for different F_y, kL, etc.) so that comparisons of the data could be made.

4.1.1.2 Taby Method. The ultimate capacity of the dented, ungrouted tubular members was calculated by the Taby method (Taby 1981, 1985). This method is derived based on simple beam theory. An example of the dent geometry assumed for this method is shown in Figure 4.1. Behavior of the specimen is assumed to occur in three phases: 1) first yield in the dent, 2) full plastification over the dented cross section, and 3) post-ultimate or collapse behavior. After plastification of the dent occurs, it is assumed not to carry additional load. Failure occurs at full plastification over the dented cross section; therefore, the plastification yield criterion is assumed. An iterative solution is needed to determine this ultimate capacity.

Taby 1981: In 1981, Taby published the first paper concerning his model for dented tubular members. The ultimate capacity is determined by:

$$P_u = P_{dp} + \Delta P_u \qquad 4.6)$$

where P_u = ultimate capacity

P_{dp} = load required to form a fully plastic hinge at the dent

ΔP_u = the increase of the load above P_{dp}

$$D = O.D.-t$$

where D = the diameter to the mid-thickness of the member wall

O.D. = the outside diameter

t = the wall thickness

$$R = D/2$$

where R = the radius to the mid-thickness of the member wall

$$\alpha = \arccos\left(1 - \frac{d_d}{R}\right)$$

where α = the angle shown in Figure 4.1

d_d = dent depth

$$a = \frac{R\sin(\alpha)}{\pi - \alpha}$$

where a = the distance between the centroid of the undamaged section and the centroid of the damaged section.

$$\eta = R\left(\frac{\sin(\alpha)}{\alpha} - \cos(\alpha)\right)$$

where η = the distance shown in Figure 4.1

$$P_p = \pi D t \sigma_y \qquad 4.7)$$

where P_p = the fully plastic compressive strength of the member

σ_y = the static yield stress of the steel

$$P_{dp} = P_p\left[\sqrt{4\left(\frac{\eta}{t}\right)^2 + 1} - 2\left(\frac{\eta}{t}\right)\right] \qquad 4.8)$$

$$I^* = R^3 t\left(\pi - \alpha - \sin(\alpha)\cos(\alpha) - \frac{2\sin^2(\alpha)}{\pi - \alpha}\right)$$

where I^* = the moment of inertia of the dented region about the neutral axis

$$\delta_b = \frac{l_1 l_d a \Delta P_u}{EI^*\left(1 + \frac{l_1}{l_2}\right)}$$

where δ_b = the deflection at the middle of the dent caused by the eccentricity of the load at the middle of the dent

E = modulus of elasticity for steel (29,000 ksi)

l_1, l_2, l_d = the lengths as shown in Figure 4.2

$$P_E = \frac{\pi^2 EI^*}{(kL)^2}$$

where P_E = the Euler buckling load

k = the effective length factor

$$\gamma = P_u / P_E$$

$$c = \frac{kL}{2l_2 + l_d} \sin\left(\frac{\pi\left(l_1 + \frac{l_d}{2}\right)}{kL}\right)$$

where c = a correction factor in the event the dent is not at midspan

c = 1, if the dent is at midspan

$$mf = 1 - \frac{\gamma(1-c)}{1-\gamma}$$

where mf = a magnification factor

mf = 1, if the dent is at midspan

$$\delta = \delta_b mf$$

where δ_b = the total deflection at the center of the dent at peak load

$$Z^* = \frac{I^*}{a + R\cos(\alpha)}$$

where Z^* = the section modulus of the pipe in the dented region

$$A^* = Dt(\pi - \alpha)$$

where A^* = the effective area in the dented region

$$\Delta P_u\left(\frac{1}{A^*} + \frac{a + \delta}{Z^*}\right) + P_{dp}\left(\frac{\delta}{Z^*}\right) = \sigma_y\left(1 - \frac{P_{dp}}{P_p}\right) \qquad 4.9)$$

Taby 1985: In 1985, Taby refined his earlier model to account for local buckling (D/t) effects. The ultimate capacity, P_u, is obtained by solving the quadratic equation:

$$\sigma_y = \frac{P_u}{A_r} + \frac{P_u(a + \delta)}{W_r} - \left(\frac{F_{dp}}{A_r} + \frac{M_{dp}}{W_r}\right) \qquad 4.10)$$

where $A_r = \pi(O.D.^2 - I.D.^2)/4$

$W_r = 2I_r/O.D.$

$$D = O.D. - t$$

where D = the diameter to the mid-thickness of the steel

O.D. = the outside diameter

t = the pipe's wall thickness

$$\alpha = \arccos\left(1 - \frac{2d_d}{D}\right)$$

where α = the angle shown in Figure 4.1

d_d = dent depth

$$\eta = \frac{D}{2}\left(\frac{\sin(\alpha)}{\alpha} - \cos(\alpha)\right)$$

where η = the distance shown in Figure 4.1

If D/t > 50

$$F_{dp} = \sigma_y D\alpha\left[\sqrt{4\eta^2 + t^2} - 2\eta\right] \qquad 4.11)$$

If $D/t \leq 50$

$$F_{dp} = 80\, t\, \sigma_y\, \alpha \left[\sqrt{4\eta^2 + t^2} - 2\eta\right] \qquad 4.12)$$

where F_{dp} = the force which causes a fully plastic hinge to form at the dent

σ_y = the static yield stress of the steel

$$A_d = D\alpha t$$

where A_d = the area of the dented portion of the cross section

$$a = \frac{D \sin(\alpha)}{2(\pi - \alpha)}$$

where a = the distance between the centroid of the undamaged section and the centroid of the damaged section

$$M_{dpmax} = \sigma_y A_d (D/2 - e + a) \qquad 4.13)$$

where M_{dpmax} = the maximum plastic moment that can develop at the hinge

$$F_{dpmax} = \frac{M_{dpmax}}{\frac{D}{2} - e + a + \eta} \qquad 4.14)$$

where F_{dpmax} = the maximum load that can occur at the dent

If $F_{dp} > F_{dpmax}$, then set $F_{dp} = F_{dpmax}$

$$M_{dp} = F_{dp}\left(\frac{D}{2} - e + a + \eta\right) \qquad 4.15)$$

where M_{dp} = the plastic moment at the dented section

$$I^* = \frac{D^3 t}{8}\left(\pi - \alpha - \sin(\alpha)\cos(\alpha) - \frac{2\sin^2(\alpha)}{\pi - \alpha}\right)$$

where I^* = the moment of inertia of the dented region about the neutral axis

$$P_E = \frac{\pi^2 E I^*}{(kL)^2}$$

where P_E = the Euler buckling load

k = the effective length factor

$$C = \frac{kL}{2l_2 + l_d} \sin\left(\frac{\pi\left(l_1 + \frac{l_d}{2}\right)}{kL}\right) \qquad 4.16)$$

where C = a correction factor in the event the dent is not at midspan

l_1, l_2, l_d = the distances shown in Figure 4.2

C = 1 if the dent is at midspan

$$\delta_o' = \frac{(l_1 - l_d)\, l_d\, (P_u a - M_{dp})}{EI_r(1 + l_1/l_d)} \qquad 4.17)$$

where δ_o' = the lateral deflection caused by the eccentricity of the load

P_u = the ultimate load

I_r = the moment of inertia of the undamaged cross section

E = modulus of elasticity for steel (29,000 ksi)

$$I_r = \pi (O.D.^4 - I.D.^4)/64$$

where O.D. = outside diameter

I.D. = inside diameter

$$\delta = \left(\delta_o' + \delta_o\right)\left(1 + \frac{CP_u}{P_E - P_u}\right) \qquad 4.18)$$

where δ = the total deflection at the dent at peak load

δ_o = the initial out-of-straightness of the dent

4.1.1.3 Ellinas Method. The ultimate capacity of the dented, ungrouted members was also computed by a method developed by Ellinas. Ellinas also uses simple beam theory to model the tubular member (Ellinas, 1984). The main difference between the Taby method and the Ellinas method is that the Ellinas method assumes "failure" when the maximum stress at the dent reaches the yield stress. The dent geometry assumed for this method is shown in Figure 4.3. After yield, the member is replaced with a beam-column section with reduced section properties. This method tends to underpredict the capacity due to the failure criterion used. The ultimate load P_u, is determined by substituting the applicable root of Eqn. 4.19 into Eqn. 4.20.

$$\frac{\sigma_u^2}{\sigma_e} - \left[1 + \alpha\lambda_d + \frac{A_d e_d}{Z_d} + \frac{\rho_y}{\sigma_e}\right]\sigma_u + \rho_y + \sigma_{pd}\left(\frac{A_d e_d}{Z_d}\right) = 0 \qquad 4.19)$$

σ_u = stress at ultimate load, P_u

$P_u = \sigma_u A$ 4.20)

A = area of undented section

$= \pi Dt$

D = O.D.-t

r = radius of gyration of undamaged region

$$r = \frac{\sqrt{O.D.^2 + I.D.^2}}{4}$$

σ_e = the Euler buckling stress

$$\sigma_e = \frac{\pi^2 E r^2}{(kL)^2}$$

d_o = initial out-of-straightness

$A_d = \frac{Dt\theta}{2}$ (θ in radians)

δ_d = dimensionless dent depth parameter = $\frac{d_d}{D}$

d_d = dent depth

If $\delta_d \geq 0.2$

$$\theta = 2\pi - 2\arcsin\left(2\sqrt{\delta_d(1 - \delta_d)}\right)$$

If $\delta_d < 0.2$

$$\theta = 2\pi - 4\sqrt{\delta_d}$$

$$\delta_o = \frac{d_o}{L}$$

If $\delta_o \leq 0.0015$

$$\alpha = 0.001167 + 0.875\left(\frac{\sigma_y}{E}\right)$$

If $\delta_o > 0.0015$

$$\alpha = \sqrt{2}\ \delta_o - 0.000954 + 0.875\left(\frac{\sigma_y}{E}\right)$$

$$\sigma_{pd} = \frac{D\sigma_y}{t}\left[\sqrt{\frac{16}{9}\delta_d^2 + \left(\frac{t}{D}\right)^2} - \frac{4\delta_d}{3}\right]$$

$$\lambda_d = \frac{kL}{r_d} - 0.2\pi\sqrt{\frac{E}{\sigma_y}}$$

σ_y = static yield stress

$$r_d = \frac{D}{2}\sqrt{\frac{1}{2}\left(1 + \frac{\sin\theta}{\theta} - \frac{8\sin^2\left(\frac{\theta}{2}\right)}{\theta^2}\right)}$$

$$Z_d = \frac{D^2 t}{8}\left[\frac{\theta + \sin\theta - \frac{8\sin^2\frac{\theta}{2}}{\theta}}{1 - 2\delta_d + \frac{2e_d}{D}}\right]$$

$$e_d = \frac{D\sin\left(\frac{\theta}{2}\right)}{\theta}$$

$$\rho_y = (\sigma_y - \sigma_{pd})\frac{A_d}{A} + \sigma_{pd}$$

4.1.1.4. Zhou Method. The ultimate capacity of the dented, ungrouted members was also computed by a method developed by Zhou. The Zhou method uses the full plastification yield criterion in the same manner as the Taby method (Zhou, 1991). The dent geometry used by the Taby method, as shown in Figure 4.1, is also used by Zhou. This method incorporates a different ultimate load interaction relationship between axial load and bending moment than the Taby or Ellinas methods. However, the Zhou method does use the same three phases of specimen behavior and geometric cross section used by the Taby method. This method has been found in previous research to most accurately predict the capacity of specimens with small dent depth to diameter ratios (d/D<0.15) (Ritter, 1992). The ultimate capacity is determined by substituting the appropriate root of Eqn. 4.21 into Eqn. 4.22.

$$\frac{A\left[\sigma_u(d_o + e_d) - \sigma_{pd}e_d\right]}{M_o\left(1 - \frac{\sigma_u}{\sigma_e}\right)} - \frac{te_d(\pi\sigma_u - \alpha\sigma_{pd})}{P_o} - \cos\left[\frac{\alpha}{2} + \frac{\pi tD(\pi\sigma_u - \alpha\sigma_{pd})}{2P_o}\right] + \frac{\sin\alpha}{2} = 0 \qquad (4.21)$$

σ_u = stress at ultimate load, P_u

$$P_u = \sigma_u A \qquad (4.22)$$

where $A = \pi Dt$

D = O.D. - t

$$\alpha = \arccos\left(1 - 2\frac{d_d}{D}\right)$$

d_d = dent depth

$M_o = D^2 t\sigma_y$

= full plastic moment capacity

σ_y = yield stress

$P_o = \pi D t \sigma_y$

= full plastic axial capacity

$$\eta = \frac{D}{2}\left(\frac{\sin(\alpha)}{\alpha} - \cos(\alpha)\right)$$

$$\sigma_{pd} = \sigma_y\left(\sqrt{4\eta^2 + t^2} - 2\eta\right)/t$$

$$e_d = \frac{D\sin(\alpha)}{2(\pi - \alpha)}$$

$$\sigma_e = \frac{\pi^2 E r^2}{(kL)^2}$$

$$r = \sqrt{\frac{O.D.^2 + I.D.^2}{4}}$$

4.1.1.5 ACI Method. For the grouted, undamaged tubular members, the capacity was calculated using the American Concrete Institute composite method (ACI, 1989). This method was used for the undamaged, grouted members since they behave as composite columns. The Euler buckling equation with a modified EI is used to predict the ultimate capacity. It is not, however, valid in the inelastic range. P_u is computed by:

$$P_u = \frac{\pi^2 EI}{(kL)^2} \qquad 4.23)$$

where $$EI = \frac{\frac{E_c I_g}{5}}{1 + \beta_d} + E_s I_t$$

I_g = moment of inertia of the grout core

$$= \frac{\pi}{64}(I.D.)^4$$

I_t = moment of inertia of the steel tube

$$= \frac{\pi}{64}(O.D.^4 - I.D.^4)$$

E_c = modulus of elasticity of the grout

E_s = modulus of elasticity of the steel

β_d is the ratio of the maximum factored dead load moment to maximum factored total load moment and is used to account for long term creep effects due to dead load. β_d was assumed to be 0 since there were no long term creep effects for any of the specimens tested.

4.1.1.6 Parsanejad Method 1. For dented, grouted tubular members, the first analytical method considered was developed by S. Parsanejad (Parsanejad, 1987). In this method the dent geometry used is the same as used by Taby and is shown in Figure 4.1. The response of the entire member is modeled as a beam column with uniform cross-sectional properties represented by the dented zone. It is also assumed that the grout and the steel tube remain fully bonded at ultimate load. The ultimate capacity is determined by solving for σ_u in the quadratic equation, Eqn. 4.24, and substituting the appropriate root into Eqn. 4.25.

$$\left(\frac{\sigma_u}{\sigma_y}\right)^2 - \left(\frac{1 + k}{\lambda^2} + m\right)\left(\frac{\sigma_u}{\sigma_y}\right) + \frac{m}{\lambda^2} = 0 \qquad 4.24)$$

where $k = A_{tr}\frac{e_t}{Z_{tr}}$, $\lambda = \frac{KL}{\pi r_{tr}}\sqrt{\frac{\sigma_y}{E_s}}$, $m = \frac{A_{tr}}{A_{tr}^{\star}}$

and:

A_{tr} = transformed cross section of the dent

A_{tr}^{*} = transformed cross-sectional area of undamaged section,

Z_{tr} = section modulus of the transformed section at the dent,

r_{tr} = transformed radius of gyration of the dent,

e_t = ecc + δ + e_{tr}

ecc = load eccentricity

K = effective length factor

δ = out of straightness

$$e_{tr} = \frac{A_s e_s + \frac{A_s e_g}{n}}{A_{tr}}$$

$$A_g = \text{area of grout} = \frac{D^2}{4}\left(\pi - \alpha + \frac{\sin^2\alpha}{2}\right)$$

$$A_s = \text{area of steel} = \pi D t$$

$$e_s = \frac{D}{2\pi}(\sin\alpha - \alpha\cos\alpha)$$

$$e_g = \frac{(D\sin\alpha)^3}{12 A_g}$$

$$\alpha = \arccos\left(1 - \frac{2d_d}{D}\right)$$

where d_d = dent depth

α = angle shown in Figure 4.1

$$n = E_s/E_g$$

where n = modular ratio

E_s = modulus of elasticity for steel (29000 ksi)

E_g = modulus of elasticity for grout

$$A_{tr} = A_s + \frac{A_g}{n}$$

$$I_s = \frac{D^3 t}{4}\left[\frac{\pi - \alpha}{2} - \frac{\sin(2\alpha)}{4} + \alpha\cos^2\alpha - \frac{(\sin\alpha - \alpha\cos\alpha)^2}{\pi}\right]$$

where I_s = the moment of inertia of the steel in the dented region

$$I_g = \frac{D^4}{64}\left(\pi - \alpha + \frac{\sin(4\alpha)}{4}\right) - \frac{(D\sin\alpha)^6}{144 A_g}$$

where I_g = the moment of inertia of the grout in the dented region

$$I_{tr} = I_s + I_g/n + A_s(e_{tr} - e_s)^2 + \frac{A_g}{n}(e_g - e_{tr})^2$$

where I_{tr} = the transformed moment of inertia at the dent

$$Z_{tr} = \frac{I_{tr}}{\left(\frac{D}{2}\right)\cos\alpha + e_{tr}}$$

$$r_{tr} = \sqrt{\frac{I_{tr}}{A_{tr}}}$$

where r_{tr} = the transformed radius of gyration of the member at the dent

$$A_{tr}^{*} = A_s + \frac{\pi D^2}{4n}$$

$$P_u = \sigma_u A_{tr}^{*} \qquad 4.25)$$

4.1.1.7 Parsanejad Method 2. S. Parsanejad presented a method in 1988 that was published in 1990 for partially filled grouted members (Parsanejad, 1990). This method defines the ultimate load by the intersection of the pre-ultimate behavior curve and the post-ultimate behavior curve. This is determined by plotting the lateral deflection versus the ratio of the applied load to the load determined by the yield stress. This is different from the simple beam theory as presented in the previous analytical method by S. Parsanejad which assumes a first yield failure criterion. It is also assumed that the grout supports the dented region and allows the steel section to reach and retain the full plastic moment capacity. Eqn. 4.26 is iteratively solved to obtain P_u.

$$\frac{k}{\left(1 - \frac{P_u}{P_y}\lambda^2\right)} = \frac{2\sin\left[\frac{\pi}{2}\left(1 - \frac{P_u}{P_y}\right)\right] - (\sin\alpha - \alpha\cos\alpha)}{2\pi\frac{P_u}{P_y}} \qquad 4.29)$$

where $\alpha = \arccos\left(1 - \frac{2e}{D}\right)$

$P_y = \pi D t \sigma_y$

$k = \frac{e_t}{D}$

D = O.D. - t

$e_t = ecc + \delta + e_s$

e_s = eccentricity of the member caused by the dent

δ = initial out of straightness

ecc = external eccentricity of the applied load

$\lambda = \sqrt{\frac{P_y}{P_e}}$

$$P_e = \frac{\pi^2 E_s I}{(Kl)^2}$$

where P_e = the Euler buckling load

K = the effective length factor

A_s, A_g, n, A_{tr}, E_s, I_s, I_g, e_g, e_s, e_{tr}, I_{tr} are the same as in the Parsanejad Method 1.

$$I_s' = \pi D^3 t/8$$

where I_s' = the moment of inertia of the ungrouted, undamaged steel section

$$I = \left(I_{tr} l_g + I_s'(l - l_g)\right)/l$$

where l = length of pipe

l_g = length of grout

I = the member's effective moment of inertia

$I = I_{tr}$ if the member is fully grouted

4.1.1.8 Parsanejad Method 3. Finally, a third method was proposed by S. Parsanejad in 1988 and is very similar to the method presented in 1987 (Parsanejad, 1988). This method assumes that the response of the damaged member can be better represented by an equivalent uniform

bending rigidity along the length of the member. In the previous methods by Parsanejad, the bending rigidity of the dent was used for the entire length of the tubular member. In addition, this method also assumes that the bonding between the grout and the steel tubular has failed at ultimate load. The ultimate load is found by substituting the appropriate root from Eqn. 4.27 into Eqn. 4.28.

$$\left(\frac{\sigma_u}{\sigma_y}\right)^2 - \left(\frac{1+k}{\lambda^2}+1\right)\left(\frac{\sigma_u}{\sigma_y}\right) + \frac{1}{\lambda^2} = 0 \qquad 4.27)$$

A_s, α, A_g, n, A_{tr}, I_g, I_s, I_s', e_g, e_s, e_{tr}, I_{tr}, and I are defined the same as in the previous Parsanejad methods. Now,

$$Z_s = \frac{I_s}{\left(\frac{D}{2}\right)\cos\alpha + e_s}$$

where Z_s = the section modulus of the steel at the dented region

$$r_s = \sqrt{\frac{I_s}{A_s}}$$

where r_s = the radius of gyration of the steel at the dented region

$$r = r_s\sqrt{\frac{I}{I_s}}$$

where r = the member's effective radius of gyration

$$\sigma_e = \frac{\pi^2 E_s r^2}{(Kl)^2}$$

$$e_t = ecc + \delta + e_s$$

$$\lambda = \sqrt{\frac{\sigma_y}{\sigma_e}}$$

$$k = A_s e_t / Z_s$$

$$P_u = \sigma_u A_s \qquad 4.28)$$

4.1.1.9 Poston Method. The ultimate capacity of specimen nos. 01-08 were predicted by a method developed by Poston. The Poston method was developed by Dr. Randall W. Poston for nonlinear analysis of reinforced concrete beam-columns subjected to static loads (Poston, 1986). This method is implemented through the computer program, PIER. The members were modeled with a concrete core and continuous spiral reinforcement with 0.01 inches of concrete cover. The value of 0.01 was assumed as a negligible thickness of concrete cover since a value of zero is not a valid option for the program. In addition, it was assumed that there was no debonding between the grout and the steel tubular prior to ultimate load. Reduced section properties based on the dent profiles shown in Figures 2.1 and 2.2 were used in the dented regions of the damaged members. In order to initiate buckling, an initial transverse deflection had to be assumed at midspan for the specimen. Table 4.3 presents the various deflections assumed for each specimen. The assumed deflections correspond to the measured initial out-of-straightness values for each member. Dr. Poston and his colleagues at Schupack-Suarez Engineering, Inc., S. Norwalk, CT, performed all the analyses with the PIER program. The Poston method was not used to predict the capacities of specimens 09-12. By the time these specimens were tested, Dr. Poston was not available to perform the analysis.

4.2 Evaluation of Experimental Results.

A summary of all test specimen properties used for the determination of P_u by the Cox formula is shown in Table 4.4. A summary of the computed P_{Cox} values with (Eqn. 4.2) and without (Eqn. 4.1) moment correction (interaction) is shown in Table 4.5. The experimental ultimate capacities are plotted against the LRFD-Cox ultimate capacities without bending moment correction in Figure 4.4 and with bending moment correction in Figure 4.5. It is clear when comparing the two graphs, (Figures 4.4 and 4.5), and also the values given on Table 4.5 that bending moment generally decreases the ultimate axial capacity. This decrease in the ultimate axial capacity due to the moments is as expected based on the interaction defined by Eqn. 4.2.

In the following sections, the most significant findings of the experimental program will be presented. **In these sections, the analysis of the data will be based on the ultimate capacities computed by the Cox-LRFD formula with the correction for moment interaction. It is assumed that these values most correctly represent the ultimate axial capacity of the members in an undamaged, ungrouted condition.** Specimen 12 was the only undamaged, ungrouted member tested in the program. The P_{Exp}/P_{Cox} value for this specimen is 1.14 which indicates that the Cox-LRFD formula provides a reasonable lower bound value for the capacity of these members.

4.2.1 Effect of Dent Damage. As previously mentioned, all specimens were dented to a dent depth to diameter ratio of approximately 0.40 (d/D = 0.40). Specimens 01 (D = 12.75-in.) and 10 (D = 16.00-in.) were the only two ungrouted, dented specimens tested. The P_{Exp}/P_{Cox} ratios for these specimens were 0.76 and 0.62 respectively. This indicates that the dents reduced the capacity of these members 24% and 38% respectively.

4.2.2 Effect of Grouting Undamaged Members. Specimens 02, 05, 07, and 09 were the grouted, undamaged members tested. The experimental ultimate capacity of specimen 07 is suspect for the reason discussed in Chapter 3 and will not be included in this discussion. The P_{Exp}/P_{Cox} ratios for specimens 02, 05, and 09 were 1.79, 1.57, and 2.04. Based on this data, the grout provided a minimum increase in capacity of 57% in the undamaged members.

4.2.3 Effect of Grouting Dented Members. Specimens 03 & 06 (D/t = 34.0), 04 & 08 (D/t = 51.0), and 11 (D/t = 42.7) were the dented/grouted members tested. The P_{Exp}/P_{Cox} ratios for these members were 1.46, 1.45, 1.32, 1.36, and 1.15 respectively. These ratios indicate that the grout can compensate for the loss in capacity due to the dent damage and restore the strength to a level that exceeds the original design capacity of the member.

When comparing the P_{Exp}/P_{Cox} ratios for these members to the ratios of identical dented/ungrouted members, specimens 01 (D/t = 34.0) and 10 (D/t = 42.7), there is very significant increase in capacity. Computing the ratio, $\frac{(P_{Exp}/P_{Cox})_{Dented/Grouted}}{(P_{Exp}/P_{Cox})_{Dented/Ungrouted}}$, for each set of

specimens indicates that the grout increases the strength from 83% to 85% in the dent-damaged members.

4.2.4 Effect of D/t. The D/t ratios for the specimens tested (34.0, 42.7, and 51.0) were less than 60 where any local buckling effects would not be expected. No local buckling failures were observed during any of the tests. The P_{Exp}/P_{Cox} ratios are presented in Tables 4.6 & 4.7 for undented/grouted and dented/grouted members respectively. Based on the values presented in Table 4.7, it appears that D/t has little effect on the increase in strength provided by the grout in the dented members. The same cannot be concluded for the undented/grouted members based on the values presented in Table 4.6. Since the P_{Exp} value for specimen 07 is suspect (for reasons previously discussed), there is insufficient data to make any broad based conclusions about the effect of D/t on the capacity of these members.

4.2.5 Replicate Tests. Three replicate tests (05, 06, & 08) were conducted on three of the first four specimens (02, 03, & 04) tested. This was done to verify the results obtained from these initial tests. Table 4.8 summarizes the results. Again, the P_{Exp}/P_{Cox} values were used as the basis for comparison because P_{Cox} accounts for different effective length (kL) and yield strength (Fy) values. As can be seen from Table 4.8, the maximum difference in replicate tests for P_{Exp}/P_{Cox} ratios is 13.1%. This difference is within an acceptable limit considering the tolerances on all the variables (i.e., dent depth, grout strength, yield strength, etc.) that must be duplicated in these tests. Therefore, it is concluded that the results from specimens 05, 06, and 08 replicate and validate the results from specimens 02, 03, and 04.

4.3 Accuracy of Analytical Methods.

The ultimate capacity of each specimen was predicted by the applicable method(s) discussed in section 4.1.1. A summary of these methods is presented in Table 4.1. The section/material properties used in these calculations are summarized in Table 4.2. In the following sections the accuracy of these methods will be evaluated based on the results from the experimental program.

4.3.1 Dented/Ungrouted Members. The ultimate capacities of specimens 01 and 10 were computed by the Zhou, Taby, Poston, and Ellinas methods. A summary of these results is

shown in Table 4.9. The capacity of specimen 10 was not computed by the Poston method for reasons previously discussed. The data presented in Table 4.9 shows that the Ellinas, Zhou, and 1981 Taby methods provide extremely conservative predicted ultimate strength values. In the extreme case, the predicted capacity was 1/4 of the capacity determined experimentally (Ellinas, specimen 10). In all cases, these methods predicted capacities that were less than 1/3 the experimental capacity.

The Poston and 1985 Taby methods provided conservative but somewhat more reasonable predicted capacities. Both of these methods provided capacities within 10% of the experimental capacity for specimen 01. The 1985 Taby method, however, produced an ultimate capacity that was 74% less than the experimental capacity for specimen 10. This method has been implemented into a computer program called DENTA (Taby 1988). This program has been shown to provide capacities that agree very well with experimentally measured capacities (Ricles, et al., 1993) and is widely accepted as one of the better analytical methods for determining the strength of dent-damaged members. It should be noted that Taby's method is based on transverse dents and the geometry shown in Figure 4.1. The method is also limited to dent-depth to diameter ratios of 0.30 ($d/D < 0.30$). The dents used in this study are longitudinal, with $d/D = 0.40$, and the geometry shown in Figures 2.1, 2.2, 2.3, and 2.4. These dents appear to be much "stiffer" than the assumed dent in the Taby method which could account for differences between the measured and predicted values shown in Table 4.9.

4.3.2 Undamaged/Grouted Members. The ultimate capacities of the grouted, undamaged specimens, (02, 05, 07, and 09), were computed by the ACI and Poston methods. A summary of the predicted strengths is presented in Table 4.10. The ACI method consistently provided capacities that were larger than the experimental capacity. In the extreme case (specimen 05), the predicted capacity was 31% greater than the experimental capacity. This is due to the fact that the ACI method uses Euler's formula which is only valid for elastic buckling. All of the undamaged/grouted specimens tested failed at an ultimate load that resulted in inelastic behavior of the steel tube. Thus, the ACI formula may not be valid for these members.

The Poston method also overpredicted the experimental capacity of specimen 01 (by 1%) and specimen 07 (by 15%). However, it is not surprising that the method would not accurately predict the capacity of specimen 07 since the model used by Poston did not account for the poor quality of grout that existed in this member.

In the case of specimen 05, this method underpredicted the experimental capacity by 23%. In general, it is expected that the Poston method would provide lower bound values reasonably close to the experimental values. This is due to the fact that the model used is much more refined than the ACI method in that it accounts for the inelastic behavior of the member and more accurately models the confining effect of the steel on the grout.

4.3.3 Dented/Grouted Members. The capacities of the grouted, damaged tubular members (specimens 03, 04, 06, 08, and 11) were computed using the three Parsanejad methods (1987, 1988, 1990) and the Poston method. A summary of these calculations is shown in Table 4.11. All of the methods proposed by Parsanejad consistently provided capacities that were less than the experimental capacities. For all specimens, the 1988 and 1990 methods produced capacities less than 1/2 of the experimental capacities. In the extreme case, the capacity was underpredicted by 159% (1988, specimen 11). The 1987 method provided conservative, but somewhat more reasonable, lower bound ultimate capacities. Again, it should be mentioned that Parsanejad's method is based on the sharp, transverse dent geometry shown in Figure 4.1. The dents used in this study (shown in Figures 2.1-2.4) are longitudinal and appear to be much "stiffer" than assumed by Parsanejad. This could account for the rather large difference in predicted and experimental capacities.

The Poston method proved to accurately predict the capacities of specimens 03 and 04, although it overpredicted the capacity of specimen 04 by 4%. However, the method was conservative (underpredicted by 24%) for specimen 06 and unconservative for specimen 08 (overpredicted by 21%). However, the difference in predicted and measured capacities of specimen 08 may be explained by the fact that Poston used an initial out-of-straightness of 1.25 in. when the actual member out-of-straightness was 2.00 in. This indicates that the Poston method, while generally

more accurate and less conservative than the Parsanejad's methods, may provide unconservative capacities for some members.

4.4 Comparison of Experimental Ultimate Capacities with Design Capacities of Undamaged/Ungrouted Members.

In Section 4.2 of this chapter, comparisons were made between the experimentally measured ultimate capacities with the capacities of undamaged/ungrouted (pristine) members. The Cox-LRFD formula, 4.1, was used in conjunction with the AISC-LRFD interaction equation, 4.2, using the actual static yield strength, F_y, from tensile coupon tests, to obtain the predicted ultimate capacity of a pristine member. The yield strength values, F_y, used and the ultimate capacities obtained, are again presented in Table 4.12.

As can be seen in Table 4.12, the actual yield strength of all specimens exceeded the nominal 35 ksi yield strength specified for API 5L Gr. B steel. The capacity of each member was computed again using the Cox and AISC formulas, except the nominal yield strength (35 ksi) was used instead of the actual yield strength. These values are presented on Table 4.12 and are the true design capacities of the members (excluding the resistance factor). Also presented in Table 4.12 are the (P_{Exp}/P_{Cox}) ratios using the actual and nominal values for F_y. As expected, the (P_{Exp}/P_{Cox}) ratio based on nominal F_y values is, in some specimens, significantly larger than the ratio based on actual F_y values. The ratio (P_{Exp}/P_{Cox} Nominal F_y) is a measure of the true reserve capacity of the member over its design capacity. For the grouted specimens, this reserve ranged from 35% to 228%. If a resistance factor of 0.85 or 0.90 is used in the design of the member, the reserve capacity is even greater.

Presented in Table 4.13 is the static tensile yield capacity, P_y, of each specimen. This value excludes any local buckling effects, elastic or inelastic global buckling, etc., and represents the maximum (upper bound) yield capacity of the member. Also shown in Table 4.13 is the ratio (P_{Exp}/P_y). These values represent the ratio of the measured capacity to the maximum possible capacity of the member. For the grouted specimens, this percentage varies from 29% below to 83% above the yield capacity.

Figure 4.1. IDEALIZED DENTED MEMBER FOR TABY, ZHOU, AND PARSANEJAD METHODS

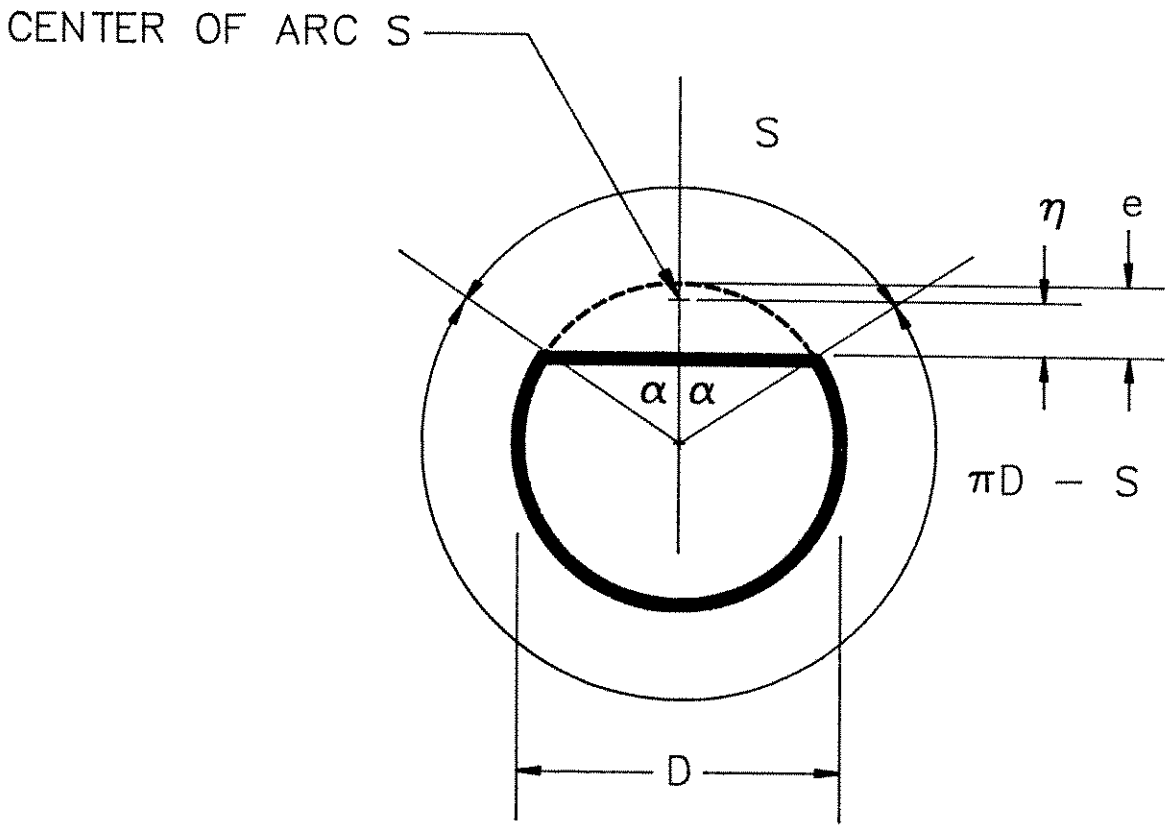

Figure 4.2. LENGTH PARAMETERS FOR TABY METHOD

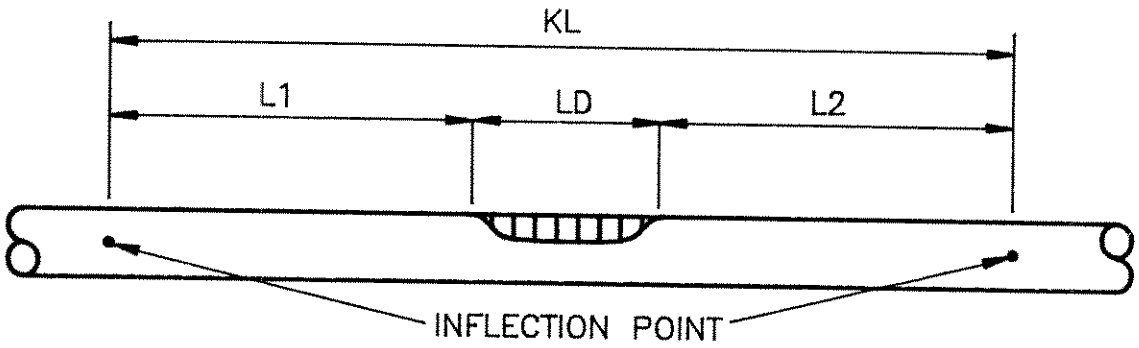

Figure 4.3. IDEALIZED DENTED MEMBER FOR ELLINAS METHOD

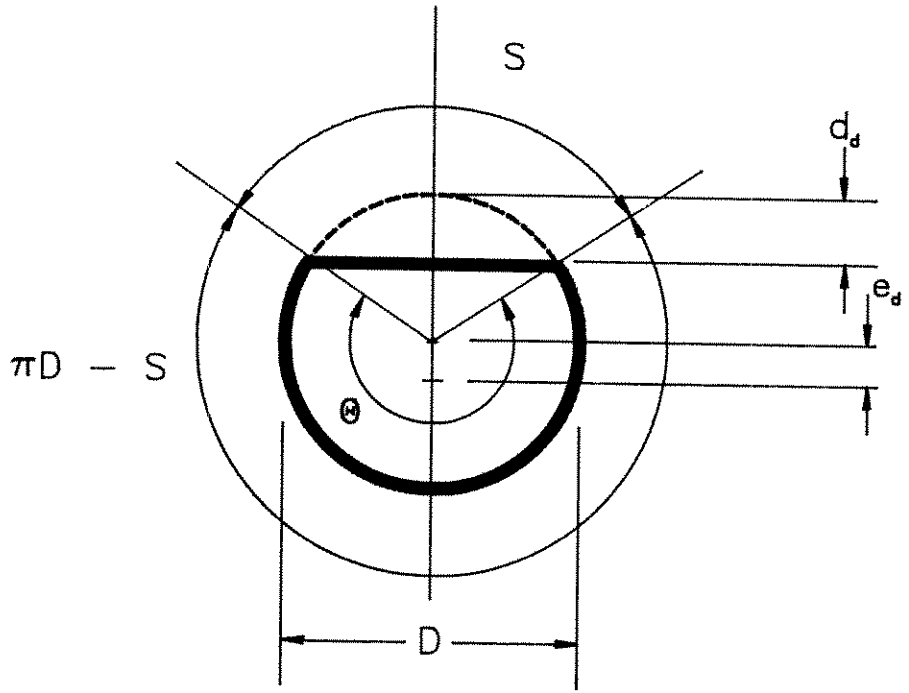

DENT GEOMETRY

Figure 4.4. COMPARISON OF EXPERIMENTAL CAPACITIES WITH COX WITHOUT BENDING CORRECTION

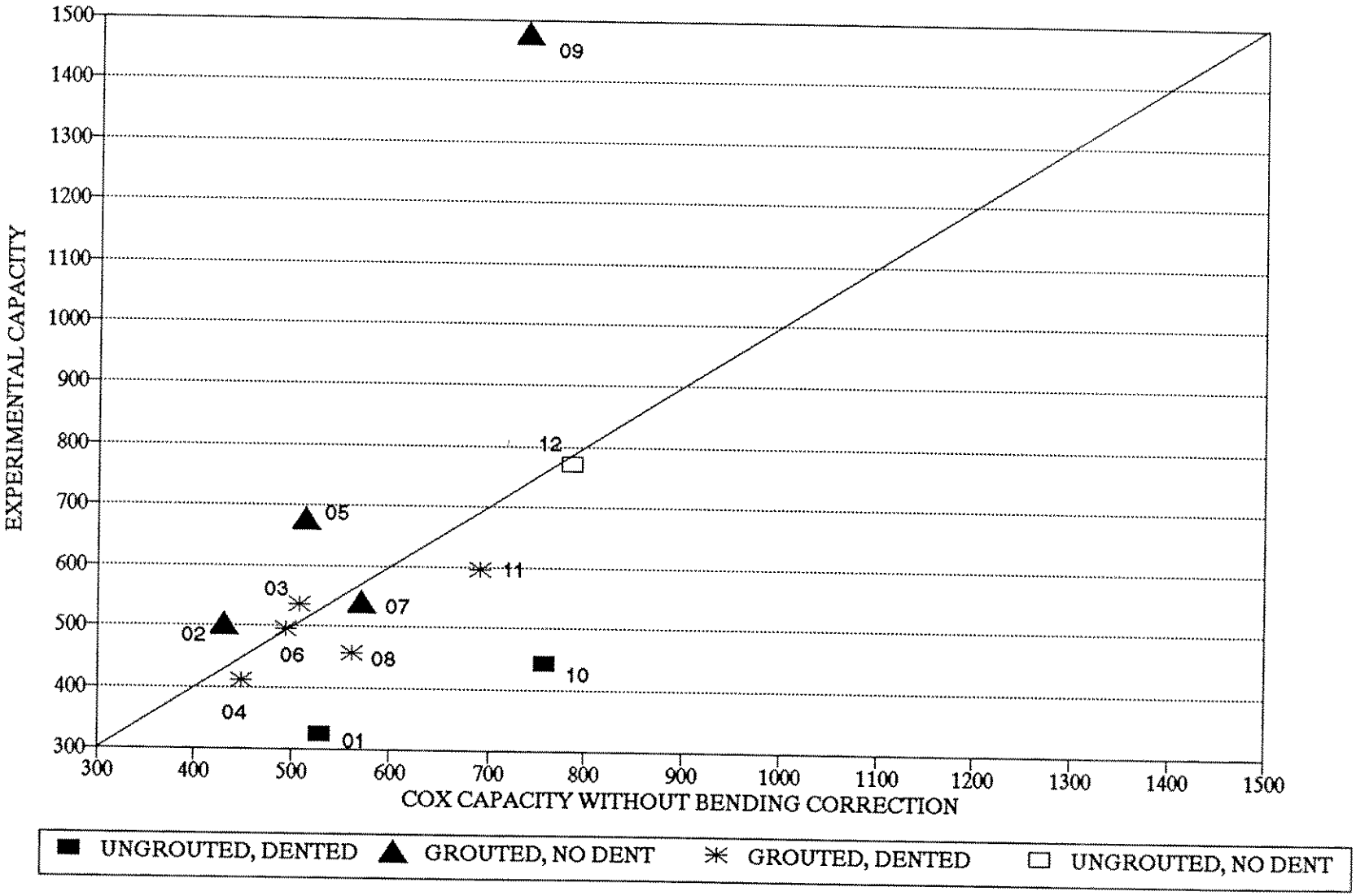

Figure 4.5. COMPARISON OF EXPERIMENTAL CAPACITIES
WITH COX WITH BENDING CORRECTION

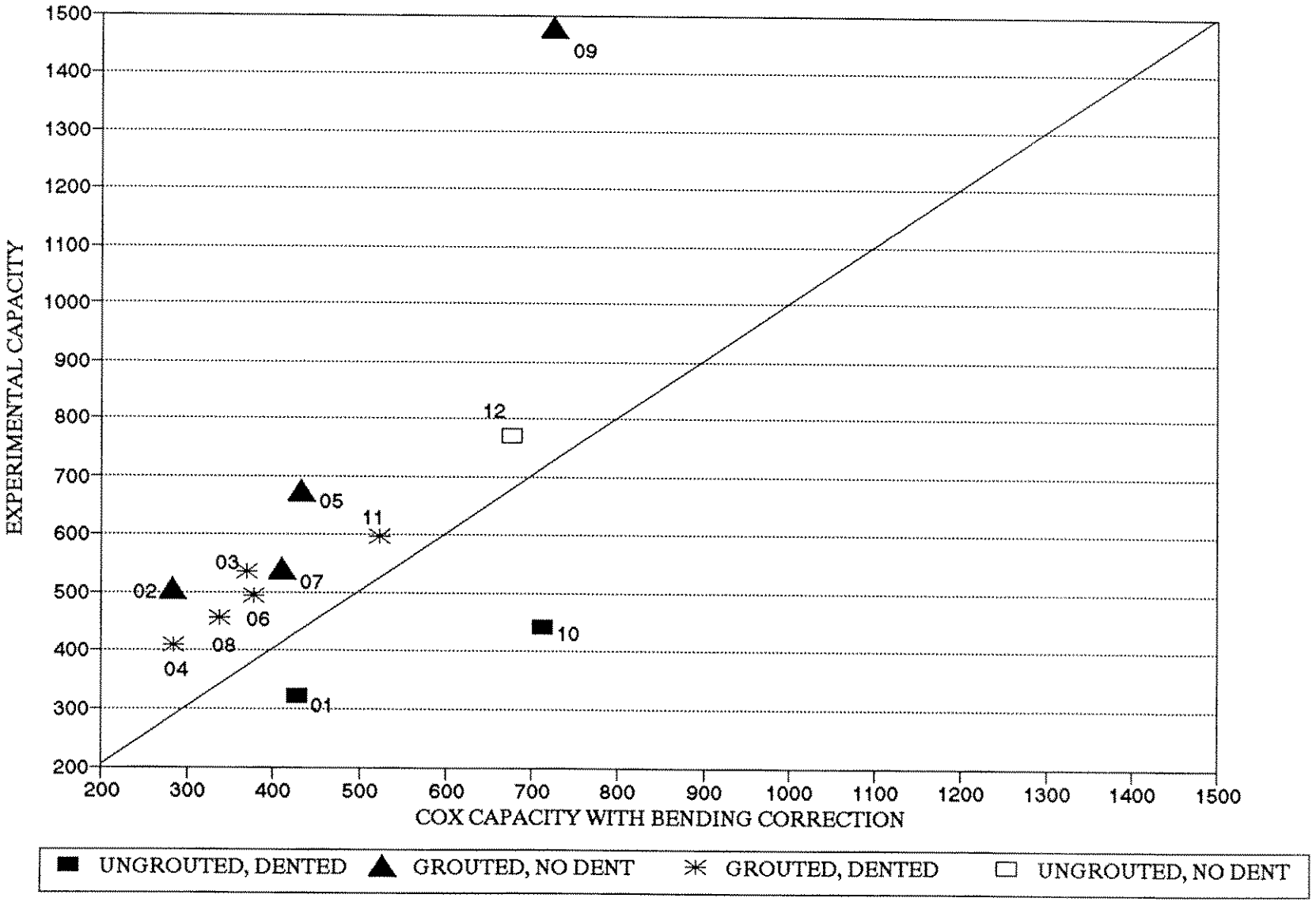

Table 4.1. Analytical Method Summary

Specimen No.	Specimen Parameters	Analytical Methods
ALL		LRFD-Cox w/ and w/o bending correction
01	Dented/Ungrouted	Taby, Ellinas, Zhou, and Poston
02,05,07	Undented/Grouted	ACI and Poston
06	Dented/Grouted	Poston
03,04,08	Dented/Grouted	Parsanejad - 1987, 1988, 1990, and Poston
10	Dented/Ungrouted	Taby, Ellinas, and Zhou
09	Undented/Grouted	ACI
11	Dented/Grouted	Parsanejad - 1987, 1988, and 1990

Table 4.2. Specimen Properties Used in Analytical Ultimate Capacities

Specimen No.	Length (ft.)	Diameter[5] (in.)	Wall[5] Thickness (in.)	Yield Strength (ksi)	Effective Length Factor
01[4]	40.19	12.75	0.375	38.9	0.50
02	40.19	12.75	0.375	36.5	0.78
03[4]	40.15	12.75	0.375	37.8	0.54
04[4]	40.15	12.75	0.250	51.8	0.54
05	40.27	12.75	0.375	40.4	0.62
06[4]	40.25	12.75	0.375	36.1	0.50
07	40.21	12.75	0.250	74.2	0.58
08[4]	40.19	12.75	0.250	65.9	0.50
09	40.06	16.00	0.375	44.0	0.66
10	39.96	16.00	0.375	42.7	0.50
11	39.96	16.00	0.375	40.8	0.66
12	40.00	16.00	0.375	46.1	0.60

Notes:
1) For steel, E = 29,000 ksi
2) Nominal compressive strength of grout=4000 psi
3) For grout, E = 3,650 ksi
4) For members 1, 3, 4, 6, and 8, dent depth is 5 in.
   For members 10 and 11, dent depth is 6 3/8 in.
   For all members, the dent length is 36 in.
5) Specified nominal values

Table 4.3. Results from PIER Program

Specimen No.	P_{Exp} (kips)	P_{PIER} (kips)	P_{Exp}/P_{PIER}	$\Delta_{CENTERLINE}$	Comments
01	324	320	1.01	1	k=0.5
02	506	510	0.99	1	k=0.7
03	538	510 450	1.05 1.20	1 2	k=0.5 k=0.5
04	411	430 540 230	0.96 0.76 1.79	1 1 2	k=0.5 F_y=51.8 ksi, k=0.5
05	677	590 550 660	1.15 1.23 1.03	1 1 0.75	k=0.5 k=0.62 k=0.5
06	496	400 380 460	1.24 1.31 1.08	1.5 1.5 1.25	k=0.5 k=1.0,L=0.5* L K=0.5
07	543	720 640 670	0.75 0.85 0.81	1 1 1.25	k=0.5 k=0.58 k=0.5
08	458	700 580	0.65 0.79	1 1.25	k=0.5 k=0.5

Notes:
1) Specimen 01-04 assumed F_y = 36,500 psi.
2) Other properties shown in Table 4.2.
3) At dent, assumed dented grout area is 3/4 of gross grout area.
   The gross area of the steel tube was used in dented area.
4) E_c = 3650 ksi.
5) $\Delta_{centerline}$ = assumed initial deflection (out-of-straightness) at midspan.

Table 4.4. Summary of Test Specimen Properties Used to Compute P_u by the Cox Formula

Specimen No.	D[3] (in.)	t[3] (in.)	D/t	r (in.)	d/D	e[4] (in.)	Grout Strength (psi)	k	L (in.)	$\frac{KL}{r}$	F_y (ksi)
01	12.75	0.375	34.0	4.38	0.39	-0.17	N.A.	0.50	482.25	55.09	38.9
02	12.75	0.375	34.0	4.38	0.00	-1.57	4140	0.78	482.25	85.93	36.5
03	12.75	0.375	34.0	4.38	0.39	-1.57	4140	0.54	481.75	59.43	37.8
04	12.75	0.250	51.0	4.42	0.39	-2.21	4140	0.54	481.75	58.85	51.8
05	12.75	0.375	34.0	4.38	0.00	-0.89	4020	0.62	483.25	68.45	40.4
06	12.75	0.375	34.0	4.38	0.39	-1.60	4210	0.50	483.00	55.17	36.1
07	12.75	0.250	51.0	4.42	0.00	-1.38	4210	0.58	482.50	63.31	74.2
08	12.75	0.250	51.0	4.42	0.39	-2.41	4210	0.50	482.25	54.55	65.9
09	16.00	0.375	42.7	5.53	0.00	-0.37	5070	0.66	480.75	57.42	44.0
10	16.00	0.375	42.7	5.53	0.40	-1.72	N.A.	0.50	479.50	43.39	42.7
11	16.00	0.375	42.7	5.53	0.40	-2.11	5070	0.66	479.50	57.27	40.8
12	16.00	0.375	42.7	5.53	0.00	-0.20	N.A.	0.60	480.00	52.12	46.1

Notes:
1) All specimens API 5L Grade B steel.
2) All dented members dented at midspan.
   Length of dent = 36"
   Width of dent = 10.2"
3) Nominal specified values (i.e., not measured)
4) Average eccentricity of load at ends A and B from end moments at peak load.

Table 4.5. Summary of Experimental Data and P_{Cox}

Specimen No.	P_{Exp} (kips)	P_{Cox} [1] without Bending (kips)	P_{Exp}/P_{Cox} without Bending	P_{Cox} with [2] Bending (kips)	P_{Exp}/P_{Cox} with Bending
01[3]	324	528	0.61	427	0.76
02[4]	506	430	1.18	283	1.79
03[5]	538	507	1.06	369	1.46
04[5]	411	449	0.92	284	1.45
05[4]	677	515	1.32	432	1.57
06[5]	496	494	1.00	377	1.32
07[4]	543	572	0.95	411	1.32
08[5]	458	562	0.82	338	1.36
09[4]	1479	738	2.00	726	2.04
10[3]	443	758	0.58	713	0.62
11[5]	598	691	0.87	522	1.15
12[6]	772	785	0.98	677	1.14

Notes:
1) P_u based on Eqn. 4.1. No correction made for the interaction of bending moment.
2) P_u based on Eqn. 4.2. Correction made for the interaction of bending moment.
3) Dented, ungrouted specimen.
4) Undented, grouted specimen.
5) Dented, grouted specimen.
6) Undented, ungrouted specimen.

Table 4.6. P_{Exp}/P_{Cox} for Undented Grouted Members

Specimen No.	D/t	P_{Exp}/P_{Cox} with Bending Correction
02	34.0	1.79
05	34.0	1.57
07	51.0	1.32
09	42.7	2.04

Table 4.7. P_{Exp}/P_{Cox} for Dented Grouted Members

Specimen No.	D/t	P_{Exp}/P_{Cox} with Bending Correction
03	34.0	1.46
06	34.0	1.32
04	51.0	1.45
08	51.0	1.36
11	42.7	1.15

Table 4.8. Summary of Replicate Tests

Specimen No.	Dented	D/t	P_{Exp}/P_{Cox} with Bending	$(P_{Exp}/P_{Cox})_{avg}$ with Bending	% Difference between Replicate Tests
02	No	34.0	1.79	1.68	13.1
05	No	34.0	1.57		
03	Yes	34.0	1.46	1.39	10.1
06	Yes	34.0	1.32		
04	Yes	51.0	1.45	1.41	6.4
08	Yes	51.0	1.36		

Note: All specimens filled with grout (nominal strength = 4100 psi)

Table 4.9. Analytical and Experimental Results for Dented, Ungrouted Specimens

Specimen No.	P_{Exp} (kips)	P_{Cox} (kips) with	P_u,Zhou (kips)	P_u,Taby 1981 (kips)	P_u,Taby 1985 (kips)	P_u,Poston (kips)	P_u,Ellinas (kips)
01	324	507	100	86	301	320	85
P_{Exp}/P_u, Method	NA	0.64	3.24	3.77	1.08	1.01	3.81
10	443	713	114	117	254	NC	110
P_{Exp}/P_u, Method	NA	0.62	3.89	3.79	1.74	NC	4.03

Notes: NA = Not applicable.
NC = Capacity not computed by this method.

Table 4.10. Analytical and Experimental Results for Undented, Grouted Specimens

Specimen No.	P_{Exp} (kips)	P_{Cox} (kips) with	P_u,ACI (kips)	P_u,Poston (kips)
02	506	283	616	510
P_{Exp}/P_u, Method	NA	1.79	0.82	0.99
05	677	432	975	550
P_{Exp}/P_u, Method	NA	1.57	0.69	1.23
07	543	411	803	640
P_{Exp}/P_u, Method	NA [1)]	1.32	0.68	0.85
09	1479	726	1788	NC
P_{Exp}/P_u, Method	NA	2.04	0.83	NC

Notes: NA = Not applicable.
NC = Capacity not computed by this method.
1) Peak load occurred after bond failure between the grout and the steel tube.

Table 4.11. Analytical and Experimental Results for Dented, Grouted Specimens

Specimen No.	P_{Exp} (kips)	P_{Cox} (kips) with	P_u,P-87[1] (kips)	P_u,P-90[2] (kips)	P_u,P-88[3] (kips)	P_u,Poston (kips)
03	538	369	302	229	237	510
P_{Exp}/P_u, Method	NA	1.46	1.78	2.35	2.27	1.05
04	411	283	263	185	189	430
P_{Exp}/P_u, Method	NA	1.45	1.56	2.22	2.17	0.96
06	496	377	MD	MD	MD	400
P_{Exp}/P_u, Method	NA	1.32	MD	MD	MD	1.24
08	458	338	323	229	234	580
P_{Exp}/P_u, Method	NA	1.36	1.42	2.00	1.96	0.79
11	598	522	318	231	239	NC
P_{Exp}/P_u, Method	NA	1.15	1.88	2.59	2.50	NC

Notes: 1) Parsanejad Method 1.
2) Parsanejad Method 2.
3) Parsanejad Method 3.
NA = Not applicable.
MD = Capacity not computed by this method. Missing initial out-of-straightness data.
NC = Capacity not computed by this method.

Table 4.12. Summary of Experimental Data and P_{Cox} Using Actual and Nominal Yield Strength Values

Specimen No.	F_y (ksi)	P_{Exp} (kips)	P_{Cox} Actual F_y (with Bending) (kips)	P_{Cox} [1] Nominal F_y (with Bending) (kips)	$\frac{P_{EXP}}{P_{COX}\ Actual\ F_y}$	$\frac{P_{EXP}}{P_{COX}\ Nominal\ F_y}$
1[2]	38.9	324	427	383	0.76	0.85
2[3]	36.5	506	283	271	1.79	1.87
3	37.8	538	369	338	1.46	1.59
4	51.8	411	284	174	1.45	2.37
5[3]	40.4	677	432	379	1.57	1.79
6	36.1	496	377	364	1.32	1.37
7[3]	74.2	543	411	202	1.32	2.68
8	65.9	458	338	139	1.36	3.28
9[3]	44.0	1479	726	593	2.04	2.50
10[2]	42.7	443	713	587	0.62	0.76
11	40.8	598	522	443	1.15	1.35
12[2],[3]	46.1	772	677	514	1.14	1.50

Notes: 1) Computed value using nominal F_y = 35 ksi for API 5L Gr. B Steel
2) Specimen not grouted.
3) Specimen not dented.

Table 4.13. Summary of Static Yield Capacities

Specimen No.	P_{Exp} (kips)	F_y (ksi)	P_y (kips)	P_{Exp}/P_y
1[2)]	324	38.9	567	0.57
2[3)]	506	36.5	532	0.95
3	538	37.8	551	0.98
4	411	51.8	509	0.81
5[3)]	677	40.4	589	1.15
6	496	36.1	526	0.94
7[3)]	543	74.2	728	0.75
8	458	65.9	647	0.71
9[3)]	1479	44.0	810	1.83
10[2)]	443	42.7	786	0.56
11	598	40.8	751	0.80
12[2),3)]	772	46.1	849	0.91

Note: 1) $P_y = F_y A_g$
2) Specimen not grouted.
3) Specimen not dented.

7) Grouting is a viable method for strengthening undamaged tubular members. Based on the experimental data, grouting members without any initial damage can increase the strength 32% to 104% above the original ultimate capacity. Specimen 07 contained extremely poor and incomplete grout; however, the grout still increased the strength of the member 32% above the original ultimate capacity. Specimen 09 contained quality grout the full length of the member which resulted in a 104% increase above the original ultimate capacity.

8) Grouting is also a viable method for repairing dent-damaged tubular members. Grout can inhibit local buckling and prevent any further reduction of the cross section at the location of the dent. In all the grout-repaired/dented members tested, the ultimate capacity exceeded the original (undamaged/ungrouted) ultimate capacity of the member. The increase in strength above the original ultimate capacity varied from 15% to 46%. This results in an 83% to 85% increase above the dented/ungrouted capacity.

9) Grouting may be a viable repair method for members with significant out-of-straightness damage. Specimen 11 contained an initial out-of-straightness of 4.50 in. ($\delta/L = 0.0095$) as well as an initial 6.40 in.-deep dent ($d/D = 0.40$). Grouting increased the strength of the member to 15% above the original ultimate capacity.

10) All grouted members were able to sustain large resultant (X and Y) lateral displacements with less deterioration in strength than identical ungrouted specimens.

11) Most of the existing analytical methods provided very conservative (lower bound) values for the predicted ultimate strength of dented/ungrouted and dented/grouted members. For some members, the predicted strength was 1/3 of the experimentally measured capacity. This could be attributed to the fact that these analytical methods assume a transverse dent geometry while the dents used in this study were

longitudinal dents. Typically, these dents appear to be stiffer than the transverse dents.

12) There were some members in which two of the methods (ACI and Poston) produced unconservative (overpredicted) ultimate capacities. There are circumstances (i.e., poor quality grout, incorrect assumptions about initial out-of-straightness) which can explain why the Poston method overpredicts the ultimate capacity. The ACI method is based on elastic behavior of the steel tubular. All of the specimens tested failed at ultimate loads in the inelastic region of the steel. Thus, the ACI formula may not be valid for these members.

13) Post-test destructive examination of the grouted members revealed significant differences in the completeness and quality of grout. Members that were pumped full without interruption generally contained a larger volume of quality grout.

5.2 Recommended Studies

The results of this research indicates that future research efforts should be considered to further evaluate and understand the behavior of damaged and grouted tubular members. There are many parameters that must be addressed in order to further validate grout as a viable repair method for damaged tubulars. It is recommended that the following items be considered in these efforts:

1) Damage parameters should be varied in order to best represent the range of dent properties that exist on in-service members. The effects of dent location, depth, and orientation on the pre- and post-ultimate behavior should be fully evaluated. In addition, members with multiple damage sites should be investigated since in-service members often suffer multiple forms of damage.

2) Generally, the mechanism that causes dent-damage will also produce out-of-straightness damage. Thus, the effects of out-of-straightness in combination with dent-damage should be further evaluated. Based on the experimental results from specimen 11, it appears that grouting is more effective in restoring strength to members with out-of-straightness

damage than indicated by previous studies. In addition, tests should be conducted to determine what is "significant" (or "insignificant") out-of-straightness.

3) Corrosion is the most prevalent damage that is experienced in the offshore environment. Grout repaired, corroded members should be thoroughly studied. This warrants testing of members that have been salvaged from in-service platforms or members that have been subjected to artificially induced corrosion.

4) Damaged/grout repaired members should also be studied under more complex loading conditions. In particular, dynamic (fatigue) loadings should be investigated to determine if there is any deterioration in the member strength.

5) More accurate analytical methods need to be developed for predicting the ultimate capacity of dent-damaged/grouted and dent-damaged/ungrouted members.

REFERENCES

American Institute of Steel Construction, "Load and Resistance Factor Design," First Edition, American Institute of Steel Construction, Inc., Chicago, IL, 1986.

American Institute of Steel Construction, "Specification for the Design, Fabrication and Erection of Structural Steel for Buildings," American Institute of Steel Construction, Inc., Chicago, IL, 1969.

American Concrete Institute, "Building Code Requirements for Reinforced Concrete," ACI 318-89, Detroit, MI, 1989.

American Petroleum Institute, "Recommended Practice for Planning, Designing and Constructing of Fixed Offshore Platforms," API RP2-A, Washington, DC, 1991.

American Society for Testing and Materials, "Standard Test Methods of Tension Testing of Metallic Materials," ASTM E8-88, Part 3, ASTM Annual Standards, Philadelphia, PA, 1988.

"B.7: SSRC Technical Memorandum No. 7: Tension Testing," Guide to Stability Design Criteria for Metal Structures, 4th Edition, pp. 744-749, Editor: Galambos, T. V., John Wiley & Sons, New York, NY, 1988.

Boswell, L. F., and D'Mello, C. A., "Residual and Fatigue Strength of Grout Filled Damaged Tubular Members," OTH89 314 Department of Civil Engineering, City University, London, U.K., 1989.

Cox, J. W., "Tubular Member Strength Equations for LRFD, "Final Report, API PRAC Project 86-55, TERA, Inc., Houston, TX, Prepared for the American Petroleum Institute, Dallas, TX, 1987.

Ellinas, C. P., "Ultimate Strength of Damaged Tubular Bracing Members," Journal of Structural Engineering, Vol. 110, No. 2, pp. 245-259, American Society of Civil Engineers, 1984.

Marek, D. L., "Evaluation of Compression Members with Non-Ideal End Conditions," Thesis presented to Texas A&M University, College Station, TX, in partial fulfillment of the requirements for the degree of Master of Science, 1993.

Moehlman, S. A., "Testing and Evaluation of Damaged Tubular Jacket Braces," Thesis presented to Texas A&M University, College Station, TX, in partial fulfillment of the requirements for the degree of Master of Science, 1990.

Parsanejad, S., Tyler, S., and Chin, K. Y., "Experimental Investigation of Grout Filled Damaged Tubular Members," Proceedings of the International Conference of Structural Faults and Repair, Great Britain, July, 1987.

Parsanejad, S., "Strength of Grout-Filled Damaged Tubular Members," ASCE Structural Engineering Journal, Vol. 113, No. 3, pp. 590-603, 1987.

Parsanejad, S., and Gusheh, P., "Behavior of Partially Grout Filled Damaged Tubular Members," Civil Engineering Monograph, No. CE 88/2 STE, University of Technology, Sydney, Australia, 1988.

Parsanejad, S., and Gusheh, P., "Analytical Expression for Ultimate Strength Analysis of Partially Grout Filled Damaged Tubular Members," Transactions of the Institution of Civil Engineers, Civil Engineering, Vol. CE 32, No. 1, pp. 14-21, Australia, 1990.

Poston, R., "Nonlinear Analysis of Concrete Bridge Piers," ASCE Structural Engineering Journal, Vol. 112, No. 9, pp. 2041-2056, 1986.

Renault, J. P., and Quillevere, J. P., "Offshore Structures: Repair of Dented Members by Internal Grouting," Proceedings of the 9th International Conference on Offshore Mechanics and Arctic Engineers, 1990.

Ricles, J. M., Gillum, T. E., and Lamport, W. B., "Grout Repair of Dent-Damaged Steel Tubular Bracing," OTC 7151, presented at the 25th Annual Offshore Technology Conference, Houston, TX, 1993.

Ritter, J., "Development of a Failure Prediction Method for Damaged Tubular Members," Thesis presented to Texas A&M University, College Station, TX, in partial fulfillment of the requirements for the degree of Master of Science, 1992.

SAA STEEL STRUCTURES CODE, Australian Standard 1250-1981, Association of Australia, Sydney, Australia, 1981.

Taby, J., and Moan, T., "Theoretical and Experimental Study of the Behaviour of Damaged Tubular Members in Offshore Structures," Norwegian Maritime Research, No. 2, pp. 26-33, 1981.

Taby, J., and Moan, T., "Collapse and Residual Strength of Damaged Tubular Members," Behavior of Offshore Structures, Elsevier Science Publishers, Amsterdam, 1985.

Taby, J., "DENTA II - Users Manual (VAX Version 1.01)," Department of Marine Technology, The Norwegian Institute of Technology, The University of Trondheim, 1988.

Wimpey Engineering Report, "Grout Filled Tubular Members," Wimpey Offshore, Houston, TX, 1984.

Zhou, Y. X., Chen, W. M., and Chen, T. Y., "A Plastic Model for Limit Analysis of Dented Tubular Members," Proceedings of the 10th International Conference on Offshore Mechanic and Arctic Engineering, Vol. III, Part B, pp. 427-432, Materials Engineering, American Society of Mechanical Engineers, 1991.